Late Paleozoic tectonic evolution of the North Tianshan Belt: New structural and geochronological constraints from meta-sedimentary rocks and migmatites in the Harlik Range (NW China)

Xinghua Ni, Bo Wang, Dominique Cluzel, Jiashuo Liu, Zhiyuan He, Flavien Choulet, Yuruo Shi, Wei Xie, Xinshui Wang, Yuanyuan Zhang

Journal of Asian Earth Sciences

Late Paleozoic tectonic evolution of the North Tianshan Belt: New structural and geochronological constraints from meta-sedimentary rocks and migmatites in the Harlik Range

--Manuscript Draft--

Manuscript Number:	JAES-D-20-00960R1
Article Type:	Research Paper
Keywords:	Central Asian Orogenic Belt; East Junggar; North Tianshan (Tien Shan); accretionary orogeny; post-orogenic crustal thinning; migmatization
Corresponding Author:	Bo Wang, PhD Nanjing University Nanjing, CHINA
First Author:	Xinghua Ni
Order of Authors:	Xinghua Ni
	Bo Wang, PhD
	Dominique Cluzel
	Jiashuo Liu
	Zhiyuan He
Abstract:	The North Tianshan Belt (NTB) formed by the subduction and accretion of the Junggar Ocean is a key area for reconstructing the Paleozoic tectonic evolution of the southern Central Asian Orogenic Belt (CAOB). Despite numerous studies, the interpretation of the late Paleozoic tectonic evolution of the NTB meets no consensus yet. We conducted field investigations and LA-ICP-MS zircon U-Pb dating on metamorphic rocks from the Julideneng Metamorphic Complex (JMC) in the Harlik Range, which is located between the Turpan-Hami Basin to the south and the East Junggar Belt to the north. The metamorphic rocks are exposed in a NW-SE striking, ~10 km-wide belt and mainly composed of migmatites, garnet-sillimanite mica schists, andalusite schists, and low-grade meta-sandstones. Detrital zircons from the low-grade meta-sandstone yielded ages of 1400 Ma to ~425 Ma. Three micaschists contain zircon populations of from 2500 Ma to ~346 Ma, and a youngest age peak at ~322 Ma. Two samples of leucocratic dykes in migmatites yielded comparable age populations with two major peaks at 322 Ma and 297 Ma. On the basis of structural features, zircon textures and U-Pb ages, combined with already published data, we propose that: (1) the meta-sedimentary rocks of the JMC were deposited after 425 Ma and before 322 Ma; (2) the Precambrian detrital zircons in the meta-sedimentary rocks were probably derived from the Central Tianshan Block; and (3) the migmatization and coeval granitic plutonism occurred at ~322-297 Ma, most likely associated with crustal thinning resulted from continent-based intra-arc or back-arc or post-orogenic extension.
Suggested Reviewers:	Johan de Grave Ghent University johan.degrave@ugent.be Expert in geology of the CAOB, Tianshan belt and geochronology
	Flavien Choulet University of Franche-Comté flavien.choulet@univ-fcomte.fr Expert in tectonics of the CAOB and Junggar domain
	Yuruo Shi Chinese Academy of Geological Sciences shiyuruo@bjshrimp.cn Expert in the CAOB, Tianshan belt and in geochronology
	Wei Xie Hohai University weixie@hhu.edu.cn

	Expert in the CAOB, Tianshan belt and in geochronology
	Xinshui Wang China University of Geosciences (Wuhan) wangxinshui@cug.edu.cn Expert in the CAOB and Tianshan belt
	Yuanyuan Zhang Peking University yy-zhang@pku.edu.cn Expert in the CAOB, Eastern Junggar and Tianshan belts
Opposed Reviewers:	

Dr. Bo Wang
School of Earth Sciences and Engineering
Nanjing University
bwang@nju.edu.cn; burh_cw@yahoo.com

Dear Editor-in Chief Prof. Zhou,

Dear the Editor Prof. Uysal,

February 3, 2021

Thank you very much for your efforts and positive evaluation on our manuscript. We also appreciate very much both reviewers for their constructive comments and thoughtful suggestions. All the comments and suggestions were carefully considered and the manuscript was revised accordingly.

All the comments and concerns were replied in the point-by-point answers to the reviewers. In addition, we have read through the manuscript carefully for several times, and corrected and revised the text, figures and tables. The English of the text was also polished by several colleagues who are good at English writing. We also checked the reference list and citations. Moreover, we append the short biography of each author at the end of this letter. We hope that the manuscript has been satisfactorily improved to fit the publication in the journal.

Your consideration and handling of this manuscript are greatly appreciated.

Sincerely,

Bo Wang

On behalf of coauthors

Xinghua Ni is a Ph.D. Candidate at School of Earth Sciences and Engineering of Nanjing University, China, where he started his Ph.D. subject since 2020. He received his M.Sc. degree in 2020 at Nanjing University. His research involves Paleozoic tectonic evolution of the Tianshan Orogenic Belt, focusing on metamorphism, structural geology, geochronology and geochemistry.

Bo Wang is a Professor at School of Earth Sciences and Engineering of Nanjing University, China. He received his joint Ph.D. degree from Nanjing University (China) and Université d'Orleans (France) in 2006. His main research interests include structural and kinematic analysis of deformed rocks, tectonic evolution of orogenic belts, plate tectonics and continental reconstruction, mainly in the Tianshan and South China.

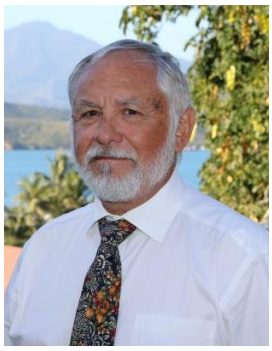

Dominique Cluzel is professor emeritus at the Institut des Sciences Exactes et Appliquées (Institute of Pure and Applied Sciences), University of New Caledonia. He researches on Structural Geology and Geodynamics through a multidisciplinary approach. His current research interests are tectonics and geodynamic evolution and mineral resources of New Caledonia, Paleozoic geodynamic evolution of the Central Asian Orogenic Belt (Xinjiang Region, China).

Jiashuo Liu is a Ph.D. Candidate at School of Earth Sciences and Engineering of Nanjing University, China, where he started his Ph.D. subject since 2020. Before that, he studied as a Master student at Nanjing University in 2018. His research interests focus on the evolution of orogenic belts using the structural geology, geochronology and geochemistry, and the thermal modeling related to Raman spectrum of carbonaceous material.

Zhiyuan He received his M.Sc. degree in 2018 from Nanjing University. His research involves Paleozoic tectonics and structural geology of the Tianshan, focusing on regional ductile shear zones. He is currently undertaking Ph.D. research at the Ghent University using an integrated approach of field mapping, structural geology and thermochronology to reveal the thermal-tectonic history of the Tianshan and Junggar.

*Author Agreement

We the undersigned declare that this manuscript is original, has not been published before and is not currently being considered for publication elsewhere.

We confirm that the manuscript has been read and approved by all named authors and that there are no other persons who satisfied the criteria for authorship but are not listed. We further confirm that the order of authors listed in the manuscript has been approved by all of us.

We understand that the Corresponding Author is the sole contact for the Editorial process. He/she is responsible for communicating with the other authors about progress, submissions of revisions and final approval of proofs.

Signed by the corresponding author:

Research highlights:

- Protoliths of the Julideneng Metamorphic Complex were deposited between 425 Ma and 322 Ma.
- Metamorphism/migmatization occurred at ~322-297 Ma in continent-based intra-arc/back-arc or post-orogenic setting.
- Precambrian detrital zircons were likely derived from the Central Tianshan.
- Accretionary orogeny in the North Tianshan terminated in the Permian.

Ms. Ref. No.: JAES-D-20-00960

Title: Late Paleozoic tectonic evolution of the North Tianshan Belt: New structural and geochronological constraints from meta-sedimentary rocks and migmatites in the Harlik Range

Journal of Asian Earth Sciences

Dear Dr. Wang,

The reviewers/editor have commented on your above paper and they ask you to undertake minor revision.

Please carefully address the issues raised in the comments. If you are submitting a revised manuscript, please also:

a) explain how and where each point of the reviewers' and Editor's comments has been incorporated (point by point) in a separate "Detailed Response to Reviewers" file. Your response must be made very clear.

b) indicate all the corrections "in red" in the revised manuscript, so that the Editor could easily identify the places of change. (that is a version use a size 12-point font and without annotations)

c) should you disagree with any part of the reviews, please explain why.

Your revision should be resubmitted within 45 days. I look forward to receiving your revised manuscript.

Yours sincerely,

On behalf of Editor-in Chief Mei-Fu Zhou

Miss Diane Chung

Journal of Asian Earth Sciences

Dear Editor-in Chief Prof. Zhou,

Dear the Journal Manager Miss Chung,

Thank you very much for sending us the referee's reports and for your positive evaluation on our manuscript JAES-D-20-00960. In careful consideration of the referee's helpful comments and suggestions, we have revised our manuscript seriously. In the following, we reply point-by-point all the comments and suggestions raised by both reviewers. We hope the manuscript has been satisfactorily improved and it will be accepted for publication in the journal.

Thanks again for your kind consideration.

Best regards,

Bo Wang and co-authors

Reviewers' comments:

Dear Dr. Wang,

Thank you for submitting your manuscript to JAES. The review process of your manuscript has now been completed and I received the comments from two expert. Both reviewers agree that the manuscript is well prepared and contains valuable data which deserve to be published. However, they both think that the current version needs some minor improvements before publication. Below, you will find the suggestions provided by two reviewers, and I believe that implementation of their comments will make your manuscript better in shape. Therefore, I kindly ask you to take into account all the comments, given below, in revision of your manuscript, and have the revised text polished for English language before re-submision.

Kind regards,

Ibrahim Uysal

Editor

Dear the Editor Prof. Uysal,

Thanks a lot for your handling and positive evaluation of our manuscript. We considered carefully all the constructive comments and suggestions by both reviewers, and revised the manuscript accordingly. The English of the text was also polished by several colleagues who are good at English writing. In the following, we reply point-by-point to all the comments and suggestions.

Best regards,

Bo Wang and co-authors

Reviewer #1: This paper presents field relationship and structures, geochronological and zircon isotopic data of meta-sedimentary rocks and migmatites in the Harlik Range, and further discusses their petrogenesis and late Paleozoic tectonic evolution of the North Tianshan Belt. The study is valuable, but this paper can be accepted with moderate revision.

Thanks a lot for the positive opinion by Reviewer #1.

1. It is important to distinguish different zircon groups due to different origins. It should be better if type 1-4 are labeled besides the zircons in figures.

A: Thanks for this meaningful suggestion. In revised Fig. 5 different types of zircons are grouped and labeled in order better to distinguish their origins.

Authors have discussed the type 3 zircons in 12TS119E are of hydrothermal origin (line 412-415). How about type 3 zircons in 12TS119A and 12TS119B? How about the Th/U ration? Not metamorphic origin? What the age of type 3 zircons in 12TS119A?

Check if type 3 zircons from these 3 samples have similar Th/U. From what you described in the text, Th/U ratios of type 3 zircons differ from these 3 samples

A: Based on the morphology, Th/U ratios and REE patterns of the zircons, we concluded that the type 3 zircons in sample 12TS119E are similar to hydrothermal zircons (Hoskin, 2005). Actually, as we discussed in line 396-398, the three youngest zircons in sample 12TS119B also belong to type 3, displaying homogeneous dark to black CL images (Figs. 5c and S1) and Th/U ratios around 0.4 (Table S1; Fig. 6f). Although we do not have REE patterns of these zircons, it is quite possible that they are also of a hydrothermal origin.

However, there is no type 3 zircon in sample 12TS119A, from which all zircons belong

to the type 1 and type 2 (Figs. 5b and S1). The youngest nine ages are obtained exclusively from type 2 zircons with Th/U ratios mostly lower than or near 0.4 (Table S1; Fig. 6d), showing bright or dark cores characterized by surface-controlled alteration (Corfu et al., 2003) and encircled by thin and dark rims (Figs. 5b and S1) (line 386-390). This kind of zircons was considered to be related with metamorphic event (Hoskin and Schaltegger, 2003) (line 359-367). Therefore, the youngest age (~322 Ma) of these zircons probably corresponds to the timing of the metamorphism (line 467-469).

For zircon morphology, how about migmatite samples? 2 out of four types are shown in migmatite samples ? Any meaning? Maybe it needs further discussion.

A: Thanks for this important comment.

Indeed, as suggested by the reviewer, there are two types of zircons in the migmatite samples. A few grains with vague dark rims are similar to type 1 zircons and they yielded ages mostly of ~322 Ma and minor older ages, and the other zircons without visible rims are comparable with type 4 zircons and they yielded ages of ~322 Ma and 297Ma (Fig. 8) (line 471-478). However, all the dated zircons display clear oscillatory zoning, Th/U ratios higher than or close to 0.4 (Fig. 8) and steeply-rising REE patterns characterized by enrichment of HREE relative to LREE, mostly positive Ce anomalies and negative Eu anomalies (Figs. 7c and 7d), indicating a magmatic origin (line 422-425 and 438-441). In addition, we calculated the apparent temperature of zircon crystallization by using Ti-in-zircon thermometer (Watson et al., 2006), which was not presented in the manuscript. As shown in figures below (Fig. R1), zircons of different ages don't show significant difference in apparent crystallization temperature. As these zircons yielded two U-Pb ages at ~322 Ma and ~297Ma, and sometimes different zircons yielded same ages, while similar zircons sometimes yielded different ages,

we proposed that these two ages likely represent two episodes of zircon crystallization (similar origin), and the dark rims of some zircons may have resulted from slight overgrowth during the second episode of crystallization at 297 Ma (line 475-478).

We have discussed in the revised manuscript the origins and meanings of zircons from the migmatite samples on the basis of their texture and morphology. On the fact that detrital zircons in meta-sedimentary rocks have complex textures, we divided them into four types. But considering that zircons of the migmatites are relatively simple, we do not recommend classifying them in order not to make things complex.

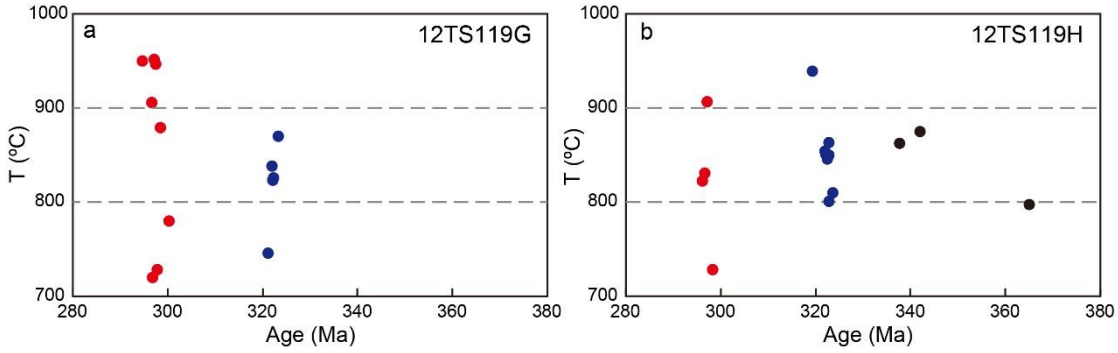

Fig. R1 Calculated crystallization temperature of zircons from two migmatite samples.

What's the temperature for hydrothermal zircon? It seems that the hydrothermal zircon ages are older than metamorphic and magmatic ages you discussed in Section 6.1.

A: Yes, we also calculated the apparent temperatures for zircons of the schist sample 12TS119E by using Ti-in-zircon thermometer (Watson et al., 2006). The results show that the hydrothermal zircons (green spots in Fig. R2) have apparent crystallization temperatures at 780-1080 ℃. Such high temperatures probably correspond to Ti-rich fluids that form the hydrothermal zircons. The reason why ages of the hydrothermal zircons are older than metamorphic age may be resulted from age mixing between primary cores and recrystallized areas or overgrowths (line 469-470) (Corfu et al., 2003) or fluids-related high U and Th

abundances (Zhao et al., 2014). This can be additionally proved by the weak concordance of the ages for these hydrothermal zircons (Fig. 6g).

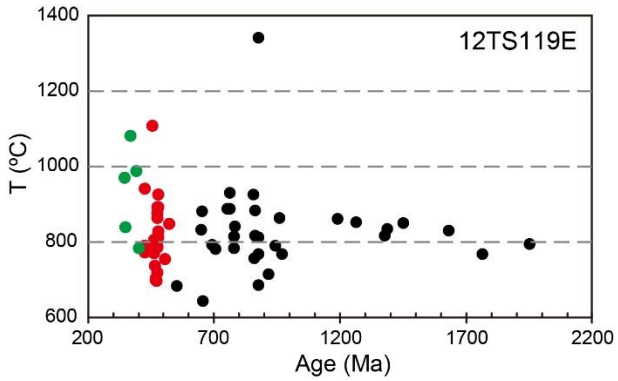

Fig. R2 Calculated crystallization temperature of zircons from the schist sample 12TS119E.

2. The metamorphic ages are constrained to be 322Ma and 297Ma, so should the deposition age of the meta-sedimentary rocks be between 425 and 322Ma at least? Line 41 is not consistent with Line 629.

A: I guess the reviewer was supposed to say, "Line 451 is not consistent with Line 629". Yes, the metamorphism is suggested to occur during 322 Ma to 297 Ma, so the deposition age of protoliths of the meta-sedimentary rocks can be roughly constrained between 425 and 322Ma. The crosscutting granite pluton dated at 320 ± 3 Ma (Song et al., 2018) provides additional evidence. We rephrased this sentence as follows: "The metamorphic ages at 322 Ma and 297 Ma provide a constraint on the minimum sedimentary age (see discussion below). Thus, the deposition of protoliths of the meta-sedimentary rocks may have occurred between 425 Ma and 322 Ma. The maximum deposition age is also defined by the crosscutting granite dated at 320 ± 3 Ma (Song et al., 2018)."

Line 549-550 it is not certain that the Central Tianshan Block is the source area for the early Paleozoic zircons of the meta-sediments in the Qincheng area. Line 570-572 the Central Tianshan Block is the most probable provenance area for the Precambrian detrital zircons in

the studied meta-sedimentary rocks. The zircons of Precambrian ages should be polycyclic. How about the morphology of these zircons?

A: Thanks for this suggestion and question. We fully agree that the Precambrian zircons are polycyclic. The Precambrian zircons mostly belong to type 1 and type 2, displaying complex texture with cores and rims (Figs. 5 and S1). Some of them even show more than one rim, which is solid evidence for polycyclic reworking. In order to better explain our interpretations, we added several sentences to discuss this point in the new version.

In addition, Line590-595 the North Tianshan was likely connected with the northern margin of the Central Tianshan Block before the Late Carboniferous…. This discussion should indicate the Central Tianshan Block might have sourced the early Paleozoic zircons. So line 549-550 need more consideration.

A: Thanks for this suggestion. We reconsidered this sentence and rephrased it as "According to the studies on ophiolites of the North Tianshan Suture zone and Kangguer belt (Xu et al., 2006a, 2006b; Chen et al., 2019), the North Tianshan (or Kangguer) Ocean opened during the mid-late Carboniferous. Considering that the Precambrian zircons most likely came from the Central Tianshan Block (see discussion below), it is possible that the Central Tianshan Block have also provided certain early Paleozoic detritus for the sediments in the Qincheng area."

3. Too many citations in some part, e.g. line 65, 128, 140…. Some representative references are enough.

A: You are right. We have checked and cited the most representative references only and deleted some references properly.

4. The English writing of this manuscript is fine, but small problems still exist. I am certain authors can correct after re-check the text.

A: Thanks a lot for this positive comment. We have re-checked the text and polished the English with the help of several colleagues good at English writing.

Reviewer #3: Comments on the paper by Xinghua Ni, Bo Wang et al.

This paper focuses on the Julideneng Formation of Carboniferous age in the Harlik Range of the North Tianshan Belt (NTB) in China. It includes plenty of U-Pb zircon age data conducted on the detrital zircons from the 4 parametamorphic rocks and igneous zircons from the 2 cross-cutting igneous (granitic) dikes. Based on the data obtained, the authors try to constrain the provenance, maximum and minimum depositional ages of the detrital zircons and then adapt a tectonic scenario for the evolution of the NTB (Harlik Range). Provenance of sediments is well constrained but depositional ages of detrital protoliths appear to need some more improvement. Also, a tectonic model can help understanding of the Pre-Carboniferous evolution of the Harlik region.

Thanks to Reviewer #3 for the encouraging opinion on our study. Yes, we tried to propose a carton model included in the revised manuscript to discuss the Paleozoic evolution of the study area and adjacent regions.

Comments keyed to the text

Line 23

I do not recommend using the term "Formation" for nomenclature of the metamorphic rocks, particularly those that lost their primary structures (e.g., bedding) during metamorphism. Instead, using of "Julideneng Metamorphic Complex" or "Julideneng Massif" is suggested.

A: Thank you so much for this meaningful suggestion. We agree that the use of “Julideneng Metamorphic Complex (JMC)” would be better on account of the high-grade yet relatively localized metamorphism. We have replaced it throughout the manuscript.

Except for the granitoids, the other units, which are shown in the legend of the map (Fig. 1c), are not defined clearly. It is noteworthy to identify whether they are metamorphic or sedimentary in origin.

A: According to references (e.g. XBMGR, 1993; Sun, 2007) and our own field investigations, most of rocks around the granitoids are sedimentary rocks and were locally deformed and metamorphosed up to greenschist facies. For example, middle Devonian strata that occur along the ridge of the Harlik Range were folded and locally reworked by shear zones, but the metamorphic grade of these rocks is very low.

We revised the text to clarify this point in the new version.

Lines 450-451

I recommend using "deposition of detrital protoliths of the meta-sedimentary rocks" instead "deposition of meta-sedimentary rocks".

A: Ok, it is rephrased as “the deposition of protoliths of the meta-sedimentary rocks”, and many thanks.

Lines 444-507

Based on the age data from a cutting granitoid at 320 Ma (Song et al., 2018), an inference reached is that 320 Ma is the minimum depositional age of the detrital protoliths of the metasedimentary rocks (line 451). This is not true. This age only provides a definite constraint on the minimum depositional age, not more. The minimum depositional age must be somewhat before the intrusion of the middle Carboniferous granitoids. Looking at the map

(Fig. 1c), it is shown that the post-collisional Carboniferous granitoids have the largest outcropping area totally after the other Carboniferous rocks. Such high-volumes of crustal melting in orogenic belts occur generally after delamination, which needs at least 30 Ma after the final closure of the Ocean (slab breakoff ~10-15 Ma, crustal thickening ~15 Ma and then delamination). Hence, it can be concluded that the deposition must be completed at least 30 Ma before the intrusion of the post-collisional granitoids, e.g., at 350 Ma (early Carboniferous) or somewhat before (late Devonian).

A: Thanks a lot for this very constructive comment and suggestion.

Yes, we strongly agree that the ages of crosscutting granitoids and migmatites only provide a minimum limit on the depositional age of protoliths of the meta-sedimentary rocks. The true depositional age should be older than the age of the metamorphism, migmatization and granitoids emplacement considering the processes of diagenesis of sediments, crustal thickening and uplifting related to orogeny, and large-scale crustal melting, such processes usually take several tens of million years, but it is difficult to precisely constrain up to now with the available methodologies.

Indeed, the post-collisional granitoids in some typical collisional orogenic belts, such as the Himalaya belt, formed 30 million years later after the collision began (e.g., Turner et al., 1996; Chung et al., 2005). However, in some accretionary orogenic belt, for example, the Newfoundland Appalachians, post-collisional magmatism occurred rapidly following arc-continent collision (<10 Ma; Whalen et al., 2006).

In adopting the reviewer's reasonable suggestion with great caution of un-constrainable time gap between the sedimentation and magmatic intrusion, we just use "Pre-late Carboniferous" (>322 Ma) as a minimum limit for the deposition timing of the protoliths of

meta-sedimentary rocks.

No clear distinction on the origin of migmatization has been presented (lines 468-497). One group of migmatites occur on a regional scale in the transition of high-grade metamorphism and anatexis at depths greater than 22-25 km where geothermal gradient is higher than 650 º C. Other group of migmatites can form in metamorphic rocks near large intrusions when some of the magma is injected into the neighbouring metamorphic rocks. It is unclear which one of these processes is the cause of migmatization?

A: We are happy to learn from this very thoughtful comment and we totally agree with the reviewer's opinion. In section 6.3, we had some discussions about the origins of migmatization, and in the revise manuscript, we added some sentences to further discuss the possible different mechanisms of the migmatization and associated metamorphism and magmatism.

According to Sun (2007) and our field observations, the garnet-sillimanite-bearing meta-sedimentary rocks are likely the protoliths of the migmatites and associated felsic melts (anatexis). The generally N-dipping foliations bearing ~NW-SE stretching lineation likely resulted from sinistral transtension (Sun, 2007). In addition, the HT-LP metamorphism and migmatization are coeval with the emplacement of high-K calc-alkaline undeformed granites (320-316 Ma) with positive whole-rock εNd(t) and zircon εHf(t) values, probably related to the intrusion of neighboring granitoids, both of which are diagnostic of decompression melting in an extensional setting (Song et al., 2018). Similarly, in the nearby Bogda Belt, Carboniferous (350-315 Ma) volcanic rocks are thought to have formed in an intra-arc (Zhang et al., 2017; Wali et al., 2018) or back-arc extensional setting (Chen et al., 2013; Xie et al., 2016b). Therefore, we consider that the meta-sedimentary rocks and migmatites are likely

parts of the Harlik arc root, and the migmatization probably occurred due to decompression partial melting in an intra-arc or back-arc extensional setting and intrusion of large volume magma (Line 601-611).

If migmatization occurred at 320 Ma, coeval with large plutonism, re-metamorphism (overprinting) and partly igneous crystallization of the previous metamorphic rocks (schists) in areas near large intrusions of granite seems likely. However, cross-cutting relationship of granites with migmatites strongly argues against this and implies that migmatization should have been concerned with regional metamorphism (lines 479). Hence, granite migmatization at 320 Ma through regional metamorphism seems unreasonably as it involves swift burial to the depths > 22 km and then denudation.

A: As replied above, the metamorphism and migmatization likely occurred at an intra-arc or back-arc extensional setting. Such an extensional setting allows for heat flow from asthenosphere, resulting in high thermal gradients, and consequent HT-LP metamorphism and partial melting of the crust in a shallow depth (e.g. Zheng and Chen, 2017). According to Zhao et al. (1997) and Zhou (2004), the temperature of the metamorphism is as high as 680℃, while the pressure of the metamorphism is about 0.23-0.4 Gpa responding to 9-15 km depth. Therefore, the partial melting of the supra-crustal rocks (similar phenomenon with anatexis) in an extensional setting with significant addition of heat by magmatism may do not need to bury these sedimentary rocks to a depth of >22 km. In addition, it is not certain that 320 Ma zircons came from granites. Alternatively, small-scale mid-Carboniferous felsic dykes may have been remelted/assimilated. Moreover, the magmatism could be a long-term process over several tens of million years, and the later (younger) granitoids could crosscut the early ones and metamorphic rocks.

In order to avoid confusions, we revised the text here to better explain this point, and many thanks for this important comment.

Lines 509-581

This section presents clear estimations on possible provenances of the detrital zircons. However, paleogeographic position of the basin (NTB) relative to the source areas providing sediments are not sufficiently depicted. Early Paleozoic (Ordovician to Silurian) sediments are considered to have been derived from the Harlik-Dananhu arc in the NTB. What is the position of the basin in relation to this arc?

A: It is true that we just discussed the possible provenances of the detrital zircons and did not precisely point out possible paleogeographic position of the sedimentary basin. In fact, based on the previous studies, we have proposed that the study area might have been an intra-arc basin between the Harlik arc (to the north of the study area) and the Dananhu arc (to the south of the study area) to receive sediments during the deposition of protoliths of the meta-sedimentary rocks (line 599-604). In the revised manuscript, following the suggestion of the reviewer, we propose a carton model in which the relative position of this sedimentary basin is shown in Fig. 11A.

Was this arc occurred due to the southward subduction of the Kalamaili Ocean or northward subduction of the Kangguer Ocean?

A: As written in line 143-150, the generation of the Harlik and Dananhu arcs is still under debate. Some geologists considered these arcs were generated by southward subduction of the Kalamaili Ocean (Yuan et al., 2010; Xie et al., 2016c), while some others proposed that the Harlik and Dananhu arcs were produced by the northward subduction of the North Tianshan (or Kangguer) Ocean (Li et al., 2006; Zhang et al., 2017, 2018; Du et al., 2018a; Han and

Zhao, 2018; Chen et al., 2019) or by the both (Xiao et al., 2004; Ma et al., 2015).

According to the available data (XBGMR, 1993), the Harlik and Dananhu arcs were active since Silurian up to late Carboniferous. However, the existence of Kangguer Ocean in early Paleozoic is not documented up to now. Thus, the early Paleozoic magmatic activities in the Harlik and Dananhu arcs most likely resulted from southward subduction of the Kalamaili Ocean which existed at least since Ordovician to Silurian.

Carboniferous N-MORB-like ophiolitic basalts were considered as the relics of the oceanic plate of the Kangguer Ocean (e.g., Chen et al., 2019). Thus, the Kangguer Ocean could have existed in Carboniferous. In addition, arc magmatism in the Dananhu Arc shows a general southward younging tendency (Xiao et al., 2004; Li et al., 2006; Zhang et al., 2018). Moreover, the Kalamaili Ocean was likely already closed in mid-Carboniferous. Therefore, we consider that the northward subduction of the Kangguer Ocean played a significant role in the formation of Dananhu and Harlik arc magmatism during the Carboniferous.

In the revised version, we added sentences to further discuss this point and provide a carton model to illustrate the evolution scenario related to the subduction of Kalamaili and Kangguer oceanic plates.

Also, Kangguer Ocean is placed to the south between the NTB and CTB. If so, when was this ocean opened?

A: As have replied for the last comment above, according to studies on ophiolitic basalts in the Kangguer belt (e.g., Chen et al., 2019), the Kangguer Ocean was likely open in mid-late Carboniferous. But the Kangguer belt was intensively reworked by a strike-slip shear zone (Wang et al., 2008, 2014a), and it is now difficult to recognize the ophiolitic rocks related to the Kangguer Ocean, its existence and duration remain unclear, and further studies are in

need.

Furthermore, there is not an obvious description how and when the Mesoproterozoic and Neoproterozoic components (zircons) transported from their provenance (CTB) to the basin (NTB) lying to the north of the Kangguer Ocean.

A: Thanks a lot for this important comment.

As mentioned in the revised manuscript and replied above, although there is no direct evidence for the timing and mechanism of opening of the Kangguer Ocean, the existing geochemical data of ophiolitic basalts in the Kangguer belt show SSZ-like signatures (e.g., Chen et al., 2019), indicating that the Kuangger Ocean was likely a back-arc basin probably due to southward subduction of the Kalamaili Ocean. Before its opening, the study area (intra-arc basin between the Dananhu and Harlik arcs in the North Tianshan Belt (NTB) was connected with the Central Tianshan Block (CTB). Thus, the Mesoproterozoic to Neoproterozoic detritus (including zircons) could be transported from the source area (CTB) northward to the sedimentary basin (NTB); they may have deposited directly in the basin before Carboniferous or might be recycled again later.

In the revised manuscript, we added sentences to further explain this possibility as “The Precambrian zircons in the meta-sedimentary rocks are anhedral in shape and show complex core-rim textures (Figs. 5 and S1), indicating that they were multiple-cycled. Thus, these Precambrian zircons were probably transported from the Central Tianshan Block to the North Tianshan Belt (Dananhu Arc) before the opening of the North Tianshan (or Kangguer) Ocean, and thereafter re-transported into the Harlik area. This is in agreement with the fact that zircon populations of Devonian flyschs in the Dananhu Arc are comparable with that of the Central Tianshan Block (Wang et al., 2019). However, due to uncertainty on their deposition age,

these zircons could have been transported directly from the Central Tianshan Block as well."

Line 596-599

If the granites cut the migmatites at 322 Ma, the migmatites should be older than this age. Also, taking the intrusion depths of the granites into account (<7 km), such shallow depths are not convenient for the migmatization concerning with the regional metamorphism.

A: Yes, we totally understand and agree with the reviewer's comment. However, in most migmatitic zone, only small-scale melts migrate along (sub-parallel to) the foliations of migmatite and/or restites. Once the melts aggregate to form larger magma body, they can ascend driven by buoyancy and crosscut the migmatite and country rocks (Sawyer, 1998). Logically, this kind of larger felsic magma form dykes and intrusion of which is certainly later than migmatization. But the processes of migration, aggregation and intrusion (crosscutting the migmatites) of a single pack of melts could occur in a relatively short period of time (Sawyer, 1994; Wang et al., 2014b) and the available zircon U-Pb method cannot recognize (within its errors) the relative different ages of migmatization (partial melting) and melt crystallization.

In addition, in a migmatization zone, granitic intrusions of different origins and different depths can co-exist, some granitic intrusions originated from great depths having nothing to do with the migmatization could intrude in the migmatites and country rocks, but this is not the topic of discussion in our manuscript.

Line 601-602

Regional migmatization and granitic magmatism can be coeval but do not display cross-cutting relationship due to the involvement of different depths for migmatization and granite emplacement.

A: As replied for the last comment above, according to the previous observations of Sayer (1998) and our studies in the migmatite zone (Wang et al., 2014b), granitic intrusions can crosscut the "coeval" migmatites, by saying that they are coeval because the available most reliable zircon U-Pb dating method cannot distinguish the ages of S-type granitic rocks from the timing of migmatization. Granitic magma can crosscut its source rocks (migmatites) via magma migration and associated cooling and crystallization.

Line 609-611

Above you mentioned that the Kangguer Ocean was closed in the Late Carboniferous. If so, this closure corresponds to the late orogenic extensional period.

A: Thanks for this comment. Yes, the closure of the Kangguer Ocean was usually supposed to occur at 320-300 Ma (Zhang et al., 2020). This period corresponds to the late (final) stage of orogenic processes of the Tianshan Belt. During the late Carboniferous, the Tianshan belt was located in an overall convergent regime, but due to the closure of the Kalamaili Ocean and the South Tianshan Ocean before ~320 Ma, the study area was also affected by post-orogenic extension while the Kangguer back-arc basin was in the process of closure. Thus, the migmatization at ~322 Ma could probably result from both the post-orogenic extension (related to the Kalamaili-East Junggar orogeny) and the back-arc or intra-arc extension during the closure of the Kangguer Ocean. We rephrased the sentences to better clarify this point.

A figure including cartoons on the tectonic evolution of the NTB and neighboring terranes can supply a substantial contribution to understanding of the early to middle Paleozoic events.

A: Thanks a lot for this thoughtful suggestion. We agree and tried to propose a carton model (Fig. 11) to show the tectonic evolution of the study area and adjacent regions on the basis of previous data and our own results.

Addition references:

Chen, X.J., Shu, L.S., Santosh, M., Zhao, X.X., 2013. Island arc bimodal magmatism in the eastern Tianshan Belt, Northwest China: Geochemistry, zircon U-Pb geochronology and implications for the Paleozoic crustal evolution in Central Asia. Lithos 168-169, 48-66.

Chen, Z.Y., Xiao, W.J., Windley, B.F., Schulmann, K., Mao, Q.G., Zhang, Z.Y., Zhang, J.E., Deng, C., Song, S.H., 2019. Composition, Provenance, and Tectonic Setting of the Southern Kangurtag Accretionary Complex in the Eastern Tianshan, NW China: Implications for the Late Paleozoic Evolution of the North Tianshan Ocean. Tectonics 38, 2779-2802.

Chung, S.L., Chu, M.F., Zhang, Y., Xie, Y., Lo, C.H., Lee, T.Y., Lan, C.Y., Li, X., Zhang, Q., Wang, Y., 2005. Tibetan tectonic evolution inferred from spatial and temporal variations in post-collisional magmatism. Earth Sci. Rev. 68, 173-196.

Corfu, F., Hanchar, J.M., Hoskin, P.W.O., Kinny, P., 2003. Altas of zircon textures. Rev. Mineral. Geochem. 53, 469-500.

Du, L., Long, X.P., Yuan, C., Zhang, Y.Y., Huang, Z.Y., Sun, M., Zhao, G.C., Xiao, W.J., 2018a. Early Paleozoic dioritic and granitic plutons in the Eastern Tianshan Orogenic Belt, NW China: Constraints on the initiation of a magmatic arc in the southern Central Asian Orogenic Belt. J. Asian Earth Sci. 153, 139-153.

Han, Y.G., Zhao, G.C., 2018. Final amalgamation of the Tianshan and Junggar orogenic collage in the southwestern Central Asian Orogenic Belt: Constraints on the closure of the Paleo-Asian Ocean. Earth Sci. Rev. 186, 129-152.

Hoskin, P.W., Schaltegger, U., 2003. The composition of zircon and igneous and metamorphic

petrogenesis. Rev. Mineral. Geochem. 53, 27-62.

Hoskin, P.W.O., 2005. Trace-element composition of hydrothermal zircon and the alteration of Hadean zircon from the Jack Hills, Australia. Geochim. Cosmochim. Acta 69, 637-648.

Li, J.Y., Wang, K.Z., Sun, G.H., Mo, S.G., Li, W.Q., Yang, T.N., Gao, L.M., 2006. Paleozoic active margin slices in the southern Turfan–Hami basin: geological records of subduction of the Paleo-Asian ocean plate in Central Asian regions. Acta Petrol. Sin. 22, 1087-1102 (in Chinese with English abstract).

Ma, X.H., Chen, B., Wang, C., Yan, X.L., 2015. Early Paleozoic subduction of the Paleo-Asian Ocean: Zircon U-Pb geochronological, geochemical and Sr-Nd isotopic evidence from the Harlik pluton, Xinjiang. Acta Petrol. Sin. 31, 89-104 (in Chinese with English abstract).

Sawyer, E.W., 1994. Melt segregation in the continental crust. Geology 22, 1019-1022.

Sawyer, E.W., 1998. Formation and evolution of granite magmas during crustal reworking: the significance of diatexites. J. Petrol. 39, 1147-1167.

Song, P., Tong, Y., Wang, T., Huang, H., Zhang, J.J., Huang, W., 2018. Zircon U-Pb ages, genetic evolution and geological significance of Carboniferous granites in the Harlik Mountain, East Tianshan, Xinjiang. Geol. Bullet. China 37, 790-804 (in Chinese with English abstract).

Sun, G.H., 2007. Structural deformation and tectonic evolution of Harlik Mountain, in Xinjiang since Paleozoic (in Chinese). Ph.D. thesis, Chinese Academy of Geological Science.

Turner, S., Arnaud, N., Liu, J., Rogers, N., Hawkesworth, C., Harris, N., Kelley, S., van Calsteren, P., Deng, W.-M., 1996. Post-collisional, shoshonitic volcanism on the Tibetan

plateau: implications for convective thinning of the lithosphere and the source of ocean island basalts. J. Petrol. 37, 45-71.

Wali, G., Wang, B., Cluzel, D., Zhong, L.L., 2018. Carboniferous-Early Permian magmatic evolution of the Bogda Range (Xinjiang, NW China): Implications for the Late Paleozoic accretionary tectonics of the SW Central Asian Orogenic Belt. J. Asian Earth Sci. 153, 238-251.

Wang, B., Cluzel, D., Jahn, B.M., Shu, L.S., Chen, Y., Zhai, Y.Z., Branquet, Y., Barbanson, L., Sizaret, S., 2014a. Late paleozoic pre- and syn-kinematic plutons of the Kangguer-Huangshan Shear zone: Inference on the tectonic evolution of the eastern Chinese north Tianshan. Am. J. Sci. 314, 43-79.

Wang, B., Liu, H.S., Shu, L.S., Jahn, B.M., Chung, S.L., Zhai, Y.Z., Liu, D.Y., 2014b. Early Neoproterozoic crustal evolution in northern Yili Block: insights from migmatite, orthogneiss and leucogranite of the Wenquan metamorphic complex in the NW Chinese Tianshan. Precambrian Res. 242, 58-81.Wang, G.C., Zhang, M., Feng, J.L., Liao, Q.A., Zhang, X.H., Kang, L., Guo, R.L., Xuan, Z.Y., Han, K.Y., 2019. New understanding of the tectonic framework and evolution during the Neoproterozoic-Paleozoic era in the East Tianshan Mountains. J. Geomech. 25, 798-819 (in Chinese with English abstract).

Wang, G.C., Zhang, M., Feng, J.L., Liao, Q.A., Zhang, X.H., Kang, L., Guo, R.L., Xuan, Z.Y., Han, K.Y., 2019. New understanding of the tectonic framework and evolution during the Neoproterozoic-Paleozoic era in the East Tianshan Mountains. J. Geomech. 25, 798-819 (in Chinese with English abstract).

Watson, E.B., Wark, D.A., Thomas, J.B., 2006. Crystallization thermometers for zircon and rutile. Contrib. Mineral. Petrol. 151, 413-433.

Whalen, J.B., McNicoll, V.J., van Staal, C.R., Lissenberg, C.J., Longstaffe, F.J., Jenner, G A., van Breeman, O. 2006. Spatial, temporal and geochemical characteristics of Silurian collision-zone magmatism, Newfoundland Appalachians: an example of a rapidly evolving magmatic system related to slab break-off. Lithos, 89, 377-404.

XBGMR (Xinjiang Bureau of Geology and Mineral Resources), 1993. Regional Geology of Xinjiang Uygur Autonomy Region. Geology Publishing House, Beijing, pp. 1-841 (in Chinese).

Xiao, W.J., Zhang, L.C., Qin, K.Z., Sun, S., Li, J.L., 2004. Paleozoic accretionary and collisional tectonics of the Eastern Tianshan (China): Implications for the continental growth of Central Asia. Am. J. Sci. 304, 370-395.

Xie, W., Xu, Y.G., Luo, Z.Y., Chen, Y.B., Hong, L.B., Ma, L., Ma, Q., 2016b. Petrogenesis and geochemistry of the Late Carboniferous rear-arc (or back-arc) pillow basaltic lava in the Bogda Mountains, Chinese North Tianshan. Lithos 244, 30-42.

Xie, W., Xu, Y.G., Luo, Z.Y., Liu, H.Q., Hong, L.B., Ma, L., 2016c. Petrogenesis and geodynamic implications of the Late Carboniferous felsic volcanics in the Bogda belt, Chinese Northern Tianshan. Gondwana Res. 39, 165-179.

Xu, X.Y., Li, X.M., Ma, Z.P., Xia, L.Q., Xia, Z.C., Peng, S.X., 2006a. LA-ICP-MS zircon U-Pb dating of gabbro from the Bayingou ophiolite in the northern Tianshan Mountains. Acta Geol. Sin. 80, 1168-1176 (in Chinese with English abstract).

Xu, X.Y., Xia, L.Q., Ma, Z.P., Wang, Y.B., Xia, Z.C., Li, X.M., Wang, L.S., 2006b. SHRIMP zircon U-Pb geochronology of the plagiogranites from Bayingou ophiolite in North Tianshan Mountains and the petrogenesis of the ophiolite. Acta Petrol. Sin. 22, 83-94 (in Chinese with English abstract).

Yuan, C., Sun, M., Wilde, S., Xiao, W.J., Xu, Y.G., Long, X.P., Zhao, G.C., 2010. Post-collisional plutons in the Balikun area, East Chinese Tianshan: Evolving magmatism in response to extension and slab break-off. Lithos 119, 269-288.

Zhang, Y.Y., Sun, M., Yuan, C., Long, X.P., Jiang, Y.D., Li, P.F., Huang, Z., Du, L., 2018. Alternating trench advance and retreat: Insights from Paleozoic magmatism in the eastern Tianshan, Central Asian Orogenic Belt. Tectonics 37, 2142-2164.

Zhang, Y.Y., Yuan, C., Long, X.P., Sun, M., Huang, Z.Y., Du, L., Wang, X.Y., 2017. Carboniferous bimodal volcanic rocks in the Eastern Tianshan, NW China: Evidence for arc rifting. Gondwana Res. 43, 92-106.

Zhang, Y.Y., Yuan, C., Sun, M., Long, X.P., Huang, Z.Y., Jiang, Y.D., Li, P.F., Du, L., 2020. Two late Carboniferous belts of Nb-enriched mafic magmatism in the Eastern Tianshan: Heterogeneous mantle sources and geodynamic implications. Geol. Soc. Am. Bull. 132, 1404-1418.

Zhao, K.D., Jiang, S.Y., Ling, H.F., Palmer, M.R., 2014. Reliability of LA-ICP-MS U-Pb dating of zircons with high U concentrations: A case study from the U-bearing Douzhashan Granite in South China. Chem. Geol. 389, 110-121.

Zhao, M., Shu, L.S., Wang, C.Y., 1997. Characteristics of metamorphism in the Harlik Metamorphic Belt, east Xinjiang, and its tectonic envorionment. Geol. J. China Univ. 3, 40-50 (in Chinese with English abstract).

Zheng, Y.F., Chen, R.X., 2017. Regional metamorphism at extreme conditions: implications for orogeny at convergent plate margins. J. Asian Earth Sci.145: 46-73.

Zhou, G.Q., 2004. The two-fold-contact metamorphic rocks occurring at Xiaopu, Hami, Eastern Xinjiang, their mineral paragenesis analysis and PTt path. Acta Mineral. Sin. 24,

290-300 (in Chinese with English abstract).

Late Paleozoic tectonic evolution of the North Tianshan Belt: New structural and geochronological constraints from meta-sedimentary rocks and migmatites in the Harlik Range

Xinghua Ni [a], Bo Wang [a, b, *], Dominique Cluzel [c], Jiashuo Liu [a], Zhiyuan He [a]

[a] *State Key Laboratory for Mineral Deposits Research, School of Earth Sciences and Engineering, Nanjing University, 210023 Nanjing, China*

[b] *Institute of continental geodynamics, Nanjing University, 210023 Nanjing, China*

[c] *Institut de Sciences Exactes et Appliquées, Université de la Nouvelle-Calédonie, BP R4, 98851 Noumea Cedex, New Caledonia*

* Corresponding author: (B. Wang)

Address: School of Earth Sciences and Engineering, Nanjing University, 163# Xianlin Avenue, Nanjing 210046, P.R. China

Email: bwang@nju.edu.cn; burh_cw@yahoo.com

Abstract

The North Tianshan Belt (NTB) formed by the subduction and accretion of the Junggar Ocean is a key area for reconstructing the Paleozoic tectonic evolution of the

21 southern Central Asian Orogenic Belt (CAOB). Despite numerous studies, the
22 interpretation of the late Paleozoic tectonic evolution of the NTB meets no consensus
23 yet. We conducted field investigations and LA-ICP-MS zircon U-Pb dating on
24 metamorphic rocks from the Julideneng Metamorphic Complex (JMC) in the Harlik
25 Range, which is located between the Turpan-Hami Basin to the south and the East
26 Junggar Belt to the north. The metamorphic rocks are exposed in a NW-SE striking,
27 ~10 km-wide belt and mainly composed of migmatites, garnet-sillimanite mica
28 schists, andalusite schists, and low-grade meta-sandstones. Detrital zircons from the
29 low-grade meta-sandstone yielded ages of 1400-1250, 1000-850, ~780, ~580, ~490,
30 ~445 and ~425 Ma. Three micaschists contain zircon populations of 2500-2175,
31 1800-1600, 1500-1100, 1000-850, 800-500, ~475, ~425, 420-380, ~346 Ma, and a
32 youngest age peak at ~322 Ma. Two samples of leucocratic dykes in migmatites
33 yielded comparable age populations with two major peaks at 322 Ma and 297 Ma,
34 which are interpreted as two stages of successive partial melting and anatectic melts
35 crystallization. On the basis of structural features, zircon textures and U-Pb ages,
36 combined with already published data, we propose that: (1) the meta-sedimentary
37 rocks of the JMC were deposited after 425 Ma and before 322 Ma (latest Silurian to
38 late Carboniferous); (2) the Precambrian detrital zircons in the meta-sedimentary
39 rocks were probably derived from the Central Tianshan Block, which was once
40 connected with the NTB; and (3) the migmatization and coeval granitic plutonism
41 occurred at ~322-297 Ma (late Carboniferous), most likely associated with crustal

thinning resulted from continent-based intra-arc or back-arc or post-orogenic extension.

Keywords: Central Asian Orogenic Belt; East Junggar; North Tianshan (Tien Shan); accretionary orogeny; post-orogenic crustal thinning; migmatization

1. Introduction

The Tianshan Orogen is located in the southernmost part of the Central Asia Orogenic Belt (CAOB), which is one of the largest Phanerozoic orogenic systems on the Earth (Şengör et al., 1993; Windley et al., 2007; Xiao et al., 2013; Safonova, 2017). It recorded the Paleozoic consumption of the southern Paleo-Asian Ocean domains (i.e., the Junggar-North Tianshan Ocean and Paleo-Tianshan Ocean or Turkestan Ocean), successive accretion of island arcs, accretionary wedges and microcontinents, as well as the final amalgamation/collision between the Kazakhstan and Tarim blocks (e.g., Gao et al., 1998, 2009; Li, 2004; Xiao et al., 2004, 2013; Charvet et al., 2007, 2011; Han et al., 2011; Wang et al., 2011a, 2018a). Deciphering the subduction-accretion processes of this belt is therefore helpful for a better understanding of the Paleozoic evolution of the southwestern CAOB and Phanerozoic Asia crustal growth (Han and Zhao, 2018; Huang et al., 2020).

Numerous studies on the Tianshan Orogen were conducted focusing on

kinematic analysis (e.g., Charvet et al., 2007, 2011; Lin et al., 2009; Wang et al., 2010), characteristics of ophiolites (e.g., Shu and Wang, 2003; Dong et al., 2006; Xu et al., 2006a, 2015a; Wang et al., 2011a, 2018a; Jiang et al., 2014), geochemistry of arc-related magmatic rocks (e.g., Chen et al., 2013; Xie et al., 2016a; Zhang et al., 2017; Wali et al., 2018) and post-collisional magmatism (e.g., Gu et al., 1999; Wang et al., 2009a, 2014a; Yuan et al., 2010; Chen et al., 2011; Muhtar et al., 2020). Based on these results, various tectonic models were proposed but no consensus has been achieved (e.g., Gao et al., 2009; Charvet et al., 2011; Xiao et al., 2013; Han and Zhao, 2018). The controversy arises over (1) the regional correlation of various magmatic arcs, and (2) the timing of the final amalgamation of the Tianshan Orogen. Late Paleozoic magmatic arcs were diversely correlated with the subduction of the South Tianshan Ocean, the Junggar-North Tianshan Ocean and the Kalamaili Ocean (e.g., Xiao et al., 2004, 2013; Charvet et al., 2007, 2011; Han and Zhao, 2018). The termination of accretion was controversially estimated to be Devonian-early Carboniferous (Xia et al., 2002, 2012; Ma et al., 2015), late Carboniferous-early Permian (Gao et al., 1998, 2009; Charvet et al., 2007, 2011; Han et al., 2010, 2011; Wang et al., 2014a; Han and Zhao, 2018), or end-Permian to mid-Triassic (Xiao et al., 2009; Chen et al., 2020).

The Harlik Range is the northeastern part of the Tianshan Orogen where the latter connects with the East Junggar Belt. It is a key area for unraveling the tectonic evolution of the Tianshan Orogen (Xiao et al., 2004; Huang et al., 2018). The tectonic

setting and evolution of the Harlik Range remain a matter of debate. Xia et al. (2002, 2012) proposed that it underwent intra-continental rifting in Carboniferous to Permian time; while some other authors suggested a volcanic arc setting during the Ordovician-Carboniferous (Xiao et al., 2004; Han and Zhao, 2018). Additionally, Sun (2007) proposed that it experienced an Ordovician-Silurian arc and a Devonian-Carboniferous back-arc extension.

Meta-sedimentary rocks and migmatites are well exposed in the southern Harlik Range (Fig. 2b), they may provide key evidence for the Paleozoic tectonic evolution of the North Tianshan Belt. However, these metamorphic rocks were poorly studied. They were ever considered as late Carboniferous in age (XBGMR, 1966; Sun et al., 2007a), but the depositional ages of their protoliths were not well constrained (Cao et al., 2009). Furthermore, the timing and tectonic setting of the metamorphism were diversely interpreted as (i) two-stage regional metamorphism associated with Carboniferous intra-arc rifting and Permian collision (Zhao et al., 1997); (ii) contact metamorphism during the Carboniferous and Permian magmatism (Zhou et al., 2004); or (iii) Permian dynamic metamorphism during post-collisional extension (Sun, 2007).

In this study, we present new field structural observations and zircon LA-ICP-MS U-Pb ages of the meta-sedimentary rocks and migmatites from the Harlik Range. These new results combined with previously published data allow us to better constrain the timing of protoliths deposition and metamorphism of these

meta-sedimentary rocks, to discuss the provenances of the sediments, and to tentatively replace the high-temperature metamorphism and anatexis in the framework of the late Paleozoic tectonic evolution of the North Tianshan Belt.

2. Geological background

2.1. *Regional tectonic framework*

The Chinese segment of the Tianshan Orogen is geographically divided into eastern and western parts along the Urumqi-Korla line. The eastern Chinese Tianshan is further divided into three tectonic units as the South Tianshan, Central Tianshan and North Tianshan belts (Fig. 1b; Xiao et al., 2004; Li et al., 2006; Charvet et al., 2007). These units are separated from each other by two major faults (namely the Main Tianshan Shear Zone and Baluntai-Xingxingxia Fault), which are dextral strike-slip faults active mainly during the Permian along reactivated older suture zones (Laurent-Charvet et al., 2003; Charvet et al., 2007; Wang et al., 2008, 2014a; de Jong et al., 2009; He et al., 2021).

The South Tianshan Belt (STB) is connected with the northern margin of the Tarim Block and mainly consists of ophiolitic mélanges and Cambrian to Carboniferous sedimentary and volcanic rocks (XBGMR, 1993). These rocks are locally metamorphosed and imbricated within several thrust-and-fault belts (Charvet et al., 2011). The western STB was formed by the amalgamation of the Tarim Block

and the Central Tianshan Belt following the closure of the South Tianshan Ocean and several back-arc basins (Gao et al., 1998, 2009; Xiao et al., 2004; Han et al., 2011; Wang et al., 2011a, 2018a; Huang et al., 2018; Zhong et al., 2019). In contrast, the eastern STB (also named the Beishan Belt) was formed by the accretion of several Precambrian-based magmatic-arc terranes (Yuan et al., 2015; Yu et al., 2016; Zong et al., 2017; He et al., 2018a) and ophiolitic mélanges during the Paleozoic (Xiao et al., 2010; Ao et al., 2012; Song et al., 2015; Shi et al., 2018).

The Central Tianshan Belt (CTB) is composed of a Precambrian basement (Hu et al., 2000, 2010; Liu et al., 2004; Ma et al., 2012b; He et al., 2014; Wang et al., 2017; Han and Zhao, 2018; Huang et al., 2019), Ordovician to early Devonian arc-related volcanic and sedimentary sequences, and Paleozoic intrusive rocks (Xiao et al., 2004, 2013; Shi et al., 2007; Lei et al., 2011; Ma et al., 2013; Zhong et al., 2015; Han and Zhao, 2018; He et al., 2018b). Both the basement and arc-type rocks are unconformably overlain by unmetamorphosed Carboniferous to Permian sediments (XBGMR, 1993). The CTB is considered either as an independent Precambrian micro-continent involved in the accretion of the Tianshan Orogen (Hu et al., 2000; Huang et al., 2015, 2017) or as a part of the northern Tarim, which was drifted off and then re-amalgamated with Tarim due to the opening and closure of the South Tianshan back-arc basins (Charvet et al., 2007; Lei et al., 2011; Ma et al., 2014; Gao et al., 2015; Zhong et al., 2017).

The North Tianshan Belt (NTB) refers to the domain between the CTB to the

144 south and the East Junggar Belt to the north (Fig. 1b). This belt is predominantly
145 composed of Ordovician to Carboniferous volcano-sedimentary sequences crosscut by
146 Paleozoic granitoids (XBGMR, 1993). It is considered as a Paleozoic arc system
147 formed by southward subduction of the Kalamaili Ocean (Xiao et al., 2004; Yuan et
148 al., 2010; Xie et al., 2016c), and/or by northward subduction of the North Tianshan
149 Ocean (Ma et al., 2015; Zhang et al., 2018; Du et al., 2018a; Han and Zhao, 2018;
150 Chen et al., 2019). The NTB is further divided into three sub-units, i.e., the
151 Harlik-Dananhu Arc, Bogda Arc and Kangguer-Yamansu Arc (e.g., Xiao et al., 2004)
152 unconformably covered by the Mesozoic-Cenozoic Turpan-Hami Basin (Fig. 1b;
153 XBGMR, 1993).

154 The Harlik-Dananhu Arc occurs on both north and south sides of the
155 Turpan-Hami Basin, either formed by the breakup of a single arc due to intra-arc
156 rifting (Xiao et al., 2004; Ma et al., 2015) or resulted from southward migration of the
157 magmatic front that generated the Harlik and Dananhu arcs successively (Sun, 2007).
158 The Bogda Arc is generally interpreted as a Carboniferous magmatic arc and Permian
159 post-collisional magmatic belt (Shu et al., 2011; Chen et al., 2011; Xie et al., 2016a;
160 Wali et al., 2018), although some authors suggested a Carboniferous to Permian rift
161 (Gu et al., 2000, 2001; Xia et al., 2008, 2012). The Kangguer-Yamansu Arc is a late
162 Paleozoic arc/fore-arc system (Xiao et al., 2004; Han and Zhao, 2018) reworked by
163 Permian intracontinental dextral ductile shear zone (Wang et al., 2008, 2014a;
164 Branquet et al., 2012; Zhu et al., 2019).

2.2. Geological background of the Harlik Range

The Harlik Range (or Harlik Arc) is situated between the Turpan-Hami Basin to the south and the East Junggar Belt to the north (Fig. 1b). The oldest stratigraphic unit is the Ordovician Huangcaopo Group, which occurs along the northern foot of the Harlik Range. It mainly consists of weakly metamorphosed marine clastic rocks and tuffs (Ma et al., 1997; Chen et al., 2014). The Silurian strata are barely exposed in the Harlik Range (XBMGR, 1993; Sun, 2007). Ordovician-Silurian (470-420 Ma) intrusions in the Harlik Range mostly belong to calc-alkaline or tholeiitic series and show typical subduction-related geochemical features associated with mantle-like whole-rock $\varepsilon_{Nd}(t)$ and zircon $\varepsilon_{Hf}(t)$ values (Ma et al., 2015; Wang et al., 2016, 2018b; Du et al., 2018a; Han and Zhao, 2018).

The Devonian strata, according to regional facies correlation, are mainly composed of volcanic rocks, carbonates and siliciclastic rocks (XBGMR, 1993). The Lower Devonian Dananhu Formation is distributed along the southern Harlik Range and the southern margin of the Turpan-Hami Basin (Fig. 1c). The Middle Devonian Tousuquan Formation is recognized along the ridge of the Harlik Range. Some rhyolites from this formation, however, yielded zircon U-Pb ages of 469 ± 9 Ma (Li et al., 2017) and were intruded by granitoids dated at 446 ± 3 Ma to 448 ± 7 Ma (Cao et al., 2006; Liu et al., 2017), indicating that some rocks in the Tousuquan Formation should be assigned to the Ordovician. Meanwhile, Upper Devonian sediments are rare

in the Harlik Range and thus were poorly investigated.

The Carboniferous strata can be divided into lower and upper units. The lower unit includes the Jiangbasitao and Xiaorequanzi formations, which mainly consist of volcaniclastic and volcanic rocks (XBMGR, 1993). The upper unit, previously named as Julideneng Formation, is distributed along the southern foot of the Harlik Range and is mainly composed of tuffs, sandstones and tuffaceous sandstones (Sun, 2007). However, to the north of the Qincheng Town, some of these rocks were metamorphosed into greenschist to amphibolite facies (Zhao et al., 1997; Zhou, 2004; Sun, 2007) and their protoliths ages and timing of metamorphism remain unclear. In this study, we separate these metamorphic rocks from the Julideneng Formation and call them as the Julideneng metamorphic complex (JMC). The Carboniferous calc-alkaline diorites and granites from the Harlik Range were formed at 320-300 Ma. These granitoids were likely emplaced during the tectonic transition from convergence to extension (Sun et al., 2005; Song et al., 2018; Zhu et al., 2018).

The Lower Permian strata, unconformably overlying the pre-Permian rocks, are mainly composed of terrestrial conglomerates, sandstones and siltstones intercalated with volcanic rocks (Sun, 2007; Shu et al., 2011; Chen et al., 2014). The Permian granitoids are transitional from calc-alkaline to alkaline and yielded zircon U-Pb ages of 298-280 Ma (Wang et al., 2009c; Yuan et al., 2010; Chen et al., 2016). They are usually associated with coeval mafic dykes, both were formed in an extensional or transtensional setting (Gu et al., 1999; Wang et al., 2009c; Yuan et al., 2010; Chen et

al., 2016).

3. Field geology and sample descriptions

Our field investigations were conducted along a section from Qincheng Town to Xiaopu Village, southern Harlik Range (Fig. 2a-b). The southern part of the section is dominated by schistose tuffs, sandstones and tuffaceous sandstones belonging to the Upper Carboniferous Julideneng Formation. The northern part of this section consists of middle Devonian sandstones, tuffaceous sandstones and limestones, which were silicified and crosscut by numerous diabase dykes showing NE-SW or nearly E-W strikes (Fig. 2b; XBGMR, 1966; Sun, 2007). The central part is a NW-SE-striking belt of >30 km long and ~10 km wide (Fig. 2a-b; Zhao et al., 1997, 2002; Sun, 2007), this belt is made of metamorphic rocks of the Julideneng metamorphic complex (JMC), including low-grade meta-sandstones, andalusite schists, garnet-sillimanite micaschists and migmatites (Zhao et al., 1997; Zhou, 2004; Sun, 2007).

In the southern part of the JMC, the sedimentary rocks were weakly deformed and slightly metamorphosed. The bedding (S0) can be easily recognized and cleavage (S1) is well developed, both dip to the northeast with S1 steeper than S0 (Figs. 2b-c and 3a), indicating a normal sequence. Further northwards, S0 is gradually transposed into sub-vertical schistosity with increasing metamorphic grade (Sun, 2007). A migmatite zone of ~1 km wide occurs in the northern part of the JMC. Migmatites are typically flow-folded (Sawyer, 2008) and contain centimeter-thick, garnet-bearing

leucocratic dykes. They display all the intermediates between folded and boudinaged leucosome ribbons, foliated (orthogneissic) sills and slightly foliated crosscutting dykes. Leucosomes are surrounded by melanosomes with biotite-rich boundaries and restites of meta-sandstone (Fig. 3b). Foliation in the migmatites is roughly in accordance with that in the surrounding meta-sedimentary rocks (Fig. 3c). Flow-folded migmatites and slightly folded small-scale garnet-bearing leucocratic dykes (Fig. 3b and 3d) indicate a continuum from pre- to late-tectonic in situ partial melting and short-distance transport of anatectic melts. A progressive lateral change from quartzites, schists and crinoidal limestone into migmatites can be observed to the west of the main road, and restites of quartzite and limestone (changed into calc-silicate) locally occur in migmatites.

The southwestern border of the migmatite zone is in fault contact with weakly deformed meta-sandstones (Figs. 2c and 3e). The fault zone, ~5-10 meters in width, was strongly sheared with schistosity/cleavage dipping 70-75° to the south. Considering the difference in metamorphic grade, there was probably a bulk normal-fault motion (Fig. 2c). In addition, the complex deformation of the fault zone likely suggests a polyphase motion. The northern side of the migmatite zone was crosscut by a coarse-grained K-feldspar granite dated at 297 ± 2 Ma (zircon U-Pb age; Chen and Shu, 2010). To the north, the granite is in fault contact with low-grade meta-sedimentary rocks of the Middle Devonian Tousuquan Formation (Fig. 2b-c). The boundary is an E-W-striking mylonite zone dipping steeply to the north, which

247 bears a down-dip stretching lineation. Kinematic indicators in ductilely deformed
248 granites are consistent with a normal-fault motion. Therefore, the high-grade
249 migmatite zone appears in a kind of horst or pop-up structure surrounded by
250 lower-grade meta-sedimentary rocks. Late Carboniferous-early Permian (zircon U-Pb
251 ages of 316-295 Ma) undeformed granodiorite, biotite granite, leucogranite as well as
252 numerous NE-striking pegmatite and mafic dykes crosscut and thus post-date the
253 metamorphic belt (Wang et al., 2009c; Chen and Shu., 2010; Song et al., 2018; Zhu et
254 al., 2018). In addition, the meta-sedimentary rocks yielded Early Permian muscovite
255 and biotite $^{40}Ar/^{39}Ar$ cooling ages ranging from 301 to 277 Ma (Sun, 2007).

256 In order to constrain the age and provenance of the meta-sedimentary rocks,
257 and the timing of the migmatization, six representative samples were collected from
258 the JMC. Three micaschist samples (12TS119A, B, E) were taken from the migmatite
259 zone (Fig. 2c). The sample 12TS119A is composed of quartz (45-50 vol. %), biotite
260 (20-25 vol. %), plagioclase (10-15 vol. %), muscovite (5-10 vol. %) and a small
261 amount of sillimanite. The sample 12TS119B is a mylonitized micaschist and mainly
262 consists of quartz (30-35 vol. %), biotite (20-25 vol. %), muscovite (30-35 vol. %)
263 and plagioclase (5-10 vol. %). Another slightly altered sample 12TS119E is composed
264 of quartz (30-35 vol. %), chloritized biotite (20-25 vol. %), muscovite (10-15 vol. %),
265 sericite (20-25 vol. %) and minor sillimanite (< 5 vol. %). In these micaschists, the
266 preferred orientation of biotite and/or muscovite and elongated quartz grains define
267 well-developed foliations (Fig. 4a-c).

One sample (12TS119F; Fig. 2c) was collected from the meta-sandstones that are in fault contact with the migmatites (Fig. 3e). This meta-sandstone is mainly composed of quartz (60-70 vol. %), chloritized mica (10-15 vol. %) and plagioclase (15-20 vol. %). The chloritized micas are weakly oriented and define an almost unnoticeable foliation due to the fine-grain and equidimensional shape of quartz and plagioclase (Fig. 4d). Undulose extinction and bulging dynamic recrystallization of quartz (Fig. 4a-d) indicate ductile deformation of these meta-sedimentary rocks under moderate temperature conditions.

Two samples were taken from migmatitic gneissic-granite (12TS119G) and migmatite leucosome (12TS119H) (Fig. 3d). Both of them are mainly composed of quartz (40-45 vol. %), K-feldspar (25-30 vol. %), plagioclase (20-25 vol. %) and minor muscovite and biotite (Fig. 4e-f). The migmatitic gneissic-granite shows a clear foliation defined by the preferred orientation of micas and elongated quartz ribbons (Fig. 3c). The feldspar and quartz exhibit lattice bending, subgrains, undulose extinction and deformation bands, suggesting that these grains accommodated intracrystalline plastic deformation by dislocation creep (Fig. 4e; Gower and Simpson, 1992; Hirth and Tullis, 1992; Passchier and Trouw, 2005). In addition, typical chessboard subgrains in quartz and lobate grain boundaries between quartz and feldspar indicate high-temperature ductile deformation (Gower and Simpson, 1992; Kruhl, 1996; Stipp et al., 2002). By contrast, the migmatite leucosome (12TS119H) shows nearly equant and diamond-shaped quartz crystals enclosed by optically

289 continuous K-feldspar (Fig. 4f), indicating that quartz crystallized from anatectic
290 melts before K-feldspar crystallized from the remaining melts (Sawyer, 2008).
291 Undulose extinction and recrystallization by grain boundary migration of quartz (Fig.
292 4f) suggest localized high-temperature ductile deformation.

293 ## 4. **Analytical methods**

294 All samples were crushed and milled into powders, from which zircon grains
295 were separated by heavy liquid and magnetic separation, and finally handpicked under
296 a binocular microscope fitted with a UV light. Selected zircon grains were mounted in
297 epoxy, polished to about half of their thickness, and then coated with gold.
298 Cathodoluminescence (CL) images of zircons were obtained at the State Key
299 Laboratory for Mineral Deposits Research (SKL-MDR), Nanjing University, using a
300 Quanta 400 FEG scanning electron microscope equipped with a Gatan mini-CL
301 detector (Mono CL3+).

302 U-Pb dating and trace elements analysis of representative zircons were
303 conducted in two laboratories. The samples 12TS119A and 12TS119B were dated at
304 the SKL-MDR of Nanjing University using Agilent 7500a inductively coupled plasma
305 mass spectrometry (ICP-MS) coupled to a New Wave 193 nm laser ablation system
306 with an in-house sample cell. The detailed analytical procedures are similar to those
307 described in Jackson et al. (2004) and Liu et al. (2014). The U-Pb dating and trace
308 elements analyses of zircons from samples 12TS119E, 12TS119F, 12TS119G and

12TS119H were carried out at the State Key Laboratory of Geological Processes and Mineral Resources, China University of Geosciences (Wuhan), where laser sampling was performed using a GeoLas 2005 System and an Agilent 7500a ICP-MS instrument was used to acquire ion-signal intensities. The detailed operating conditions and analytical procedures are described in Liu et al. (2008, 2010a, 2010b).

For zircon crystals older than 1000 Ma, $^{207}Pb/^{206}Pb$ apparent ages were used to plot relative probability diagrams considering large amounts of radiogenic Pb. For zircon grains younger than 1000 Ma, $^{206}Pb/^{238}U$ apparent ages are more reliable due to the low content of radiogenic Pb and low uncertainty of common Pb correction. Uncertainties are quoted at 1σ for individual analysis and 2σ (with 95% confidence level) for weighted mean ages, respectively. The results of U-Pb isotopic dating and trace element compositions are listed in Supplementary Table S1 and Table S2, respectively.

5. Results

5.1. Meta-sandstone

A total of 55 zircon grains were chosen for U-Pb dating from the weakly metamorphosed sandstone sample 12TS119F. The CL images of all dated zircons together with their ages are shown in Supplementary Fig. S1 and those of the representative grains are presented in Fig. 5a. Most zircons have euhedral to

sub-euhedral shapes and show clear oscillatory zoning without or with narrow dark rims, indicating original magmatic sources (Connelly, 2000; Corfu et al., 2003; Hoskin and Schaltegger, 2003). A small group of zircons show stubby or sub-rounded shapes and have complex core-rim textures, comprising irregular cores with blurry or patchy zoning and structureless rims. This kind of zircons may have been produced by modification of primary igneous zircons in response to metamorphism (Corfu et al., 2003; Hoskin and Schaltegger, 2003; Rubatto, 2017). The rest few zircons are rounded and sector zoned or without zoning, indicative of metamorphic origin (Figs. 5a and S1; Corfu et al., 2003; Hoskin and Schaltegger, 2003).

Forty-five out of fifty-five grains yielded concordant ages, a large majority of which have ages < 540 Ma, with two major age peaks at 425 Ma (n = 14; 31.1%) and 445 Ma (n = 10; 22.2%), as well as a minor age peak at ca. 490 Ma. The Precambrian zircons show sub-peaks at ~580 Ma, ~780 Ma, and in a range of 850-1000 Ma; only two Mesoproterozoic grains (1280 Ma and 1372 Ma) were identified (Fig. 6a-b; Table S1). The remaining ten analyses yielded discordant ages (Fig. 6a) probably due to Pb loss or disequilibrium of their isotopic systems (Connelly, 2000).

Twenty-three zircons with ages around 445-425 Ma were analyzed for rare earth element (REE) compositions. Most grains are characterized by steeply-rising REE patterns with remarkable positive Ce and negative Eu anomalies (Fig. 7a), together with high Th/U ratios (mostly > 0.4) (Fig. 6b; Table S1), generally consistent with typical magmatic zircons (Hoskin and Schaltegger, 2003; Rubatto, 2017). Only two

zircons (Nos. 38 and 51) display relatively higher LREE values and weaker Ce anomalies in comparison to the other zircons, and their REE patterns (Fig. 7a) are similar to those of hydrothermal zircons (Hoskin, 2005).

5.2. Micaschists

From three micaschist samples, a total of 192 zircon grains were analyzed, which show various sizes, sub-rounded to sub-euhedral shapes and complicated internal textures (Figs. 5 and S1). According to their CL images, four types of zircons can be recognized. (1) Type 1 zircons have core-rim textures in which the cores are bright with oscillatory zoning and the rims are relatively dark and un-zoned, corresponding to originally magmatic zircons surrounded by metamorphic overgrowths (Hoskin and Schaltegger, 2003). (2) Type 2 zircons also show core-rim textures with bright un-zoned cores, which could be originally metamorphic then subjected to secondary metamorphic or hydrothermal overgrowth. Alternatively, they could also be originally magmatic but were intensively "reworked" (via solid-state recrystallization or local dissolution-reprecipitation) by the subsequent metamorphism or alteration so that the original magmatic oscillatory zoning was totally erased. In the latter case, the overgrowth rims may have formed synchronously with the reworking of the cores or even reflect a later metamorphic and/or hydrothermal event (Hoskin and Schaltegger, 2003). (3) Type 3 zircons have homogeneous dark to black CL images without visible oscillatory zoning, likely formed by metamorphism or hydrothermal activities

(Connelly, 2000; Corfu et al., 2003; Hoskin and Schaltegger, 2003). (4) Type 4 zircons are characterized by prismatic shapes and moderately bright CL images with clearly concentric magmatic oscillatory zoning, without visible overgrowths.

In order to obtain sufficiently representative zircon populations, all four types of zircons from each sample were analyzed. Most analyses plot on or close to the Concordia, but a few zircons show remarkable discordance, especially for the sample 12TS119E (Fig. 6c, e and g). One reason for discordant ages can be Pb loss due to metamorphic or hydrothermal alteration. In addition, analytical mixing between two parts of zircons with different origins (e.g., older cores and younger rims) is also highly possible as some of the discordant zircons with core-rim texture are quite small (Fig. S1). The geological meaning of the discordant ages is ambiguous; therefore, they are excluded from further discussion and only concordant ages (concordance > 90%) are considered.

For the micaschist sample 12TS119A, fifty-eight out of sixty dated zircons yielded concordant ages (Fig. 6c) ranging from 313 to 2175 Ma. They show a dominant age peak at 477 Ma (n = 19; 32.8%), two younger age peaks at 322 Ma (n = 4; 6.9%) and 414 Ma (n = 4; 6.9%), and other populations of 500-550, 600-750, 850-1000,1100-1500, 1600-1800 and 2175 Ma (Fig. 6d). The youngest nine ages (peaked at 322 and 414 Ma) (Fig. 6d; Table S1) are obtained exclusively from type 2 zircons with Th/U ratios mostly lower than or near 0.4 (Table S1; Fig. 6d), showing bright or dark cores characterized by surface-controlled alteration (Corfu et al., 2003)

and encircled by thin and dark rims (Figs. 5b and S1). Zircons defining the major age peak of 477 Ma mainly belong to the type 1 and type 2, and show Th/U ratios higher than 0.4 (Table S1; Figs. 5b, 6d and S1). The other older zircons cover types 1 and 2, and have variable Th/U ratios mostly higher than 0.4 (Figs. 6d and S1).

Sixty zircons were dated for the micaschist sample 12TS119B and all of them yielded concordant ages (Fig. 6e). Their age populations are very similar to those of the sample 12TS119A (Fig. 6f). Therein, three youngest zircons (380-413 Ma) belong to the type 3 displaying homogeneous dark to black CL images (Figs. 5c and S1) and Th/U ratios around 0.4 (Table S1; Fig. 6f). Twenty zircons (33.3%) of type 1 and minor type 2 and type 4 (Figs. 5c and S1) define an age peak at 477 Ma and show Th/U ratios mostly higher than 0.4 (Fig. 6f; Table S1). Other ages around 500-550, 600-750, 850-1000, 1100-1500, 1600-1800 and 2200-2500 Ma (Fig. 6f) were obtained from zircons of all four types, most of which show Th/U ratios higher than 0.4 (Table S1).

As for the sample 12TS119E, sixty-one out of seventy-two zircons provided concordant ages ranging from 346 to 1765 Ma (Fig. 6g-6h). A major age peak at 475 Ma (n = 11; 18.0%) and a minor age peak at 425 Ma (n = 5; 8.2%) are mainly defined by types 1 and 2 zircons (Figs. 5d and S1), which mostly show Th/U ratios higher than 0.4 (Fig. 6h; Table S1). These zircons show steeply-rising REE patterns, remarkable positive Ce anomalies and negative Eu anomalies (Fig. 7b). Thus, these ages are indicative of magmatic events (Hoskin and Schaltegger, 2003; Hoskin, 2005).

411 One exceptional zircon (No. 57; ~424 Ma) shows a quite high Th/U ratio (2.93; Table
412 S1). For some unclear reasons, a V-shaped REE pattern due to its high LREE content
413 is similar to that of some "hydrothermal" zircons (Fig. 7b). Five zircons of types 2
414 and 3 with dark, homogenous CL images (Figs. 5d and S1) yielded ages from 346 to
415 402 Ma, they display gently-rising REE patterns with weak Ce anomalies and Th/U
416 ratios mostly lower than 0.4 (Figs. 6h and 7b), similar to zircons of hydrothermal
417 origin (Fig. 7b). With only a few exceptions, the other age populations (500-550,
418 600-800, 850-1000, 1100-1400 and 1600-1800 Ma) correspond to all four zircon
419 types (Fig. 6g-6h) with Th/U ratios mostly higher than 0.4 (Fig. 6h; Table S1).

420 *5.3. Migmatites*

421 For two migmatite samples, a total of 38 analyses were conducted on 36 zircons.
422 Their CL images and ages are shown in Fig. 8. Almost all the dated zircons are
423 euhedral to sub-euhedral with prismatic shapes, they have clear oscillatory zoning
424 (Fig. 8) and their Th/U ratios are mostly higher than or close to 0.4 (Table S1),
425 suggesting a magmatic origin.

426 Out of twenty analyses on zircons from the migmatitic gneissic-granite
427 12TS119G, thirteen concordant ages form two age peaks at 297.4 ± 2.1 Ma (n = 8;
428 61.5%; MSWD = 0.26) and 322.2 ± 2.3 Ma (n = 5; 38.5%; MSWD = 0.066) (Fig. 8c
429 and 8e). Seven zircons yielded discordant ages (Fig. 8c; Table S1) that are not
430 considered in the following discussion.

Eighteen zircons were dated for the migmatite leucosome sample 12TS119H and fifteen analyses yielded concordant ages (Fig. 8d), defining comparable two age groups of 297.1 ± 2.7 Ma (n = 4; 26.7%; MSWD = 0.13) and 322.5 ± 2.1 Ma (n = 8; 53.3%; MSWD = 0.13) (Fig. 8f). Three zircons (Nos. 6, 10 and 16) yielded older and probably inherited ages of 338-365 Ma (Fig. 8d). The remaining three zircons (Nos. 2, 5 and 15) with discordant ages have been rejected.

The dated concordant zircons from these two samples were further analyzed for REE compositions. The results show steeply-rising Chondrite-normalized REE patterns characterized by enrichment of HREE relative to LREE, mostly positive Ce anomalies and negative Eu anomalies (Fig. 7c and 7d), in accord with an igneous origin. Only two zircons (Nos. 15 and 16) in sample 12TS119G have slightly different REE patterns with relatively higher LREE values and weaker Ce anomalies than typical magmatic zircons (Fig. 7c).

6. Discussion

6.1. Protoliths depositional and metamorphic ages of the meta-sedimentary rocks

The most remarkable age population of detrital zircons from the meta-sandstone and micaschists lies in the 540-420 Ma interval. The micaschists have dominant peaks of 477-475 Ma, while the meta-sandstone shows a peak at 425 Ma that resembles a minor peak of the micaschist 12TS119E (Fig. 6). Since these detrital zircons are

mostly of magmatic origins, their ages constrain the maximum depositional ages for the protoliths of meta-sedimentary rocks. The metamorphic ages at 322 Ma and 297 Ma provide a constraint on the minimum sedimentary age (see discussion below). Thus, the deposition of protoliths of the meta-sedimentary rocks may have occurred between 425 Ma and 322 Ma. The maximum deposition age is also defined as >320 Ma by the crosscutting granite dated at 320 ± 3 Ma (Song et al., 2018).

Zircons of ~480-420 Ma from sillimanite micaschists generally exhibit dark rims, whereas detrital zircons of ~425 Ma from the meta-sandstone usually show no overgrowth (Figs. 5 and S1). This indicates that zircons from high-grade micaschists were significantly reworked by metamorphism, in contrast to the low-grade meta-sandstone. Such reworking may also account for the occurrence of discordant detrital zircons in the meta-sedimentary rocks (Fig. 6), most likely due to incomplete metamorphic reset.

The youngest zircon group (~420-320 Ma) from the micaschists, displaying diagnostic features of metamorphic and/or hydrothermal zircons, has no equivalent in the meta-sandstone. Therefore, the younger ages suggest partial or total overprint during amphibolite facies metamorphism, although it cannot be excluded that some of them were originally (pre-sedimentation) metamorphic. The metamorphism likely occurred at ~322 Ma, which is the youngest age peak of metamorphic zircons. The older ages (420-322 Ma) possibly resulted from age mixing between primary cores and recrystallized areas or overgrowths (Corfu et al., 2003).

The two migmatite samples yielded exactly identical age peaks at 322 Ma and 297 Ma (Fig. 8). Both zircon groups show clear concentric oscillatory zonings, high Th/U ratios and steeply-rising REE patterns, indicative of magmatic origin (Fig. 8; Table S1). Thus, these two ages represent two distinct episodes of zircon crystallization. Although zircons from both groups generally show similar morphologies and internal textures, some 322 Ma grains have thin dark rims (Fig. 8a-b), which may correspond to overgrowth during the second episode of crystallization at ~297 Ma. This is also confirmed by (1) the occurrence of thin dark rims surrounding the inherited zircons of 338 Ma, 342 Ma and 365 Ma (Fig. 8a-8b), and (2) conspicuous dark rims and zoning-controlled alteration developed in discordant zircons (Fig. 8a-b).

Regional tectonics, metamorphism, and migmatization have close spatial and temporal relationships with peraluminous leucogranite genesis (e.g., Barrow, 1893; Vernon, 1982; Barton and Hanson, 1989; Okay et al., 2014). Late Paleozoic granite plutons (Figs. 2b and 9) occurred in two episodes at 330-310 Ma and 305-290 Ma (Sun et al., 2007b; Wang et al., 2009c; Chen and Shu, 2010; Chen et al., 2016; Song et al., 2018), which fit the two zircon age peaks of zircons from migmatites (322 Ma and 297 Ma) (Figs. 8 and 9). Moreover, the age of the first episode of granitic magmatism is also consistent with the youngest age peak (322 Ma) of “metamorphic” zircons of the micaschists (Fig. 9b). Therefore, ~322 Ma can be reasonably interpreted as the timing of amphibolite facies metamorphism, migmatization and the first episode of

492 magmatism. As the migmatites also contain zircons of ~297 Ma, it is likely that
493 anatectic melts were not totally crystallized at ~322 Ma probably due to high thermal
494 gradient or continuous addition of melts until ~297 Ma in connection with the second
495 episode of granitic magmatism, giving birth to the crystallization of the younger
496 zircons, while some zircons of ~322 Ma were preserved. Finally, leucogranite dykes
497 of ~308 Ma contain a few inherited zircons with 320-330 Ma ages (Zhu et al., 2018).
498 Such a genetic relationship between migmatites and granites is likely but needs to be
499 confirmed through detailed geochemical investigations.

500 It is also worth noting that mica $^{40}Ar/^{39}Ar$ apparent ages of the metamorphic
501 rocks range from 301 to 277 Ma and were considered as the timing of the
502 metamorphism in the Harlik domain (Sun, 2007). However, considering: (1) the
503 relatively low closure temperature of argon isotopic system of micas (Harrison et al.,
504 1985, 2009), (2) the occurrence of extensive Permian granitic plutons and their close
505 spatial relationships with meta-sedimentary rocks and migmatites, and (3) the good
506 match between mica $^{40}Ar/^{39}Ar$ apparent ages (301-277 Ma) and zircon U-Pb ages of
507 granites (305-290 Ma), we consider that mica $^{40}Ar/^{39}Ar$ apparent ages of
508 meta-sedimentary rocks most likely correspond to the timing of thermal reset and
509 final cooling event related to the second episode of magmatism.

510 *6.2. Provenances of the meta-sedimentary rocks*

511 The studied meta-sedimentary rocks contain both Paleozoic and Proterozoic

detrital zircons (Fig. 6). Among overall 224 concordant detrital zircons, 126 grains (56%) yielded Paleozoic ages and 98 zircons (44%) yielded Proterozoic ages. For the Paleozoic ages, as aforementioned, the U-Pb system of detrital zircons younger than 420 Ma was likely affected by post-depositional metamorphism. Thus, these zircons and their ages should be rejected for provenance investigation. The Ordovician to Silurian detrital zircons (~480-420 Ma with peaks at ~475, ~445 and ~425 Ma) are dominant constituents in the meta-sedimentary rocks (Fig. 9b). This is consistent with the study of Sun et al. (2007a) who found a predominant Ordovician to Silurian zircon population (482-418 Ma) in low-grade sandstones from the study area.

As discussed above, the early Paleozoic zircons are mainly derived from magmatic rocks. Numerous early Paleozoic magmatic rocks of 440-450 Ma were previously reported both in the Harlik and Dananhu arcs, while magmatic rocks of 420-430 Ma crop out in the Dananhu area only (Cao et al., 2006; Ma et al., 2015; Wang et al., 2016; Zhang et al., 2016a; Chen et al., 2017; Liu et al., 2017; Deng et al., 2018; Du et al., 2018a; Wang et al., 2018b; Zheng et al., 2018; Chai et al., 2019). In addition, very few ~475 Ma magmatic rocks have been reported so far in the North Tianshan, and only rhyolites of 469 ± 9 Ma were documented in the Harlik area (Li et al., 2017). The angular to sub-angular early Paleozoic detrital zircons indicate short distances of transportation (Sun et al., 2007a), while these samples are from the Qincheng area that is situated between the Harlik Arc and Dananhu Arc; thus, it is suggested that these early Paleozoic detrital zircons (~480-420 Ma) came from

magmatic rocks of the Harlik and Dananhu arcs.

Ordovician to Silurian arc-type magmatic rocks are also exposed in the Central Tianshan and East Junggar-Altai belts (Fig. 10), which are potential sources for the meta-sedimentary rocks. However, the North Tianshan was separated from East Junggar-Altai belts before the early Carboniferous (>340 Ma) by the Kalamaili oceanic basin (Li et al., 2009; Wang et al., 2009b; Huang et al., 2012; Zhang et al., 2013; Xu et al., 2015a; Du et al., 2018b; Han and Zhao, 2018; Wang et al., 2019), while the depositional age of protoliths of the meta-sedimentary rocks is roughly constrained between ~425 to ~322 Ma. Therefore, the available data cannot sufficiently prove or disprove that the East Junggar-Altai magmatic arcs might be possible sources for the Ordovician to Silurian detrital zircons of the meta-sedimentary rocks in the Qincheng area.

In addition, it is suggested that the North Tianshan (Harlik-Dananhu arcs) was amalgamated with the Yamansu Arc and Central Tianshan Block at ~320-300 Ma along the Kangguer shear zone after the closure of the Kangguer Ocean (e.g., Li, 2004; Li et al., 2006; Zhang et al., 2020; Zhao et al., 2019). However, the rock sequences on both sides of this shear zone are comparable and it might have been located within the North Tianshan belt (Wang et al., 2008, 2014a; Branquet et al., 2012). According to the studies on ophiolites of the North Tianshan Suture zone and Kangguer belt (Xu et al., 2006a, 2006b; Chen et al., 2019), the North Tianshan (or Kangguer) Ocean opened during the mid-late Carboniferous. Considering that the Precambrian zircons

most likely came from the Central Tianshan Block (see discussion below), it is possible that the Central Tianshan Block also provided certain early Paleozoic detritus for the sediments in the Qincheng area.

The main population of Proterozoic zircons in the meta-sedimentary rocks is the Neoproterozoic group (550-1000 Ma) showing a peak at ~870 Ma and a subordinate peak at ~780 Ma. Minor zircon populations of 1.1-1.5 Ga, 1.6-2.0 Ga, 2.1-2.3 Ga and ~2.5 Ga with peaks at ~1.45 Ga and ~1.7 Ga are also recognized (Fig. 10a). However, there is no Precambrian basement exposed in the NTB (Xiao et al., 2004; Zhang et al., 2016b). These Proterozoic zircons were thus most likely transported from nearby Precambrian-based continental blocks. Chen et al. (2014) suggested that the Harlik Range is a part of the Tuva-Mongol-Altai Arc. Nevertheless, the available data indicate that the Tuva-Mongol-Altai Arc and the East Junggar Belt both lack magmatic events and detrital records in the ~1.35-1.45 Ga interval (Fig. 10d-e; Jiang et al., 2011), which are common in the North Tianshan (Fig. 10a-b; Chen et al., 2014). In contrast, a large quantity of Mesoproterozoic granitic rocks of ~1.40-1.45 Ga have been documented in the Central Tianshan Block (Fig. 10c; Ma et al., 2012a; He et al., 2014, 2015; Wang et al., 2014b, 2017; Huang et al., 2015). Moreover, the Central Tianshan Block has a detrital zircon age spectrum similar to that of the Harlik Range and the entire North Tianshan, they all display zircon populations of 750-800 Ma, 850-1000 Ma, ~1.45 Ga, 1.6-1.8 Ga and ~2.5 Ga. More importantly, the igneous rocks in the Central Tianshan Block formed during ~800, ~900 Ma and ~1.45 Ga episodes,

identical with the detrital zircon age peaks of the meta-sedimentary rocks from the Harlik Range, which are absent in the other neighboring units (Fig. 10). Therefore, the Central Tianshan Block is the most probable provenance area for the Precambrian detrital zircons in the studied meta-sedimentary rocks.

The Precambrian zircons in the meta-sedimentary rocks are anhedral in shape and show complex core-rim textures (Figs. 5 and S1), indicating that they were multiple-cycled. Thus, these Precambrian zircons were probably transported from the Central Tianshan Block to the North Tianshan Belt (Dananhu Arc) before the opening of the North Tianshan (or Kangguer) Ocean, and thereafter re-transported into the Harlik area. This is in agreement with the fact that zircon populations of Devonian flyschs in the Dananhu Arc are comparable with that of the Central Tianshan Block (Wang et al., 2019). However, due to uncertainty on their deposition age, these zircons could have been transported directly from the Central Tianshan Block as well.

Clastic sediments derived from orogens are generally a mixture of multifarious detritus from metamorphic, sedimentary and igneous rocks (e.g., Han et al., 2017). Mixing and preferential elimination of certain zircons during transport can significantly modify zircon populations in sediments, especially in old multiple-cycled populations (Hay and Dempster, 2009; Han et al., 2017). Therefore, comparison of detrital zircon populations must be undertaken with much care. In the present case, provenance from the Central Tianshan Block is most likely, but considering the limited size of the database, other provenances cannot be completely

596 excluded.

597 *6.3. Implications for the late Paleozoic tectonic evolution of the North Tianshan belt*

598 Our new zircon U-Pb data indicate that the meta-sediments from the JMC were
599 deposited in the interval between late Silurian and late Carboniferous. The
600 predominant early Paleozoic detrital zircons were potentially derived from both the
601 Harlik and Dananhu arcs. In combination with the low maturity of the meta-sandstone
602 that suggests a near-source deposition (Sun et al., 2007a), an intra-arc basin
603 (Qincheng or Xiaopu basin; Zhao et al., 1997) located between these arcs can be
604 suggested (Fig. 11A). In addition, the Precambrian zircons in the meta-sedimentary
605 rocks were probably derived from the Central Tianshan Block. As a result, the North
606 Tianshan was likely connected with the northern margin of the Central Tianshan
607 Block before the Carboniferous. The North Tianshan was rifted from the Central
608 Tianshan Block in the mid-late Carboniferous (Xu et al., 2006a, 2006b; Chen et al.,
609 2019) due to the opening of the North Tianshan (or Kangguer) Ocean, and was
610 thereafter re-amalgamated to the Central Tianshan Block during the latest
611 Carboniferous (Han et al., 2010; Zhang et al., 2015b, 2020) (Fig. 11B-D).

612 As discussed above, the amphibolite-facies metamorphism and migmatization
613 occurred at ~322 Ma. According to Sun (2007) and our field observations, the
614 garnet-sillimanite-bearing meta-sedimentary rocks are most likely the source rocks of
615 the migmatites and associated felsic dykes. The N-dipping foliations that bear

616 ~NW-SE stretching lineation resulted from sinistral transtension (Sun, 2007). In
617 addition, the HT-LP metamorphism (Zhao et al., 1997) and migmatization are coeval
618 with the co-emplacement of undeformed high-K calc-alkaline I- and A-type granites
619 (320-316 Ma) that formed probably in an extensional setting (Song et al., 2018).
620 Similarly, in the nearby Bogda area, Carboniferous (350-315 Ma) volcanic rocks are
621 thought to have formed in an intra-arc (Zhang et al., 2017; Wali et al., 2018) or
622 back-arc extensional setting (Chen et al., 2013; Xie et al., 2016b). Taking all these
623 arguments into consideration, we suggest that the meta-sedimentary rocks and
624 migmatites are likely parts of the Harlik arc root, and the migmatization probably
625 occurred due to decompression partial melting in a continent-based intra-arc or
626 back-arc extensional setting (Fig. 11C).

627 The migmatites in the Harlik Range also recorded an event at ~297 Ma, which is
628 coeval with the widespread emplacement of undeformed post-orogenic K-feldspar
629 granites and leucocratic two-mica granites at 298-295 Ma (Wang et al., 2009c; Chen
630 and Shu, 2010). The occurrence of ductilely deformed granites along the northern
631 boundary of the metamorphic belt (Fig. 2b-c), and dip-slip (normal) stretching
632 lineation along the north-dipping mylonite zone (see section 3) indicate syn-kinematic
633 emplacement of granites. Therefore, the development of a large volume of latest
634 Carboniferous to earliest Permian post-orogenic granitoids (Wang et al., 2009c, 2009d;
635 Chen and Shu, 2010; Yuan et al., 2010; Chen et al., 2016), bimodal dyke swarms (Gu
636 et al., 1999) and nearly synchronous ductile normal faults correspond to the

637 exhumation of the metamorphic units under a regional post-orogenic extensional
638 regime and thus prominent crustal thinning (Fig. 11D). Final cooling at 301-277 Ma
639 revealed by mica $^{40}Ar/^{39}Ar$ apparent ages (Sun, 2007) indicates that these events
640 terminated during the Early Permian.

641 7. Conclusions

642 (1) Protoliths of the meta-sedimentary rocks from the Julideneng Metamorphic
643 Complex in the southern Harlik Range were originally deposited between the
644 latest Silurian and late Carboniferous (425-322 Ma).
645 (2) The Harlik-Dananhu magmatic arcs were likely the major sources for the
646 Ordovician to Silurian detrital zircons in the meta-sedimentary rocks, while the
647 Precambrian detrital zircons were most likely derived from the Central Tianshan
648 Block, although possible provenances from the East Junggar and Chinese Altai
649 cannot be excluded.
650 (3) High-grade metamorphism and migmatization occurred at ~322 Ma in the
651 southern Harlik Range probably related to continent-based intra-arc or back-arc
652 crust thinning. The orogenic events in the Harlik Range terminated before the
653 Early Permian.

654 Acknowledgments

655 We appreciate the kind helps of Mr. B. Wu for LA-ICP-MS zircon U-Pb dating. Dr.

K. de Jong reviewed the first version of the manuscript and provided constructive suggestions. We are very grateful to two anonymous reviewers for their constructive comments; the Editor-in-Chief Prof. Mei-Fu Zhou and Editor Dr. Ibrahim Uysal are appreciated for their editorial handling. This study was co-sponsored by the National Nature Science Foundation of China (41772225, 42011530146, 41390445, and 41311120069), the Fundamental Research Funds for the Central Universities, and by the Open Fund of State Key Laboratory for Mineral Deposits Research (ZZKT-201603).

References

Ao, S.J., Xiao, W.J., Han, C.M., Li, X.H., Qu, J.F., Zhang, J.E., Guo, Q.Q., Tian, Z.H., 2012. Cambrian to early Silurian ophiolite and accretionary processes in the Beishan collage, NW China: implications for the architecture of the Southern Altaids. Geol. Mag. 149, 606-625.

Barrow, G., 1893. On an intrusion of muscovite-biotite gneiss in the southeastern Highlands of Scotland, and its accompanying metamorphism. Q. J. Geol. Soc. 49, 330-358.

Barton, M.D., Hanson, R.B., 1989. Magmatism and the development of low-pressure metamorphic belts: Implications from the western United States and thermal modeling. Geol. Soc. Am. Bull. 101, 1051-1065.

Branquet, Y., Gumiaux, C., Sizaret, S., Barbanson, L., Wang, B., Cluzel, D., Li, G.R.,

676 Delaunay, A., 2012. Synkinematic mafic/ultramafic sheeted intrusions:
677 Emplacement mechanism and strain restoration of the Permian Huangshan
678 Ni-Cu ore belt (Eastern Tianshan, NW China). J. Asian Earth Sci. 56, 240-257.
679 Belousova, E., Griffin, W. L., O'Reilly, S. Y., Fisher, N. L., 2002. Igneous zircon: trace
680 element composition as an indicator of source rock type. Contrib. Mineral. Petrol.
681 143, 602-622.
682 Cai, K.D., Sun, M., Yuan, C., Zhao, G.C., Xiao, W.J., Long, X.P., Wu, F.Y., 2011.
683 Prolonged magmatism, juvenile nature and tectonic evolution of the Chinese
684 Altai, NW China: Evidence from zircon U-Pb and Hf isotopic study of Paleozoic
685 granitoids. J. Asian Earth Sci. 42, 949-968.
686 Cai, K.D., Sun, M., Jahn, B.-M., Xiao, W., Yuan, C., Long, X., Chen, H., Tumurkhuu,
687 D., 2015. A synthesis of zircon U-Pb ages and Hf isotopic compositions of
688 granitoids from Southwest Mongolia: Implications for crustal nature and tectonic
689 evolution of the Altai Superterrane. Lithos 232, 131-142.
690 Cao, F.G., Tu, Q.J., Zhang, X.M., Ren, Y., Li, S.L., Dong, F.R., 2006. Preliminary
691 determination of the Early Paleozoic magmatic arc in the Karlik Mountains, East
692 Tianshan, Xinjiang, China-Evidence from zircon SHRIMP U-Pb dating of
693 granite bodies in the Tashuihe area. Geol. Bullet. China 25, 923-927 (in Chinese
694 with English abstract).
695 Cao, F.G., Zhang, Y.P., Li, Y., Guan, W., Ren, Y., Dong, F.R., Guo, L., 2009. The
696 geological daracter of Nanhua system Qingshixia formation in Qincheng Hami,

Xinjiang. Xinjiang Geol. 27, 303-307 (in Chinese with English abstract).

Chai, F.M., Zhang, Z.C., Li, W.H., Santosh, M., Wang, H.P., Wang, W., Xu, Q.F., 2019. The early Paleozoic Huangtupo VMS Cu-Zn deposit in Kalatag, Eastern Tianshan: Implications from geochemistry and zircon U-Pb geochronology of volcanic host rocks. Lithos 342, 97-113.

Charvet, J., Shu, L.S., Laurent-Charvet, S., 2007. Paleozoic structural and geodynamic evolution of eastern Tianshan (NW China): welding of the Tarim and Junggar plates. Episodes 30, 162-186.

Charvet, J., Shu, L.S., Laurent-Charvet, S., Wang, B., Faure, M., Cluzel, D., Chen, Y., de Jong, K., 2011. Palaeozoic tectonic evolution of the Tianshan belt, NW China. Sci. China Earth Sci. 54, 166-184.

Chen, L., Wang, J.B., Bagas, L., Wu, X.B., Zou, H.Y., Zhang, H.Q., Sun, Y., Lv, X.Q., Deng, X.H., 2017. Significance of adakites in petrogenesis of Early Silurian magmatism at the Yudai copper deposit in the Kalatag district, NW China. Ore Geol. Rev. 91, 780-794.

Chen, X.J., Shu, L.S., 2010. Features of the post-collisional tectono-magmatism and geochronological evidence in the Karlik Mt., Xinjiang. Acta Petrol. Sin. 26, 3057-3064 (in Chinese with English abstract).

Chen, X.J., Shu, L.S., Santosh, M., 2011. Late Paleozoic post-collisional magmatism in the Eastern Tianshan Belt, Northwest China: New insights from geochemistry, geochronology and petrology of bimodal volcanic rocks. Lithos 127, 581-598.

718 Chen, X.J., Shu, L.S., Santosh, M., Zhao, X.X., 2013. Island arc bimodal magmatism
719 in the eastern Tianshan Belt, Northwest China: Geochemistry, zircon U-Pb
720 geochronology and implications for the Paleozoic crustal evolution in Central
721 Asia. Lithos 168-169, 48-66.
722 Chen, X.J., Shu, L.S., Santosh, M., Xu, Z.Q., 2014. The provenance and tectonic
723 affinity of the Paleozoic meta-sedimentary rocks in the Chinese Tianshan belt:
724 New insights from detrital zircon U-Pb geochronology and Hf-isotope analysis. J.
725 Asian Earth Sci. 94, 12-27.
726 Chen, X.J., Zhang, K.H., Zhang, G.L., Zhou, J., 2016. Characteristics, petrogenesis
727 and tectonic implications of the Permian Omoertage alkaline granites in Harlik
728 area, Xinjiang. Acta Petrol. Mineral. 35, 929-946 (in Chinese with English
729 abstract).
730 Chen, Z.Y., Xiao, W.J., Windley, B.F., Schulmann, K., Mao, Q.G., Zhang, Z.Y., Zhang,
731 J.E., Deng, C., Song, S.H., 2019. Composition, Provenance, and Tectonic Setting
732 of the Southern Kangurtag Accretionary Complex in the Eastern Tianshan, NW
733 China: Implications for the Late Paleozoic Evolution of the North Tianshan
734 Ocean. Tectonics 38, 2779-2802.
735 Chen, Z.Y., Xiao, W.J., Windley, B.F., Schulmann, K., Mao, Q.G., Zhang, Z.Y., Zhang,
736 J.E., Li, C.Y., Song, S.H., 2020. Latest Permian-early Triassic arc amalgamation
737 of the Eastern Tianshan (NW China): Constraints from detrital zircons and Hf
738 isotopes of Devonian-Triassic sediments. Geol. J. 55, 1708-1727.

739 Connelly J.N. 2000. Degree of preservation of igneous zonation in zircon as a
740 signpost for concordancy in U/Pb geochronology. Chem. Geol. 172, 25-39.
741 Corfu, F., Hanchar, J.M., Hoskin, P.W.O., Kinny, P., 2003. Altas of zircon textures.
742 Rev. Mineral. Geochem. 53, 469-500.
743 de Jong, K., Wang, B., Faure, M., Shu, L.S., Cluzel, D., Charvet, J., Ruffet, G., Chen,
744 Y., 2009. New 40Ar/39Ar age constraints on the Late Palaeozoic tectonic
745 evolution of the Western Tianshan (Xinjiang, northwestern China), with
746 emphasis on Permian fluid ingress. Int. J. Earth Sci. 98, 1239-1258.
747 Deng, X.H., Wang, J.B., Santosh, M., Wang, Y.W., Long, L.L., Zhang H.Q., Yang,
748 L.Y., Xu, J., Chen, X., Chen, L., 2018. Early Paleozoic volcanic rocks with VMS
749 mineralization from easternTianshan Orogen: Implication for tectonic evolution.
750 Geol. J. 53, 2178-2192.
751 Dong, Y.P., Zhou, D.W., Zhang, G.W., Zhao, X., Luo, J.H., Xu, J.G., 2006. Geology
752 and geochemistry of the Gangou ophiolitic melange at the northern margin of the
753 Middle Tianshan Belt. Acta Petrol. Sin. 22, 49-56 (in Chinese with English
754 abstract).
755 Du, L., Long, X.P., Yuan, C., Zhang, Y.Y., Huang, Z.Y., Sun, M., Zhao, G.C., Xiao,
756 W.J., 2018a. Early Paleozoic dioritic and granitic plutons in the Eastern Tianshan
757 Orogenic Belt, NW China: Constraints on the initiation of a magmatic arc in the
758 southern Central Asian Orogenic Belt. J. Asian Earth Sci. 153, 139-153.
759 Du, Q.X., Han, Z.Z., Shen, X.L., Han, C., Han, M., Song, Z.G., Gao, L.H., Liu, H.,

760 Zhong, W.J., Yan, J.L., 2018b. Zircon U-Pb geochronology and geochemistry of
761 the post-collisional volcanic rocks in eastern Xinjiang Province, NW China:
762 implications for the tectonic evolution of the Junggar terrane. Int. Geol. Rev. 60,
763 339-364.
764 Gao, J., Li, M.S., Xiao, X.C., Tang, Y.Q., He, G.Q., 1998. Paleozoic tectonic evolution
765 of the Tianshan Orogen, northern China. Tectonophysics 287, 213-231.
766 Gao, J., Long, L.L., Klemd, R., Qian, Q., Liu, D.Y., Xiong, X.M., Su, W., Liu, W.,
767 Wang, Y.T., Yang, F.Q., 2009. Tectonic evolution of the South Tianshan orogen
768 and adjacent regions, NW China: geochemical and age constraints of granitoid
769 rocks. Int. J. Earth Sci. 98, 1221-1238.
770 Gao, J., Wang, X.S., Klemd, R., Jiang, T., Qian, Q., Mu, L.X., Ma, Y.Z., 2015. Record
771 of assembly and breakup of Rodinia in the Southwestern Altaids: Evidence from
772 Neoproterozoic magmatism in the Chinese Western Tianshan Orogen. J. Asian
773 Earth Sci. 113, 173-193.
774 Glorie, S., De Grave, J., Buslov, M.M., Zhimulev, F.I., Izmer, A., Vandoorne, W.,
775 Ryabinin, A., Van den haute, P., Vanhaecke, F., Elburg, M.A., 2011. Formation
776 and Palaeozoic evolution of the Gorny-Altai-Altai-Mongolia suture zone (South
777 Siberia): Zircon U-Pb constraints on the igneous record. Gondwana Res. 20,
778 465-484.
779 Gower, R.J.W., Simpson, C., 1992. Phase boundary mobility in naturally deformed,
780 high-grade quartzofeldspathic rocks: evidence for diffusional creep. J. Struct.

781 Geol. 14, 301-314.
782 Gu, L.X., Hu, S.X., Chu, Q., Yu, C.S., Xiao, X.J., 1999. Pre-collision granites and
783 post-collision intrusive assemblage of the Kelameili-Harlik Orogenic Belt. Acta
784 Petrol. Sin. 73, 316-329.
785 Gu, L.X., Hu, S.X., Yu, C.S., Li, H.Y., Xiao, X.J., 2000. Carboniferous volcanites in
786 the Bogda orogenic belt of eastern Tianshan: their tectonic implications. Acta
787 Petrol. Sin. 16, 305-316 (in Chinese with English abstract).
788 Gu, L.X., Hu, S.X., Yu, C.S., Wu, C.Z., Yan, Z.F., 2001. Initiation and evolution of the
789 Bogda subduction-torn-type rift. Acta Petrol. Sin. 17, 585-597 (in Chinese with
790 English abstract).
791 Han, B.F., Guo, Z.J., Zhang, Z.C., Zhang, L., Chen, J.F., Song, B., 2010. Age,
792 geochemistry, and tectonic implications of a late Paleozoic stitching pluton in the
793 North Tian Shan suture zone, western China. Geol. Soc. Am. Bull. 122, 627-640.
794 Han, B.F., He, G.Q., Wang, X.C., Guo, Z.J., 2011. Late Carboniferous collision
795 between the Tarim and Kazakhstan-Yili terranes in the western segment of the
796 South Tianshan Orogen, Central Asia, and implication for the Northern Xinjiang,
797 western China. Earth Sci. Rev. 109, 74-93.
798 Han, S.Y., de Jong, K., Yi, K., 2017. Detrital zircon ages in Korean mid-Paleozoic
799 meta-sandstones (Imjingang Belt and Taean Formation): Constraints on tectonic
800 and depositional setting, source regions and possible affinity with Chinese
801 terranes. J. Asian Earth Sci. 143, 191-217.

Han, Y.G., Zhao, G.C., 2018. Final amalgamation of the Tianshan and Junggar orogenic collage in the southwestern Central Asian Orogenic Belt: Constraints on the closure of the Paleo-Asian Ocean. Earth Sci. Rev. 186, 129-152.

Harrison, T.M., Duncan, I., McDougall, I., 1985. Diffusion of 40Ar in biotite: Temperature, pressure and compositional effects. Geochim. Cosmochim. Acta 49, 2461-2468.

Harrison, T.M., Célérier, J., Aikman, A.B., Hermann, J., Heizler, M.T., 2009. Diffusion of 40Ar in muscovite. Geochim. Cosmochim. Acta 73, 1039-1051.

Hay, D.C., Dempster, T.J., 2009. Zircon alteration, formation and preservation in sandstones. Sedimentology 56, 2175-2191.

He, Z.Y., Klemd, R., Yan, L.L., Zhang, Z.M., 2018a. The origin and crustal evolution of microcontinents in the Beishan orogen of the southern Central Asian Orogenic Belt. Earth Sci. Rev. 185, 1-14.

He, Z.Y., Klemd, R., Zhang, Z.M., Zong, K.Q., Sun, L.X., Tian, Z.L., Huang, B.T., 2015. Mesoproterozoic continental arc magmatism and crustal growth in the eastern Central Tianshan Arc Terrane of the southern Central Asian Orogenic Belt: Geochronological and geochemical evidence. Lithos 236-237, 74-89.

He, Z.Y., Zhang, Z.M., Zong, K.Q., Xiang, H., Chen, X.J., Xia, M.J., 2014. Zircon U-Pb and Hf isotopic studies of the Xingxingxia Complex from Eastern Tianshan (NW China): Significance to the reconstruction and tectonics of the southern Central Asian Orogenic Belt. Lithos 190-191, 485-499.

He, Z.Y., Wang, B., Zhong, L.L., Zhu, X.Y., 2018b. Crustal evolution of the Central Tianshan Block: Insights from zircon U-Pb isotopic and structural data from meta-sedimentary and meta-igneous rocks along the Wulasitai-Wulanmoren shear zone. Precambrian Res. 314, 111-128.

He, Z.Y., Wang, B., Ni, X.H., De Grave, J., Scaillet, S., Chen, Y., Liu, J.S., Zhu, X., 2021. Structural and kinematic evolution of strike-slip shear zones around and in the Central Tianshan: insights for eastward tectonic wedging in the southwest Central Asian Orogenic Belt. J. Struct. Geol. 144, https://doi.org/10.1016/j.jsg.2021.104279.

Hirth, G., Tullis, J.A.N., 1992. Dislocation creep regimes in quartz aggregates. J. Struct. Geol. 14, 145-159.

Hoskin, P.W., Schaltegger, U., 2003. The composition of zircon and igneous and metamorphic petrogenesis. Rev. Mineral. Geochem. 53, 27-62.

Hoskin, P.W.O., 2005. Trace-element composition of hydrothermal zircon and the alteration of Hadean zircon from the Jack Hills, Australia. Geochim. Cosmochim. Acta 69, 637-648.

Hu, A.Q., Jahn, B., Zhang, G.X., Chen, Y.B., Zhang, Q.F., 2000. Crustal evolution and Phanerozoic crustal growth in northern Xinjiang: Nd isotopic evidence. Part I. Isotopic characterization of basement rocks. Tectonophysics 328, 15-51.

Hu, A.Q., Wei, G.J., Jahn, B.M., Zhang, J.B., Deng, W.F., Chen, L.L., 2010. Formation of the 0.9 Ga Neoproterozoic granitoids in the Tianshan Orogen, NW

China: constraints from the SHRIMP zircon age determination and its tectonic significance. Geochimica 39, 197-212 (in Chinese with English abstract).

Huang, B., Fu, D., Kusky, T., Ruan, K.P., Zhou, W.X., Zhang, X.H., 2018. Sedimentary provenance in response to Carboniferous arc-basin evolution of East Junggar and North Tianshan belts in the southwestern Central Asian Orogenic Belt. Tectonophysics 722, 324-341.

Huang, G., Niu, G.Z., Wang, X.L., Guo, J., Yu, F., 2012. Formation and emplacement age of Karamaili ophiolite: LA-ICP-MS zircon U-Pb age evidence from the diabase and tuff in eastern Junggar, Xinjiang. Geol. Bullet. China 31, 1267-1278 (in Chinese with English abstract).

Huang, H., Wang, T., Tong, Y., Qin, Q., Ma, X.X., Yin, J.Y., 2020. Rejuvenation of ancient micro-continents during accretionary orogenesis: Insights from the Yili Block and adjacent regions of the SW Central Asian Orogenic Belt. Earth Sci. Rev. 103255. https://doi.org/10.1016/j.earscirev.2020.103255

Huang, Z.Y., Long, X.P., Kröner, A., Yuan, C., Wang, Y.J., Chen, B., Zhang, Y.Y., 2015. Neoproterozoic granitic gneisses in the Chinese Central Tianshan Block: Implications for tectonic affinity and Precambrian crustal evolution. Precambrian Res. 269, 73-89.

Huang, Z.Y., Long, X.P., Wang, X.C., Zhang, Y.Y., Du, L., Yuan, C., Xiao, W.J., 2017. Precambrian evolution of the Chinese Central Tianshan Block: Constraints on its tectonic affinity to the Tarim Craton and responses to supercontinental cycles.

865 Precambrian Res. 295, 24-37.
866 Huang, Z.Y., Yuan, C., Long, X.P., Zhang, Y.Y., Du, L., 2019. From Breakup of Nuna
867 to Assembly of Rodinia: A Link Between the Chinese Central Tianshan Block
868 and Fennoscandia. Tectonics 38, 4378-4398.
869 Jackson, S.E., Pearson, N.J., Griffin, W.L., Belousova, E.A., 2004. The application of
870 laser ablation-inductively coupled plasma-mass spectrometry to in situ U-Pb
871 zircon geochronology. Chem. Geol. 211, 47-69.
872 Jiang, T., Gao, J., Klemd, R., Qian, Q., Zhang, X., Xiong, X.M., Wang, X.S., Tan, Z.,
873 Chen, B.X., 2014. Paleozoic ophiolitic mélanges from the South Tianshan
874 Orogen, NW China: geological, geochemical and geochronological implications
875 for the geodynamic setting. Tectonophysics 612-613, 106-127.
876 Jiang, Y.D., Sun, M., Zhao, G.C., Yuan, C., Xiao, W.J., Xia, X.P., Long, X.P., Wu, F.Y.,
877 2011. Precambrian detrital zircons in the Early Paleozoic Chinese Altai: Their
878 provenance and implications for the crustal growth of central Asia. Precambrian
879 Res. 189, 140-154.
880 Kruhl, J.H. 1996. Prism- and basal-plane parallel subgrain boundaries in quartz: A
881 microstructural geothermobarometer. J. Metamorph. Geol. 14(5), 581-589.
882 Laurent-Charvet, S., Charvet, J., Monié, P., Shu, L.S., 2003. Late Paleozoic strike-slip
883 shear zones in eastern Central Asia (NW China): New structural and
884 geochronological data. Tectonics 22(2), 1009, doi:10.1029/2001TC901047.
885 Lei, R.X., Wu, C.Z., Gu, L.X., Zhang, Z.Z., Chi, G.X., Jiang, Y.H., 2011. Zircon U-Pb

chronology and Hf isotope of the Xingxingxia granodiorite from the Central Tianshan zone (NW China): Implications for the tectonic evolution of the southern Altaids. Gondwana Res. 20, 582-593.

Lei, R.X., Wu, C.Z., Feng, Y.G., Xia, M.Z., Jiao, J.G., 2018. Formation age and geodynamic setting of the Neoproterozoic Shalong iron formation in the Central Tianshan, NW China: Constraints from zircon U-Pb dating, geochemistry, and Hf-Nd isotopes of the host rocks. Geol. J. 53, 345-361.

Liang, P., Chen, H., Hollings, P., Xiao, B., Wu, C., Bao, Z., Cai, K., 2016a. The Paleozoic tectonic evolution and metallogenesis of the northern margin of East Junggar, Central Asia Orogenic Belt: Geochronological and geochemical constraints from igneous rocks of the Qiaoxiahala Fe-Cu deposit. J. Asian Earth Sci. 130, 23-45.

Liang, P., Chen, H.Y., Hollings, P., Wu, C., Xiao, B., Bao, Z.W., Xu, D., 2016b. Geochronology and geochemistry of igneous rocks from the Laoshankou district, north Xinjiang: Implications for the late Paleozoic tectonic evolution and metallogenesis of east Junggar. Lithos 266-267, 115-132.

Li, D.F., Zhang, L., Chen, H.Y., Hollings, P., Cao, M.J., Fang, J., Wang, C.M., Lu, W.J., 2016. Geochronology and geochemistry of the high Mg dioritic dikes in Eastern Tianshan, NW China: Geochemical features, petrogenesis and tectonic implications. J. Asian Earth Sci. 115, 442-454.

Li, J.T., He, X.F., Liu, L., Yang, P.T., Liang, B., Su, H., Yang, Y.D., Han, H.M., Liu,

907 Y.Z., Dai, Z.H., 2017. Ordovician tectonic evolution of Harlik in Eastern
908 Tianshan of Xinjiang: Constraints from LA-ICP-MS zircon U-Pb geochronology
909 and geochemistry of volcanic rocks. Geoscience 31, 460-473 (in Chinese with
910 English abstract).
911 Li, J.Y., 2004. Late Neoproterozoic and Paleozoic tectonic framework and evolution
912 of Eastern Xinjiang, NW China. Geol. Rev. 50, 304-322 (in Chinese with English
913 abstract).
914 Li, J.Y., Wang, K.Z., Sun, G.H., Mo, S.G., Li, W.Q., Yang, T.N., Gao, L.M., 2006.
915 Paleozoic active margin slices in the southern Turfan–Hami basin: geological
916 records of subduction of the Paleo-Asian ocean plate in Central Asian regions.
917 Acta Petrol. Sin. 22, 1087-1102 (in Chinese with English abstract).
918 Li, J.Y., Yang, T.N., Li, Y.P., Zhu, Z.X., 2009. Geological features of the Karamaili
919 faulting belt, eastern Junggar region, Xinjiang, China and its constraints on the
920 reconstruction of Late Paleozoic ocean-continental framework of the Central
921 Asian region. Geol. Bullet. China 28, 1817-1826 (in Chinese with English
922 abstract).
923 Li, W., Liu, Y.Q., Dong, Y.P., Zhou, X.H., Liu, X.M., Li, H., Fan, T.T., Zhou, D.W.,
924 Xu, X.Y., Chen, J.L., 2013. The geochemical characteristics, geochronology and
925 tectonic significance of the Carboniferous volcanic rocks of the Santanghu area
926 in northeastern Xinjiang, China. Sci. China Earth Sci. 56, 1318-1333.
927 Lin, W., Faure, M., Shi, Y.H, Wang, Q.C, Li, Z., 2009. Palaeozoic tectonics of the

928 southwestern Chinese Tianshan: new insights from a structural study of the
929 high-pressure/low-temperature metamorphic belt. Int. J. Earth Sci. 98,
930 1259-1274.
931 Liu, H.S., Wang, B., Shu, L.S., Jahn, B.M., Lizuka, Y., 2014. Detrital zircon ages of
932 Proterozoic meta-sedimentary rocks and Paleozoic sedimentary cover of northern
933 Yili Block: Implications for the tectonics of microcontinents in the Central Asian
934 Orogenic Belt. Precambrian Res. 252, 209-222.
935 Liu, L., He, X.F., Li, J.T., Yang, P.T., Liang, B., Su, H., Yang, Y.D., Liu, Y.Z., Dai,
936 Z.H., 2017. Petrogenesis and tectonic significances of the Qincheng
937 Tianshengquan pluton in the Harlik Orogen of Eastern Xinjiang. Geol. Sci.
938 Technol. Info. 36, 86-96 (in Chinese with English abstract).
939 Liu, S.W., Guo, Z.J., Zhang, Z.C., Li, Q.G., Zheng, H.F., 2004. Nature of Precambrian
940 metamorphic blocks in eastern segment of the Central Tianshan: constraints from
941 geochronology and Nd geochemistry. Sci. China Ser. D Earth Sci. 47,
942 1085-1094.
943 Liu, W., Liu, X.J., Liu, L.J., 2013. Underplating generated A- and I-type granitoids of
944 the East Junggar from the lower and the upper oceanic crust with mixing of
945 mafic magma: insights from integrated zircon U-Pb ages, petrography,
946 geochemistry and Nd-Sr-Hf isotopes. Lithos 179, 293-319.
947 Liu, X.J., Liu, W., Si, C.Q., 2019. Petrogenesis and source rocks of the high-K
948 calc-alkaline and shoshonitic I-type granitoids in the northwestern part of East

949 Junggar, NW China. Lithos 326-327, 298-312.
950 Liu, Y.S., Gao, S., Hu, Z.C., Gao, C.G., Zong, K.Q., Wang, D.B., 2010a. Continental
951 and oceanic crust recycling-induced melt-peridotite interactions in the
952 Trans-North China Orogen: U-Pb dating, Hf isotopes and trace elements in
953 zircons from mantle xenoliths. J. Petrol. 51, 537-571.
954 Liu, Y.S., Hu, Z.C., Gao, S., Günther, D., Xu, J., Gao, C.G., Chen, H.H., 2008. In situ
955 analysis of major and trace elements of anhydrous minerals by LA-ICP-MS
956 without applying an internal standard. Chem. Geol. 257, 34-43.
957 Liu, Y.S., Hu, Z.C., Zong, K.Q., Gao, C.G., Gao, S., Xu, J., Chen, H.H., 2010b.
958 Reappraisement and refinement of zircon U-Pb isotope and trace element
959 analyses by LA-ICP-MS. Chin. Sci. Bull. 55, 1535-1546.
960 Long, L.L., Wang, J.B., Wang, Y.W., Mao, Q.G., Deng, X.H., Zhao, L.T., Sun, Z.Y.,
961 Sun, Y., Gao, Y. H., 2016. Discussion on the age of ore-host volcanic strata in the
962 Kalatage ore concentration area, Eastern Tianshan: Evidence from shrimp zircon
963 U-Pb dating. Miner. Explor. 7, 31-37 (in Chinese with English abstract).
964 Long, X.P., Sun, M., Yuan, C., Xiao, W.J., Lin, S.F., Wu, F.Y., Xia, X.P., Cai, K.D.,
965 2007. Detrital zircon age and Hf isotopic studies for metasedimentary rocks from
966 the Chinese Altai: Implications for the Early Paleozoic tectonic evolution of the
967 Central Asian Orogenic Belt. Tectonics 26, TC5015.
968 Long, X.P., Yuan, C., Sun, M., Xiao, W.J., Zhao, G.C., Wang, Y.J., Cai, K.D., 2010.
969 Detrital zircon ages and Hf isotopes of the early Paleozoic flysch sequence in the

970 Chinese Altai, NW China: New constraints on depositional age, provenance and
971 tectonic evolution. Tectonophysics 480, 213-231.
972 Long, X.P., Sun, M., Yuan, C., Kröner, A., Hu, A.Q., 2012a. Zircon REE patterns and
973 geochemical characteristics of Paleoproterozoic anatectic granite in the northern
974 Tarim Craton, NW China: Implications for the reconstruction of the Columbia
975 supercontinent. Precambrian Res. 222, 474-487.
976 Long, X.P., Yuan, C., Sun, M., Safonova, I., Xiao, W.J., Wang, Y.J., 2012b.
977 Geochemistry and U-Pb detrital zircon dating of Paleozoic graywackes in East
978 Junggar, NW China: Insights into subduction-accretion processes in the southern
979 Central Asian Orogenic Belt. Gondwana Res. 21, 637-653.
980 Luo, J., Xiao, W.J., Wakabayashi, J., Han, C.M., Zhang, J.E., Wan, B., Ao, S.J., Zhang,
981 Z.Y., Tian, Z.H., Song, D.F., Chen, Y.C., 2017. The Zhaheba ophiolite complex
982 in Eastern Junggar (NW China): Long lived supra-subduction zone ocean crust
983 formation and its implications for the tectonic evolution in southern Altaids.
984 Gondwana Res. 43, 17-40.
985 Ma, R.S., Shu, L.S., Sun, J.Q., 1997. Tectonic Evolution and Metallogeny of Eastern
986 Tianshan Mountains. Geological Publishing House, Beijing, pp. 1-202.
987 Ma, X.X., Shu, L.S., Jahn, B.M., Zhu, W.B., Faure, M., 2012a. Precambrian tectonic
988 evolution of Central Tianshan, NW China: Constraints from U-Pb dating and in
989 site Hf isotopic analysis of detrital zircons. Precambrian Res. 222-223, 450-473.
990 Ma, X.X., Shu, L.S., Santosh, M., Li, J.Y., 2012b. Detrital zircon U-Pb geochronology

and Hf isotope data from Central Tianshan suggesting a link with the Tarim Block: Implications on Proterozoic supercontinent history. Precambrian Res. 206, 1-16.

Ma, X.X., Shu, L.S., Santosh, M., Li, J.Y., 2013. Petrogenesis and tectonic significance of an early Palaeozoic mafic-intermediate suite of rocks from the Central Tianshan, northwest China. Int. Geol. Rev. 55, 548-573.

Ma, X.X., Shu, L.S., Meert, J.G., Li, J.Y., 2014. The Paleozoic evolution of Central Tianshan: Geochemical and geochronological evidence. Gondwana Res. 25, 797-819.

Ma, X.H., Chen, B., Wang, C., Yan, X.L., 2015. Early Paleozoic subduction of the Paleo-Asian Ocean: Zircon U-Pb geochronological, geochemical and Sr-Nd isotopic evidence from the Harlik pluton, Xinjiang. Acta Petrol. Sin. 31, 89-104 (in Chinese with English abstract).

Mao, Q.G., Yu, M.J., Xiao, W.J., Windley, B.F., Li, Y.C., Wei, X.F., Zhu, J.J., Lv, X.Q., 2018. Skarn-mineralized porphyry adakites in the Harlik arc at Kalatage, E. Tianshan (NW China): Slab melting in the Devonian-early Carboniferous in the southern Central Asian Orogenic Belt. J. Asian Earth Sci. 153, 365-378.

Muhtar, M.N., Wu, C.Z., Santosh, M., Lei, R.X., Gu, L.X., Wang, S.M., Gan, K., 2020. Late Paleozoic tectonic transition from subduction to post-collisional extension in Eastern Tianshan, Central Asian Orogenic Belt. Geol. Soc. Am. Bull. 132, 1756-1774.

1012 Okay, A.I., Sunal, G., Tüysüz, O., Sherlock, S., Keskin, M., Kylander-Clark, A.R.C.,
1013 2014. Low-pressure–high-temperature metamorphism during extension in a
1014 Jurassic magmatic arc, Central Pontides, Turkey. J. Metamorph. Geol. 32,
1015 49-69.
1016 Passchier, C.W., Trouw, R.A.J., 2005. Microtectonics, second ed. Springer, Berlin,
1017 Heidelberg, pp. 1-306.
1018 Rubatto, D., 2017. Zircon: The metamorphic mineral. Rev. Mineral. Geochem. 83,
1019 261-295.
1020 Safonova, I., 2017. Juvenile versus recycled crust in the Central Asian Orogenic Belt:
1021 Implications from ocean plate stratigraphy, blueschist belts and intra-oceanic arcs.
1022 Gondwana Res. 47, 6-27.
1023 Sawyer, E.W., 2008. Atlas of migmatites. The Canadian Mineralogist Special
1024 Publication 9. NRC Research Press, Ottawa, pp. 1-371.
1025 Şengör, A.M.C., Natal'in, B.A., Burtman, V.S., 1993. Evolution of the Altaid tectonic
1026 collage and Paleozoic crustal growth in Eurasia. Nature 364, 209-304.
1027 She, J.Z., Yang, W.Z., Xun, Q.U., Jia, J., Di, X.C., 2017. Geochemistry and zircon
1028 U-Pb dating of the Dacaotanbei mafic-ultramafic complex, eastern Tianshan and
1029 its geological significance. Bull. Mineral. Petrol. Geochem. 36, 82-91 (in
1030 Chinese with English abstract).
1031 Shi, Y.R., Liu, D.Y., Zhang, Q., Jian, P., Zhang, F.Q., Miao, L.C., 2007. SHRIMP
1032 zircon U-Pb dating of the Gangou granitoids, Central Tianshan Mountains,

Northwest China and tectonic significances. Chin. Sci. Bull. 52, 1507-1516.

Shi, Y.R., Zhang, W., Kröner, A., Li, L.L., Jian, P., 2018. Cambrian ophiolite complexes in the Beishan area, China, southern margin of the Central Asian Orogenic Belt. J. Asian Earth Sci. 153, 193-205.

Shu, L.S., Wang, B., Zhu, W.B., Guo, Z.J., Charvet, J., Zhang, Y., 2011. Timing of initiation of extension in the Tianshan, based on structural, geochemical and geochronological analyses of bimodal volcanism and olistostrome in the Bogda Shan (NW China). Int. J. Earth Sci. 100, 1647-1663.

Shu, L.S., Wang, Y.J., 2003. Late Devonian-Early Carboniferous radiolarian fossils from siliceous rocks of the Kelameili ophiolite, Xinjiang. Geol. Rev. 49, 408-412 (in Chinese with English abstract).

Song, D.F., Xiao, W.J., Windley, B.F., Han, C.M., Tian, Z.H., 2015. A Paleozoic Japan-type subduction-accretion system in the Beishan orogenic collage, southern Central Asian Orogenic Belt. Lithos 224, 195-213.

Song, P., Tong, Y., Wang, T., Huang, H., Zhang, J.J., Huang, W., 2018. Zircon U-Pb ages, genetic evolution and geological significance of Carboniferous granites in the Harlik Mountain, East Tianshan, Xinjiang. Geol. Bullet. China 37, 790-804 (in Chinese with English abstract).

Stipp, M., Stünitz, H., Heilbronner, R., Schmid, S.M., 2002. The eastern Tonale fault zone: a ‘natural laboratory’ for crystal plastic deformation of quartz over a temperature range from 250 to 700 ℃. J. Struct. Geol. 24, 1861-1884.

1054 Sun, M., Yuan, C., Xiao, W., Long, X., Xia, X., Zhao, G., Lin, S., Wu, F., Kröner, A.,
1055 2008. Zircon U-Pb and Hf isotopic study of gneissic rocks from the Chinese
1056 Altai: Progressive accretionary history in the early to middle Paleozoic. Chem.
1057 Geol. 247, 352-383.
1058 Sun, S.S., McDonough, W.F., 1989. Chemical and isotopic systematics of oceanic
1059 basalts: implications for mantle composition and processes. Geol. Soc. Lond.,
1060 Spec. Publ. 42, 313-345.
1061 Sun, G.H., Li, J.Y., Gao, L.M., Yang, T.N., 2005. Zircon SHRIMP U-Pb age of a
1062 dioritic pluton in the Harlik Mountains, eastern Xinjiang, and its tectonic
1063 implications. Geol. Rev. 51, 463-469 (in Chinese with English abstract).
1064 Sun, G.H., Li, J.Y., Zhu, Z.X., Li, Y.P., Yang, Z.Q., 2007a. Detrital zircon SHRIMP
1065 U-Pb dating of Carboniferous sandstone from the southern foot of the Harlik
1066 Mountains, eastern Xinjiang, and its geological implications. Geol. China 34,
1067 778-789 (in Chinese with English abstract).
1068 Sun, G.H., Li, J.Y., Zhu, Z.X., Li, Y.P., Yang, Z.Q., 2007b. Zircons SHRIMP U-Pb
1069 dating of gneissoid-biotite granite in Harlik Mountains, eastern of Xinjiang and
1070 its geological implications. Xinjiang Geol. 25, 1-10 (in Chinesewith English
1071 abstract).
1072 Sun, G.H., 2007. Structural deformation and tectonic evolution of Harlik Mountain, in
1073 Xinjiang since Paleozoic (in Chinese). Ph.D. thesis, Chinese Academy of
1074 Geological Science.

1075 Vernon, R.H., 1982. Isobaric cooling of two regional metamorphic complexes related
1076 to igneous intrusions in southern Australia. Geology 10, 76-81.
1077 Wali, G., Wang, B., Cluzel, D., Zhong, L.L., 2018. Carboniferous-Early Permian
1078 magmatic evolution of the Bogda Range (Xinjiang, NW China): Implications for
1079 the Late Paleozoic accretionary tectonics of the SW Central Asian Orogenic Belt.
1080 J. Asian Earth Sci. 153, 238-251.
1081 Wang, B., Cluzel, D., Shu, L.S., Faure, M., Charvet, J., Chen, Y., Meffre, S., de Jong,
1082 K., 2009a. Evolution of calc-alkaline to alkaline magmatism through
1083 Carboniferous convergence to Permian transcurrent tectonics, western Chinese
1084 Tianshan. Int. J. Earth Sci. 98, 1275-1298.
1085 Wang, B., Cluzel, D., Jahn, B.M., Shu, L.S., Chen, Y., Zhai, Y.Z., Branquet, Y.,
1086 Barbanson, L., Sizaret, S., 2014a. Late paleozoic pre- and syn-kinematic plutons
1087 of the Kangguer-Huangshan Shear zone: Inference on the tectonic evolution of
1088 the eastern Chinese north Tianshan. Am. J. Sci. 314, 43-79.
1089 Wang, B., Faure, M., Shu, L.S., de Jong, K., Charvet, J., Cluzel, D., Jahn, B.M., Chen,
1090 Y., Ruffet, G., 2010. Structural and geochronological study of High-Pressure
1091 metamorphic rocks in the Kekesu section (Northwestern China): implications for
1092 the late Paleozoic tectonics of the southern Tainshan. J. Geol. 118, 59-77.
1093 Wang, B., Shu, L.S., Faure, M., Jahn, B.M., Cluzel, D., Charvet, J., Chung, S.L.,
1094 Meffre, S., 2011a. Paleozoic tectonics of the southern Chinese Tianshan: Insights
1095 from structural, chronological and geochemical studies of the Heiyingshan

ophiolitic mélange (NW China). Tectonophysics 497, 85-104.

Wang, B.Y., Jiang, C.Y., Li, Y.J., Wu, H.E., Xia, Z.D., Lu, R.H., 2009b. Geochemistry and tectonic implications of Karamaili ophiolite in East Junggar of Xinjiang. J. Minearl. Petrol. 29, 74-82 (in Chinese with English abstract).

Wang, B., Zhai, Y.Z., Kapp, P., de Jong, K., Zhong, L.L., Liu, H.S., Ma, Y.Z., Gong, H.J., Geng, H.J., 2018a. Accretionary tectonics of back-arc oceanic basins in the South Tianshan: Insights from structural, geochronological, and geochemical studies of the Wuwamen ophiolite mélange. Geol. Soc. Am. Bull. 130, 284-306.

Wang, C., Chen, B., Ma, X.H., Yan, X.L., 2015. Petrogenesis of Early and Late Paleozoic plutons in Sanchakou area of East Tianshan and their implications for evolution of Kangur suture zone. J. Earth Sci. Environ. 5, 52-70 (in Chinese with English abstract).

Wang, C.S., Gu, L.X., Zhang, Z.Z., Wu, C.Z., Tang, J.H., Tang, X.Q., 2009c. Petrogenesis and geological implications of the Permian high-k calc-alkaline granites in Harlik Mountains of eastern Tianshan, NW China. Acta Petrol. Sin. 25, 1499-1511 (in Chinese with English abstract).

Wang, C.S., Gu, L.X., Zhang, Z.Z., Wu, C.Z., Tang, J.H., San, J.Z., Li, G.R., Li, Z.H., 2009d. Petrogenesis and tectonic implications of the Permian alkaline granite and quartz-syenite assemblage in Harlik Mountains, Xinjiang. Acta Petrol. Sin. 25, 3182-3196 (in Chinese with English abstract).

Wang, G.C., Zhang, M., Feng, J.L., Liao, Q.A., Zhang, X.H., Kang, L., Guo, R.L.,

1117 Xuan, Z.Y., Han, K.Y., 2019. New understanding of the tectonic framework and
1118 evolution during the Neoproterozoic-Paleozoic era in the East Tianshan
1119 Mountains. J. Geomech. 25, 798-819 (in Chinese with English abstract).
1120 Wang, X.S., Gao, J., Klemd, R., Jiang, T., Li, J.L., Zhang, X., Tan, Z., Li, L., Zhu,
1121 Z.X., 2014b. Geochemistry and geochronology of the Precambrian high-grade
1122 metamorphic complex in the Southern Central Tianshan ophiolitic mélange, NW
1123 China. Precambrian Res. 254, 129-148.
1124 Wang, X.S., Gao, J., Klemd, R., Jiang, T., Li, J.L., Zhang, X., Xue, S.C., 2017. The
1125 Central Tianshan Block: A microcontinent with a Neoarchean-Paleoproterozoic
1126 basement in the southwestern Central Asian Orogenic Belt. Precambrian Res.
1127 295, 130-150.
1128 Wang, Y.F., Chen, H.Y., Han, J.S., Chen, S.B., Huang, B.Q., Li, C., Tian, Q.L., Wang,
1129 C., Wu, J.X., Chen, M.X., 2018b. Paleozoic tectonic evolution of the
1130 Dananhu-Tousuquan island arc belt, eastern Tianshan: Constraints from the
1131 magmatism of the Yuhai porphyry Cu deposit, Xinjiang, NW China. J. Asian
1132 Earth Sci. 153, 282-306.
1133 Wang, Y.H., Zhang, F.F., Liu, J.J., 2016. The genesis of the ores and intrusions at the
1134 Yuhai Cu-Mo deposit in eastern Tianshan, NW China: Constraints from geology,
1135 geochronology, geochemistry, and Hf isotope systematics. Ore Geol. Rev. 77,
1136 312-331.
1137 Wang, Y.J., Yuan, C., Long, X.P., Sun, M., Xiao, W.J., Zhao, G.C., Cai, K.D., Jiang,

Y.D., 2011b. Geochemistry, zircon U-Pb ages and Hf isotopes of the Paleozoic volcanic rocks in the northwestern Chinese Altai: Petrogenesis and tectonic implications. J. Asian Earth Sci. 42 (5), 969-985.

Wang, Y.J., Long, X.P., Wilde, S.A., Xu, H.L., Sun, M., Xiao, W.J., Yuan, C., Cai, K.D., 2014c. Provenance of Early Paleozoic metasediments in the central Chinese Altai: Implications for tectonic affinity of the Altai-Mongolia terrane in the Central Asian Orogenic Belt. Lithos 210-211, 57-68.

Wang, Y., Li, J.Y., Sun, G.H., 2008. Postcollisional eastward extrusion and tectonic exhumation along the Eastern Tianshan Orogen, Central Asia: Constraints from dextral strike-slip motion and 40Ar/39Ar geochronological evidence. J. Geol. 116, 599-618.

Windley, B.F., Alexeiev, D., Xiao, W., Kröner, A., Badarch, G., 2007. Tectonic models for accretion of the Central Asian Orogenic Belt. J. Geol. Soc. Lond. 164, 31-47.

XBGMR (Xinjiang Bureau of Geology and Mineralogy Resources), 1966. Geological Map 1: 200000, Yiwu sheet (K-46-XI).

XBGMR (Xinjiang Bureau of Geology and Mineral Resources), 1993. Regional Geology of Xinjiang Uygur Autonomy Region. Geology Publishing House, Beijing, pp. 1-841 (in Chinese).

XGSC (Xi'an Geological Survey Center), 2007. Geological Map of Tianshan and Adjacent region (1:1,000,000).

Xia, L.Q., Zhang, G.W., Xia, Z.C., Xu, X.Y., Dong, Y.P., Li, X.M., 2002. Constraints

on the timing of opening and closing of the Tianshan Paleozoic ocenic basin: Evidence from Sinian and Carboniferous volcanic rocks. Geol. Bullet. China 21, 55-62 (in Chinese with English abstract).

Xia, L.Q., Xia, Z.C., Xu, X.Y., Li, X.M., Ma, Z.P., 2008. Relative contributions of crust and mantle to the generation of the Tianshan Carboniferous rift-related basic lavas, northwestern China. J. Asian Earth Sci. 31, 357-378.

Xia, L.Q., Xu, X.Y., Li, X.M., Ma, Z.P., Xia, Z.C., 2012. Reassessment of petrogenesis of Carboniferous-early Permian rift-related volcanic rocks in the Chinese Tianshan and its neighboring areas. Geosci. Front. 3, 445-471.

Xiao, B., Chen, H.Y., Wang, Y.F., Yang, J.T., 2015. Discovery of the Late Silurian granodiorite and its tectonic significance in the Tuwu-Yandong porphyry copper deposits, Dananhu-Tousuquan island arc, Eastern Tianshan. Earth Sci. Front. 22, 251-266 (in Chinese with English abstract).

Xiao, W.J., Mao, Q.G., Windley, B.F., Han, C.M., Qu, J.F., Zhang, J.E., Ao, S.J., Guo, Q.Q., Cleven, N.R., Lin, S.F., Shan, Y.H., Li, J.L., 2010. Paleozoic multiple accretionary and collisional processes of the Beishan orogenic collage. Am. J. Sci. 310, 1553-1594.

Xiao, W.J., Windley, B.F., Allen, M.B., Han, C.M, 2013. Paleozoic multiple accretionary and collisional tectonics of the Chinese Tianshan orogenic collage. Gondwana Res. 23, 1316-1341.

Xiao, W.J., Windley, B.F., Huang, B.C., Han, C.M., Yuan, C., Chen, H.L., Sun, M.,

Sun, S., Li, J.L., 2009. End-Permian to mid-Triassic termination of the accretionary processes of the southern Altaids: implications for the geodynamic evolution, Phanerozoic continental growth, and metallogeny of Central Asia. Int. J. Earth Sci. 98, 1189-1217.

Xiao, W.J., Zhang, L.C., Qin, K.Z., Sun, S., Li, J.L., 2004. Paleozoic accretionary and collisional tectonics of the Eastern Tianshan (China): Implications for the continental growth of Central Asia. Am. J. Sci. 304, 370-395.

Xiao, Y., Zhang, H.F., Shi, J.A., Su, B.X., Sakyi, P.A., Lu, X.C., Hu, Y., Zhang, Z., 2011. Late Paleozoic magmatic record of East Junggar, NW China and its significance: Implication from zircon U-Pb dating and Hf isotope. Gondwana Res. 20, 532-542.

Xie, W., Xu, Y.G., Chen, Y.B., Luo, Z.Y., Liu, H.Q., 2016a. High-alumina basalts from the Bogda Mountains suggest an arc setting for Chinese Northern Tianshan during the Late Carboniferous. Lithos 256, 165-181.

Xie, W., Xu, Y.G., Luo, Z.Y., Chen, Y.B., Hong, L.B., Ma, L., Ma, Q., 2016b. Petrogenesis and geochemistry of the Late Carboniferous rear-arc (or back-arc) pillow basaltic lava in the Bogda Mountains, Chinese North Tianshan. Lithos 244, 30-42.

Xie, W., Xu, Y.G., Luo, Z.Y., Liu, H.Q., Hong, L.B., Ma, L., 2016c. Petrogenesis and geodynamic implications of the Late Carboniferous felsic volcanics in the Bogda belt, Chinese Northern Tianshan. Gondwana Res. 39, 165-179.

Xu, X.W., Jiang, N., Li, X.H., Qu, X., Yang, Y.H., Mao, Q., Wu, Q., Zhang, Y., Dong, L.H., 2013. Tectonic evolution of the East Junggar terrane: Evidence from the Taheir tectonic window, Xinjiang, China. Gondwana Res. 24, 578-600.

Xu, X.W., Jiang, N., Li, X.H., Wu, C., Qu, X., Zhou, G., Dong, L.H., 2015a. Spatial-temporal framework for the closure of the Junggar Ocean in central Asia: New SIMS zircon U-Pb ages of the ophiolitic mélange and collisional igneous rocks in the Zhifang area, East Junggar. J. Asian Earth Sci. 111, 470-491.

Xu, X.W., Li, X.H., Jiang, N., Li, Q.L., Qu, X., Yang, Y.H., Dong, L.H., 2015b. Basement nature and origin of the Junggar terrane: New zircon U-Pb-Hf isotope evidence from Paleozoic rocks and their enclaves. Gondwana Res. 28, 288-310.

Xu, X.Y., Li, X.M., Ma, Z.P., Xia, L.Q., Xia, Z.C., Peng, S.X., 2006a. LA-ICP-MS zircon U-Pb dating of gabbro from the Bayingou ophiolite in the northern Tianshan Mountains. Acta Geol. Sin. 80, 1168-1176 (in Chinese with English abstract).

Xu, X.Y., Xia, L.Q., Ma, Z.P., Wang, Y.B., Xia, Z.C., Li, X.M., Wang, L.S., 2006b. SHRIMP zircon U-Pb geochronology of the plagiogranites from Bayingou ophiolite in North Tianshan Mountains and the petrogenesis of the ophiolite. Acta Petrol. Sin. 22, 83-94 (in Chinese with English abstract).

Yang, J.S., Xu, X.Z., Li, T.F., Chen, S.Y., Ren, Y.F., Li, J.Y., Liu, Z., 2011a. U-Pb ages of zircons from ophiolite and related rocks in the Kumishi region at the southern margin of Middle Tianshan, Xinjiang: Evidence of early Paleozoic oceanic basin.

Acta Petrol. Sin. 27, 77-95 (in Chinese with English abstract).

Yang, M., Wang, J.L., Wang, J.Q., Dang, F.P., 2012a. Studies on geochemistry, zircon U-Pb geochronology and Hf isotopes of granite in Wangfeng area at the northern margin of Middle Tianshan, Xinjiang. Acta Petrol. Sin. 28, 2121-2131 (in Chinese with English Abstract).

Yang, T.N., Li, J.Y., Zhang, J., Hou, K.J., 2011b. The Altai-Mongolia terrane in the Central Asian Orogenic Belt (CAOB): A peri-Gondwana one? Evidence from zircon U-Pb, Hf isotopes and REE abundance. Precambrian Res. 187, 79-98.

Yang, W.B., Niu, H.C., Shan, Q., Sun, W.D., Zhang, H., Li, N.B., Jiang, Y.H., Yu, X.Y., 2014. Geochemistry of magmatic and hydrothermal zircon from the highly evolved Baerzhe alkaline granite: Implications for Zr-REE-Nb mineralization. Miner. Deposita 49, 451-470.

Yang, X.F., He, D.F., Wang, Q.C., Tang, Y., Tao, H.F., Li, D., 2012b. Provenance and tectonic setting of the Carboniferous sedimentary rocks of the East Junggar Basin, China: Evidence from geochemistry and U-Pb zircon geochronology. Gondwana Res. 22, 567-584.

Yin, J.Y., Chen, W., Xiao, W.J., Yuan, C., Zhang, B., Cai, K.D., Long, X.P., 2017. Geochronology, petrogenesis and tectonic significance of the latest Devonian-early Carboniferous I-type granites in the Central Tianshan, NW China. Gondwana Res. 47, 188-199.

Yuan, C., Sun, M., Xiao, W.J., Li, X.H., Chen, H.L., Lin, S.F., Xia, X.P., Long, X.P.,

2007. Accretionary orogenesis of the Chinese Altai: Insights from Paleozoic granitoids. Chem. Geol. 242, 22-39.

Yuan, C., Sun, M., Wilde, S., Xiao, W.J., Xu, Y.G., Long, X.P., Zhao, G.C., 2010. Post-collisional plutons in the Balikun area, East Chinese Tianshan: Evolving magmatism in response to extension and slab break-off. Lithos 119, 269-288.

Yuan, Y., Zong, K.Q., He, Z.Y., Klemd, R., Liu, Y.S., Hu, Z.C., Guo, J.L., Zhang, Z.M., 2015. Geochemical and geochronological evidence for a former early Neoproterozoic microcontinent in the South Beishan Orogenic Belt, southernmost Central Asian Orogenic Belt. Precambrian Res. 266, 409-424.

Yu, J.Y., Guo, L., Li, J.X., Li, Y.G., Smithies, R.H., Wingate, M.T.D., Meng, Y., Chen, S.F., 2016. The petrogenesis of sodic granites in the Niujuanzi area and constraints on the Paleozoic tectonic evolution of the Beishan region, NW China. Lithos 256-257, 250-268.

Zeng, L., Niu, H., Bao, Z., Shan, Z., Li, H., Yang, W., 2015. Petrogenesis and tectonic significance of the plagiogranites in the Zhaheba ophiolite, Eastern Junggar orogen, Xinjang, China. J. Asian Earth Sci. 113, 137-150.

Zhang, J., Sun, M., Schulmann, K., Zhao, G.C., Wu, Q.H., Jiang, Y.D., Guy, A., Wang, Y.J., 2015a. Distinct deformational history of two contrasting tectonic domains in the Chinese Altai: Their significance in understanding accretionary orogenic process. J. Struct. Geol. 73, 64-82.

Zhang, W.F., Chen, H.Y., Han, J.S., Zhao, L.D., Huang, J.H., Yang, J.T., Yan, X.L.,

2016a. Geochronology and geochemistry of igneous rocks in the Bailingshan area: Implications for the tectonic setting of late Paleozoic magmatism and iron skarn mineralization in the eastern Tianshan, NW China. Gondwana Res. 38, 40-59.

Zhang, X.R., Zhao, G.C., Eizenhöfer, P.R., Sun, M., Han, Y.G., Hou, W.Z., Liu, D.X., Wang, B., Liu, Q., Xu, B., 2015b. Latest Carboniferous closure of the Junggar Ocean constrained by geochemical and zircon U-Pb-Hf isotopic data of granitic gneisses from the Central Tianshan block, NW China. Lithos 238, 26-36.

Zhang, X.R., Zhao, G.C., Sun, M., Eizenhöfer, P.R., Han, Y.G., Hou, W.Z., Liu, D.X., Wang, B., Liu, Q., Xu, B., 2016b. Tectonic evolution from subduction to arc-continent collision of the Junggar ocean: Constraints from U-Pb dating and Hf isotopes of detrital zircons from the North Tianshan belt, NW China. Geol. Soc. Am. Bull. 128, 644-660.

Zhang, Y.Y., Pe-Piper, G., Piper, D.J.W., Guo, Z.J., 2013. Early Carboniferous collision of the Kalamaili orogenic belt, North Xinjiang, and its implications: Evidence from molasse deposits. Geol. Soc. Am. Bull. 125, 932-944.

Zhang, Y.Y., Sun, M., Yuan, C., Long, X.P., Jiang, Y.D., Li, P.F., Huang, Z., Du, L., 2018. Alternating trench advance and retreat: Insights from Paleozoic magmatism in the eastern Tianshan, Central Asian Orogenic Belt. Tectonics 37, 2142-2164.

Zhang, Y.Y., Yuan, C., Long, X.P., Sun, M., Huang, Z.Y., Du, L., Wang, X.Y., 2017.

Carboniferous bimodal volcanic rocks in the Eastern Tianshan, NW China: Evidence for arc rifting. Gondwana Res. 43, 92-106.

Zhang, Y.Y., Yuan, C., Sun, M., Long, X.P., Huang, Z.Y., Jiang, Y.D., Li, P.F., Du, L., 2020. Two late Carboniferous belts of Nb-enriched mafic magmatism in the Eastern Tianshan: Heterogeneous mantle sources and geodynamic implications. Geol. Soc. Am. Bull. 132, 1404-1418.

Zhang, Z.W., Zang, Y.S., Wang, Y.L., Chen, S.B., 2016c. Zircon SHRIMP U-Pb age of the Yuhai prophyry copper deposit in Eastern Tianshan Mountains of Xinjiang and its tectonic implications. Acta Geosci. Sin. 37, 59-68 (in Chinese with English abstract).

Zhao, L.D., Chen, H.Y., Hollings, P., Han, J.S., 2019. Late Paleozoic magmatism and metallogenesis in the Aqishan-Yamansu belt, Eastern Tianshan: Constraints from the Bailingshan intrusive complex. Gondwana Res. 65, 68-85.

Zhao, M., Shu, L.S., Wang, C.Y., 1997. Characteristics of metamorphism in the Harlik Metamorphic Belt, east Xinjiang, and its tectonic envorionment. Geol. J. China Univ. 3, 40-50 (in Chinese with English abstract).

Zhao, M., Shu, L.S., Zhu, W.B., Wang, C.Y. Ma, R.S., 2002. Zircon U-Pb dating of the rocks from the Harlik Metamorphic Belt in eastern Xinjiang and its geological significance. Acta Geol. Sin. 76, 379-383 (in Chinese with English abstract).

Zheng, J.H., Chai, F.M., Feng, W.Y., Yang, F.Q., Shen, P., 2018. Geochemistry and

chronology of the early Paleozoic diorites and granites in the Huangtupo volcanogenic massive sulfide (VMS) deposit, Eastern Tianshan, NW China: Implications for petrogenesis and geodynamic setting. Lithos 302-303, 455-466.

Zhong, L.L., Wang, B., Shu, L.S., Liu, H.S., Mu, L.X., Ma, Y.Z., Zhai, Y.Z., 2015. Structural overprints of early Paleozoic arc-related intrusive rocks in the Chinese Central Tianshan: Implications for Paleozoic accretionary tectonics in SW Central Asian Orogenic Belts. J. Asian Earth Sci. 113, 194-217.

Zhong, L.L., Wang, B., Alexeiev, D.V., Cao, Y.C., Biske, Y.S., Liu, H.S., Zhai, Y.Z., Xing, L.Z., 2017. Paleozoic multi-stage accretionary evolution of the SW Chinese Tianshan: New constraints from plutonic complex in the Nalati Range. Gondwana Res. 45, 254-274.

Zhong, L.L., Wang, B., de Jong, K., Zhai, Y.Z., Liu, H.S., 2019. Deformed continental arc sequences in the South Tianshan: New constraintson the Early Paleozoic accretionary tectonics of the Central Asian Orogenic Belt. Tectonophysics 768, 228169.

Zhou, G.Q., 2004. The two-fold-contact metamorphic rocks occurring at Xiaopu, Hami, Eastern Xinjiang, their mineral paragenesis analysis and PTt path. Acta Mineral. Sin. 24, 290-300 (in Chinese with English abstract).

Zhu, X.H., Zhu, T., Zhang, X., Xi, R.G., Meng, Y., Wang, K., 2018. Petrogenesis and geological implications of late Carboniferous leucogranites in Harlik aera, eastern Xinjiang. Earth Sci. 43, 179-194 (in Chinese with English abstract).

Zhu, X., Wang, B., Chen, Y., Liu, H.S, 2019. Constraining the Intracontinental Tectonics of the SW Central Asian Orogenic Belt by the Early Permian Paleomagnetic Pole for the Turfan‐Hami Block. J. Geophys. Res. Solid Earth 124, 12366-12387.

Zong, K.Q., Klemd, R., Yuan, Y., He, Z.Y., Guo, J.L., Shi, X.L., Liu, Y., Hu, Z., Zhang, Z., 2017. The assembly of Rodinia: The correlation of early Neoproterozoic (ca. 900 Ma) high-grade metamorphism and continental arc formation in the southern Beishan Orogen, southern Central Asian Orogenic Belt (CAOB). Precambrian Res. 290, 32-48.

Figure and Table captions:

Fig. 1. (a) Tectonic sketch map of Eurasia showing the location of the Central Asian Orogenic Belt (modified from Sengör et al., 1993). (b) Sketch map of the northern Xinjiang area, NW China, showing tectonic subdivisions of the Chinese Tianshan (modified from Wang et al., 2014a). Abbreviations: NTB = North Tianshan Belt, CTB = Central Tianshan Belt, STB = South Tianshan Belt. (c) Geological map of the northeastern Tianshan Belt (modified from 1:1,000,000 scale geological map of the Chinese Tianshan and surrounding regions, after XGSC, 2007).

Fig. 2. (a) Geological map of the Harlik Range, North Tianshan (modified from 1:200,000 scale geological map No. K-46-XI by XBGMR, 1966). (b) Detailed

geological map of the Qincheng area, North Tianshan showing the metamorphic zone and sampling sites (modified from Sun, 2007). Dating results are from Sun, 2007; Chen and Shu, 2010. Abbreviations: Bt = Biotite Ar-Ar age, Mus = Muscovite Ar-Ar age, Zr = Zircon U-Pb age. (c) Cross-section of the Julideneng Metamorphic Complex (JMC) in the Qincheng area showing the occurrence of migmatites and sampling sites. Stereograms of the bedding and foliation are equal-area Schmidt net, lower hemisphere.

Fig. 3. Representative field photographs of meta-sedimentary rocks and migmatites in the Qincheng area, North Tianshan. (a) Weakly deformed and metamorphosed sandstone and siltstone. The cleavage S1 is steeper than the bedding S0 indicating a normal sequence. (b) Migmatite with leucosome (Leu), melanosome (Mel) and mesosome (Mes). (c) Parallel and consistent foliations in gneissic-granite and schist. (d) Migmatite with irregular transition between leucosome and melanosome. (e) Faulted contact between meta-sandstones and migmatites.

Fig. 4. Photomicrographs of metamorphic rocks and migmatites from the Qincheng area, North Tianshan. (a-c) Micaschists (12TS119A, B and E) showing preferred orientations of mica and sillimanite. (d) Meta-sandstone (12TS119F) with weak orientation of chloritized mica and tabular feldspar grains. (e) Cuspate and lobate grain boundaries between plagioclase and quartz with chessboard subgrains

(12TS119G). (f) Optically continuous K-feldspar enclosing diamond-shaped quartz crystals in leucosome (12TS119H). Mineral abbreviations: Kf = K-feldspar; Bt = biotite; Chl = chlorite; Mus = muscovite; Pl = plagioclase; Qz = quartz; Sil = sillimanite.

Fig. 5. Cathodoluminescence images for representative zircons from meta-sandstone (12TS119F) and mica schists (12TS119A, B and E) showing their apparent $^{206}Pb/^{238}U$ ages (<1000 Ma) or $^{207}Pb/^{206}Pb$ ages (>1000 Ma). Four types of zircons can be recognized. See text for more explanations. The CL images of all the dated zircons can be found in Supplementary Fig. S1.

Fig. 6. Concordia diagrams (a, c, e and g) and U-Pb age probability diagrams (b, d, f and h), and insets are plots of Th/U ratios vs. U-Pb age for detrital zircons from the meta-sedimentary rocks, southern Harlik Range.

Fig. 7. Chondrite-normalized REE patterns for detrital zircons from meta-sandstone 12TS119F (a), mica schist 12TS119E (b), and two migmatites 12TS119G and 12TS119H (c-d). Only the Paleozoic detrital zircons with $^{206}Pb/^{238}U$ ages between 425 Ma and 475 Ma were analyzed for REE abundances. The grey shaded area is the REE composition of hydrothermal zircons (after Hoskin, 2005; Yang et al., 2014) and magmatic zircons of various igneous rocks (Belousova et al., 2002; Hoskin, 2005;

Long et al., 2012a; Yang et al., 2014). Insets are plots of Th/U ratios against U-Pb age. Chondrite normalization values are from Sun and McDonough (1989).

Fig. 8. (a-b) Cathodoluminescence images showing $^{206}Pb/^{238}U$ apparent ages, (c-d) Concordia diagrams, and (e-f) U-Pb age probability diagrams for the zircons from the migmatites, Qincheng area, North Tianshan.

Fig. 9. (a) Compilation of zircon U-Pb ages for granites crosscutting the meta-sedimentary rocks of the Harlik area (data from Sun et al., 2007b; Wang et al., 2009c; Chen and Shu, 2010; Chen et al., 2016; Song et al., 2018). (b) U-Pb age spectra of Paleozoic zircons from the migmatites and meta-sedimentary rocks of the Qincheng area (this study), North Tianshan.

Fig. 10. Compilation of zircon U-Pb ages from the Qincheng area and neighboring tectonic units. The right columns show the age distributions of Precambrian zircons only. DZ: Detrital zircons from sedimentary rocks; IZ: Zircons from igneous rocks (Inherited zircons were excluded). All the reference data and corresponding literature are listed in Supplementary Table S2.

Fig. 11. Tentative cartoon model for the Paleozoic tectonic evolution of the North Tianshan Belt and adjacent areas.

Table 1. Sample description and analytical data summary.

Supplementary Fig. S1. Cathodoluminescence images for all the dated detrital zircons from the meta-sedimentary rocks, Qincheng area, North Tianshan.

Supplementary Fig. S2. Discrimination diagrams for magmatic and hydrothermal zircons of the meta-sedimentary rocks and migmatites (after Hoskin, 2005). (a, c, e and g) $(Sm/La)_N$ (chondrite-normalized Sm/La ratio) vs. La (ppm) plots. (b, d, f and h) Ce/Ce* (Ce anomaly) vs. $(Sm/La)_N$ plots. Chondrite normalization values are from Sun and McDonough (1989).

Supplementary Table S1. LA-ICP-MS zircon U-Pb analytical results of the meta-sedimentary rocks and migmatites from the Qincheng area, North Tianshan.

Supplementary Table S2. REE abundances of representative zircons of meta-sedimentary rocks and migmatites from the Qincheng area, North Tianshan.

Supplementary Table S3. Compilations of zircon U-Pb ages from the Qincheng area, North Tianshan and the neighboring Central Tianshan, East Junggar, and Chinese Altai.

1431

Late Paleozoic tectonic evolution of the North Tianshan Belt: New structural and geochronological constraints from meta-sedimentary rocks and migmatites in the Harlik Range

Xinghua Ni [a], Bo Wang [a, b,]*, Dominique Cluzel [bc], Jiashuo Liu [a], Zhiyuan He [a]

[a] *State Key Laboratory for Mineral Deposits Research, School of Earth Sciences and Engineering, Nanjing University, 210023 Nanjing, China*

[b] *Institute of continental geodynamics, Nanjing University, 210023 Nanjing, China*

[b c] *Institut de Sciences Exactes et Appliquées, Université de la Nouvelle-Calédonie, BP R4, 98851 Noumea Cedex, New Caledonia*

* Corresponding author: (B. Wang)

Address: School of Earth Sciences and Engineering, Nanjing University, 163# Xianlin Avenue, Nanjing 210046, P.R. China

Email: bwang@nju.edu.cn; burh_cw@yahoo.com

Abstract

The North Tianshan Belt (NTB) formed by the subduction and accretion of the

Junggar Ocean is a key area for reconstructing the Paleozoic tectonic evolution of the southern Central Asian Orogenic Belt (CAOB). Despite numerous studies ~~have been done~~, the interpretation of the late Paleozoic tectonic evolution of the NTB meets no consensus yet. We conducted field investigations and LA-ICP-MS zircon U-Pb dating on ~~the~~ metamorphic rocks ~~of~~from the ~~Upper Carboniferous Julideneng Formation~~ Julideneng Metamorphic Complex (JMC) in the Harlik Range, which is located between the Turpan-Hami Basin to the south and the East Junggar Belt to the north~~west~~. The metamorphic rocks are exposed in a NW-SE striking, ~10 km-wide belt and mainly composed of migmatites, garnet-sillimanite mica schists, andalusite schists, and low-grade meta-sandstones. Detrital zircons from the low-grade meta-sandstone yielded ages of 1400-1250, 1000-850, ~780, ~580, ~490, ~445 and ~425 Ma. Three mica ~~-~~schists contain zircon populations of 2500-2175, 1800-1600, 1500-1100, 1000-850, 800-500, ~475, ~425, 420-380, ~346 Ma, and a youngest age peak at ~322 Ma. Two samples of leucocratic dykes in migmatites yielded comparable age populations with two major peaks at 322 Ma and 297 Ma, which ~~may be~~are interpreted as ~~the minimum age of youngest protolith~~two stages of successive partial melting and ~~anatectic~~ anatexic ~~magma~~ melts crystallization ~~respectively~~. On the basis of structural features, zircon textures and U-Pb ages, combin~~ed~~ed~~ing~~ with ~~the~~ already published data, we propose that: (1) the meta-sedimentary rocks of the ~~Julideneng Formation~~JMC were deposited ~~between~~ after 425 Ma and before 322 Ma (latest Silurian to ~~early L~~late Carboniferous); (2) the Precambrian detrital zircons in the

meta-sedimentary rocks were probably derived from the Central Tianshan Block, which was once connected with the NTB; and (3) the ~~migmatisation~~ migmatization and coeval granitic plutonism occurred at ~322-297 Ma (l~~L~~ate Carboniferous), most likely associated with crustal thinning resulted ~~in~~from ~~a~~ continent-based~~n~~ intra-arc or back-arc ~~setting to~~or post-orogenic extension ~~setting~~. ~~a late- to post-orogenic setting.~~

Keywords: Central Asian Orogenic Belt; East Junggar~~-Balkash Ocean~~; North Tianshan (Tien Shan); accretionary orogeny; post-orogenic crustal thinning; migmatization

1. Introduction

The Tianshan Orogen is located in the southernmost part of the Central Asia Orogenic Belt (CAOB), which is one of the largest Phanerozoic orogenic systems on the Earth (Şengör et al., 1993; Windley et al., 2007; Xiao et al., 2013; Safonova, 2017). It recorded the Paleozoic ~~subduction~~consumption of the southern ~~domains of the~~ Paleo-Asian Ocean domains (i.e., the Junggar-~~Balkash~~ North Tianshan Ocean and Paleo-Tianshan Ocean or Turkestan Ocean), successive accretion of ~~various tectonic units including~~ island arcs, accretionary wedges and microcontinents, ~~and~~as well as the final amalgamation/collision ~~of~~between the Kazakhstan and Tarim blocks (e.g., Gao et al., 1998, 2009; Li ~~et al.~~, 2004~~, 2006, 2009~~; Xiao et al., 2004, 2013; Charvet et

al., 2007, 2011; Han et al., 2011; –Wang et al., 2008, 2011a, 2018a; Han et al., 2011). Deciphering the subduction-accretion processeses of this belt is therefore helpful for a better understanding of the Paleozoic evolution of the southwestern CAOB and Phanerozoic Asia crustal growth (Han and Zhao, 2018; Huang et al., 2020).

Numerous studies on the Tianshan Orogen were conducted throughfocusing on kinematic analysis (e.g., Charvet et al., 2007, 2011; Lin et al., 2009; Wang et al., 2010, 2018a), characteristics of ophiolitess geochemistry (e.g., Shu and Wang, 2003; Dong et al., 2006; Xu et al., 2006a, 2006b, 2015a; Shu et al., 2007; Wang et al., 2009b, 2011a, 2018a; Huang et al., 2012; Jiang et al., 2014), geochemistry of arc-related magmatic rocks (e.g., Chen et al., 2013; Xie et al., 2016a, 2016b, 2016c; Zhang et al., 2017; Wali et al., 2018) and post-collisional magmatism (e.g., Gu et al., 1999; Shu et al., 2005, 2011; Wang et al., 2009a, 2014a; Chen and Shu, 2010; Yuan et al., 2010; Chen et al., 2011; Muhtar et al., 2020). Based on these results, various tectonic models have beenwere proposed but no consensus washas been achieved (e.g., Gao et al., 2009; Charvet et al., 2011; Xiao et al., 2013; Wang et al., 2018a; Han and Zhao, 2018). The controversy arises mainly aboutover (1) the regional correlation of various magmatic arcs, and (2) the timing of the final amalgamation of the Tianshan Orogen. Late Paleozoic magmatic arcs were diversely correlated with the subduction of the South Tianshan Ocean, the Junggar-North Tianshan Ocean and the Kalamaili Ocean (e.g., Xiao et al., 2004, 2013; Charvet et al., 2007, 2013; Han and Zhao, 2018). The endtermination of accretion was controversially estimated to be Devonian-early

Carboniferous (Xia et al., 2002, 2012; Ma et al., 2015), late Carboniferous-early Permian (Gao et al., 1998, 2009; Charvet et al., 2007, 2011; Han et al., 2010, 2011; Wang et al., 2010, 201414a, 2018a; Han et al., 2010, 2011; Han and Zhao, 2018), or end-Permian to mid-Triassic (Xiao et al., 2009; Chen et al., 2020).

The Harlik Range is located in the northeastern part of the Tianshan Orogen and where the latter connects with the East Junggar Belt to the northeast., thus, iIt is a key area for unraveling the tectonic evolution of the Tianshan Orogen (Xiao et al., 2004; Huang et al., 2018). The tectonic setting and evolution of the Harlik Range remain a matter of debate. Xia et al. (2002, 2012) proposed that it underwent intra-continental rifting in Carboniferous to Permian time; while some other authors suggested a volcanic arc setting during the Ordovician-Carboniferous (Xiao et al., 2004; Ma et al., 2015; Du et al., 2018aHan and Zhao, 2018). Additionally, Sun (2007) proposed that it experienced an Ordovician-Silurian arc and a Devonian-Carboniferous back-arc extension.

Meta-sedimentary rocks and migmatites are well exposed in the southern Harlik Range (Fig. 2b), they may provide key evidence for the Paleozoic tectonic evolution of the North Tianshan Belt. However, these metamorphic rocks were poorly studied. They were ever considered as late Carboniferous in age (XBGMR, 1966; Sun et al., 2007a), but the depositional ages of their protoliths were not well constrained (Cao et al., 2009). Furthermore, the timing and tectonic setting of the metamorphism were diversely interpreted as (~~i~~i) two-stage regional metamorphism associated with

Carboniferous intra-arc rifting and Permian collision~~, respectively~~ (Zhao et al., 1997); (~~i~~ii) contact metamorphism during the Carboniferous and Permian magmatism (Zhou et al., 2004); or (~~iii~~iii) Permian dynamic metamorphism ~~under~~ during post-collisional extension ~~setting~~ (Sun, 2007).

In this study, we present new field structural observations and zircon LA-ICP-MS U-Pb ages ~~for~~of the meta-sedimentary rocks and migmatites from the Harlik Range. These new results combined with ~~the already~~previously ~~previous studies~~published data allow us to better constrain the ~~depositional and metamorphic ages~~timing ~~of~~ of protoliths deposition and metamorphism of these ~~metamorphic~~ meta-sedimentary rocks, to discuss the provenance~~s~~ of the ~~meta-sedimentary rocks~~sediments, and to ~~decipher the significance of the~~ tentatively replace the high-temperature metamorphism and anat~~a~~exis ~~and~~regarding in the framework of the late Paleozoic tectonic evolution of the North Tianshan Belt.

2. Geological background

2.1. *Regional tectonic framework*

The Chinese segment of the Tianshan Orogen is geographically divided into eastern and western parts along the Urumqi-Korla ~~road~~line. The eastern Chinese Tianshan is further divided into three tectonic units as~~:~~ the South Tianshan, Central Tianshan and North Tianshan belts ~~belts~~ (Fig. 1b; Xiao et al., 2004; Li et al., 2006;

Charvet et al., 2007~~, 2009~~). These units are separated from each other by two major faults~~,~~ (namely the Main Tianshan Shear Zone and Baluntai-Xingxingxia Fault), which are dextral strike-slip faults active mainly during the Permian along reactivated older suture zones ~~represented by ophiolitic mélanges~~ (Laurent-Charvet et al., ~~2002,~~ 2003; ~~Shu et al., 2002;~~ Charvet et al., 2007; Wang et al., 2008, 2009, 2014a; de Jong et al., 2009; He et al., 2021).

The South Tianshan Belt (STB) is connected with the northern margin of the Tarim Block and mainly consists of ophiolitic mélanges and Cambrian to Carboniferous sedimentary and volcanic rocks (XBGMR, 1993). These rocks are locally metamorphosed and imbricated within several thrust-and-fault belts (Charvet et al., ~~2007,~~ 2011). The western STB was formed by the amalgamation of the Tarim Block and the Central Tianshan Belt following the closure of the South Tianshan Ocean and several back-arc basins (Gao et al., 1998, 2009; Xiao et al., 2004; Han et al., 2011; Wang et al., 2011a, 2018a; Huang et al., 2018; Zhong et al., 2019). In contrast, the eastern STB (~~now corresponds to~~also named the Beishan Belt) was~~,~~ formed by the accretion of several ~~Precambrian~~ Precambrian-based magmatic-arc terranes (Yuan et al., 2015; Yu et al., 2016; Zong et al., 2017; He et al., 2018a) and ophiolitic mélanges during the Paleozoic (Xiao et al., 2010; Ao et al., 2012; Song et al., ~~2013,~~ 2015; Shi et al., 2018).

The Central Tianshan Belt (CTB) is composed of a Precambrian basement (Liu et al., 2004; Hu et al., 2010; Ma et al., ~~2012a,~~ 2012b; He et al., 2014~~, 2018b~~; Wang et

al., 2014b, 2014d, 2017; Han and Zhao, 2018; Huang et al., 2019), Ordovician to early Devonian arc-related volcanic and sedimentary sequences, and early Paleozoic to early Mesozoic intrusive rocks (Xiao et al., 2004, 2013; Shi et al., 2007; Dong et al., 2011; Lei et al., 2011; Ma et al., 2013, 2014; Zhong et al., 2015; Du et al., 2018a; Han and Zhao, 2018; He et al., 2018b). Both the basement and arc-type rocks are unconformably overlain by unmetamorphosed Carboniferous to Permian sedimentary coverssediments (XBGMR, 1993; Xiao et al., 2013). The CTB is considered either as an independent Precambrian micro-continent involved in the accretion of the Tianshan Orogen (Hu et al., 2000; Huang et al., 2015b, 2017) or as a part of the northern Tarim, which was drifted off and then re-amalgamated with Tarim due to the opening and closure of the South Tianshan back-arc basins (Charvet et al., 2007, 2011; Wang et al., 2008, 2011a, 2018a; Lei et al., 2011; Ma et al., 2012a, 2012b, 2014; Huang et al., 2015a; Gao et al., 2015; Zhong et al., 2015, 2017, 2019, 2019).

The North Tianshan Belt (NTB) refers to the domain between the CTB to the south and the East Junggar Belt to the north (Fig. 1b). This belt is predominantly composed of Ordovician to Carboniferous volcano-sedimentary sequences and crosscut by Paleozoic granitoidsassociated granitesic intrusions (XBGMR, 1993). It is considered as a Paleozoic arc system formed by southward subduction of the Kalamaili Ocean (Zhao et al., 2002; Xiao et al., 2004; Yuan et al., 2010; Xie et al., 2016a, 2016b, 2016c), and/or by northward subduction of the North Tianshan Ocean (Sun, 2007; Ma et al., 2015; Zhang et al., 2017, 2018; Du et al., 2018a; Han and Zhao,

2018; Chen et al., 2019). The NTB is further divided into three sub-units, i.e., the Harlik-Dananhu Arc, Bogda ~~Belt~~ Arc and Kangguer-Yamansu ~~Belt~~ Arc (e.g., Xiao et al., 2004) ~~covering~~ unconformably covered by the Mesozoic-Cenozoic Turpan-Hami Basin ~~whichthat is now filled bywith Mesozoic-Cenozoic sedimentary rocks~~ (Fig. 1b; XBGMR, 1993).

The Harlik-Dananhu Arc occurs on both north and south sides of the Turpan-Hami Basin, either formed by the breakup of a single arc due to intra-arc rifting (~~Zhao et al., 2002;~~ Xiao et al., 2004; Ma et al., 2015) or resulted from southward migration of the magmatic front ~~forming~~ that generated the Harlik ~~Arc~~ and Dananhu ~~A~~arcs~~,~~ successively (Sun, 2007). The Bogda ~~Belt~~ Arc is generally interpreted as a Carboniferous magmatic arc and Permian post-collisional magmatic belt (Shu et al., ~~2005,~~ 2011; Chen et al., 2011; Xie et al., 2016a~~, 2016b~~; Wali et al., 2018), although some authors suggested a Carboniferous ~~(~~to Permian~~)~~ rift ~~system~~ (Gu et al., 2000, 2001; Xia et al., 2008, 2012). The Kangguer-Yamansu ~~Belt~~ Arc is a late Paleozoic arc/fore-arc system (Xiao et al., 2004; Han and Zhao, 2018) ~~whichthat was affected~~reworked by Permian ~~post-orogenic post-collision/post-orogenic~~intracontinental dextral ductile ~~dextral~~ shear~~ing~~ zone (Wang et al., 2008, 2014a; Branquet et al., 2012; Zhu et al., 2019).

2.2. Geological background of the Harlik Range

The Harlik Range (or Harlik Arc) is situated between the Turpan-Hami Basin to

the south and the East Junggar Belt to the northeast (Fig. 1b). The oldest stratigraphic unit is the Ordovician Huangcaopo Group, which occurs along the northern foot of the Harlik Range. It mainly consists of weakly metamorphosed marine clastic rocks and tuffs (Ma et al., 1997; Chen et al., 2014). The Silurian strata are barely exposed in the Harlik Range (XBMGR, 1993; Sun, 2007). Ordovician-Silurian (470-420 Ma) intrusions in the Harlik Range mostly belong to calc-alkaline or tholeiitic series and show typical subduction-related geochemical features associated with positive mantle-like whole-rock $\varepsilon_{Nd}(t)$ and zircon $\varepsilon_{Hf}(t)$ values (Ma et al., 2015; Wang et al., 2016, 2018b; Du et al., 2018a; Han and Zhao, 2018).

The Devonian strata, previously defined byaccording to regional facies correlation, are mainly composed of volcanic rocks, carbonates and siliciclastic rocks (XBGMR, 1993). The Lower Devonian Dananhu Formation is distributed along the southern Harlik Range and the southern margin of the Turpan-Hami Basin (Fig. 1c). The Middle Devonian Tousuquan Formation is developrecognized along the ridge of the Harlik Range., from which, however, sSome rhyolites from this formation, however, yielded zircon U-Pb ages of 469 ± 9 Ma (Li et al., 2017) and were intrudinged by granitoids were dated at 446 ± 3 Ma to 448 ± 7 Ma (Cao et al., 2006; Liu et al., 2017), indicating that some rocks in the Tousuquan Formation should be assigned to the Ordovician. MIn the meanwhile, Tthe Upper Devonian sediments isare rare in the Harlik Range and thus were poorly studiedinvestigated.

The Carboniferous strata can be divided into lower and upper units. The lower

unit includes the Jiangbasitao and Xiaorequanzi formations, which mainly consist of volcaniclastic and volcanic rocks (XBMGR, 1993). The upper unitoneunit, previously named as Julideneng Formation, is distributed along the southern foot of the Harlik Range and is mainly composed of tuffs, sandstones and tuffaceous sandstones (Sun, 2007). Some of these rocks which occur THowever, tto the north of the Qincheng Town, some of these rocks were metamorphosed into greenschist to amphibolite facies (Zhao et al., 1997; Zhou, 2004; Sun, 2007) and their protoliths ages and timing of metamorphism remain unclear. In this study, we separate these metamorphic rocks from the Julideneng Formation and call them as the Julideneng metamorphic complex (JMC). The Carboniferous calc-alkaline diorites and granites from the Harlik Range were formed at 320-300 Ma. These granitoids were likely emplaced during the tectonic transition from convergence to extension (Sun et al., 2005; Song et al., 2018; Zhu et al., 2018).

The Lower Permian strata, unconformably overlying the pre-Permian rocks, are mainly composed of unconformable terrestrial conglomerates, sandstones and siltstones intercalated with volcanic rocks, unconformably overlying the older strata (Sun, 2007; Shu et al., 2011; Chen et al., 2014). The Permian granitoids are transitional from calc-alkaline to alkaline (Wang et al., 2009) and yielded zircon U-Pb ages of 298-280 Ma (Wang et al., 2009c; Yuan et al., 2010; Chen et al., 2016refs.). They are usually associated with coeval mafic dykes, both were formed in an extensional or transtensional setting (Gu et al., 1999; Wang et al., 2009c, 2009d; Chen

and Shu, 2010; Yuan et al., 2010; Chen et al., 2016).

3. Field geology and sample descriptions

FOur field investigations were conducted along a section from Qincheng Town to Xiaopu Village, southern Harlik Range (Figs. 2a-2b). The southern part of the section is dominated by variablyvarious schistose tuffs, sandstones and tuffaceous sandstones belonging to the upperUpper Carboniferous Julideneng Formation.; Tthe northern part of theis section consists of Mmiddle Devonian sandstones, tuffaceous sandstones and limestones, which were silicified and crosscut by numerous diabase dykes inshowing NE-SW or nearly E-W strikinges (Fig. 2b; XBGMR, 1966; Sun, 2007). The central part of the section, in between , is a occupied by NW-SE-striking belt of of metamorphic rocks, occurring inalong a NW-SE-striking belt, which extends for >30 km long and ~10 km wide (Figs. 2a-2b; Zhao et al., 1997, 2002; Sun, 2007).), this belt is made of These metamorphic rocks of the Julideneng metamorphic complex (JMC), includeing garnet-sillimanite mica schists, low-grade meta-sandstones, andalusite schists, low-grade meta-sandstones garnet-sillimanite mica schists and migmatites (Zhao et al., 1997; Zhou, 2004; Sun, 2007)., Consequently, we to which we propose there to give the name of suggest naming this metamorphic belt as Julideneng Metamorphic Complex (JMC).

In the southern part of the JMCmetamorphic belt, the sedimentary rocks were weakly deformed and slightly metamorphosed. The bedding (S0) can be easily

recognized ~~while~~and cleavage (S1) is well developed, both dip to the northeast with S1 steeper than S0 (Figs. 2b~~, 2~~c and 3a), indicating a normal sequence. Further northwards, S0 is gradually transposed into sub-vertical schistosity with increasing metamorphic grade (Sun, 2007). A ~~migmatite zone of ~1 km wide~~ migmatite zone of ~1 km wide occurs in the northern part of the JMC~~metamorphic belt~~. Migmatites are typically flow-folded (Sawyer, 2008) and contain ~~cm~~centimeter-thick ~~leucocratic~~, ~~locally~~ garnet-bearing leucocratic ~~bodies~~dykes.~~,~~ ~~which~~They display all the intermediates between folded and boudinaged leucosome ribbons, foliated (orthogneissic) sills and ~~crosscutting,~~ slightly foliated crosscutting dykes. Leucosomes are surrounded by melanosomes with biotite-rich boundaries and restites of meta-sandstone (Fig. 3b). Foliation in the migmatites is roughly ~~concordant~~ in accordance with that in the surrounding meta-sedimentary rocks (Fig. 3c). Flow-folded migmatites and slightly folded small-scale garnet-bearing leucocratic dykes (Fig. 3b and 3d) ~~illustrate~~indicate a continuum from pre- to late-tectonic in situ partial melting and short-distance transport of ~~anatectic~~ anatexic melts. A progressive lateral change from migmatites into quartzites, schists and crinoidal limestone can be observed farther to the west, and restites of quartzite and limestone (changed into calc-silicate) occur in migmatites more to the north.

The southwestern border of the migmatite zone is in fault contact with weakly deformed meta-sandstones (Figs. 2c and 3e). The fault zone, ~5-10 meters ~~wide~~in width, ~~is~~was strongly sheared with schistosity/cleavage dipping 70-75° to the south.

~~Owing to~~Considering the difference ~~of~~in metamorphic grade, there was probably a bulk normal-fault motion ~~is likely~~ (Fig. 2c).~~;~~ ~~however~~~~On the other hand~~In addition, the complex deformation of the fault zone likely suggests a polyphase motion. The northern side of the migmatite zone was~~is~~ crosscut by a coarse-grained K-feldspar granite dated at 297 ± 2 Ma (zircon U-Pb age; Chen and Shu, 2010). To the north, the granite is in fault contact with low-grade meta-sedimentary rocks of the Middle Devonian Tousuquan Formation (Fig. 2b~~ and 2~~-c). The boundary is an E-~~W~~ W-striking mylonite zone dipping steeply to the north, which bears a down-dip stretching lineation. Kinematic indicators in ductilely deformed granites ~~suggest a top-down-to-the-north shearing and thus~~ are consistent with a normal-fault motion. Therefore, the high-grade migmatite zone appears in a kind of horst or pop-up structure surrounded by lower-grade meta-sedimentary rocks. Late Carboniferous-~~early~~ ~~E~~early Permian (~~U-Pb~~ zircon U-Pb ages~~:~~ ~~from~~of 316~~ to ~~-295 Ma) undeformed granodiorite, biotite granite, leucogranite ~~and~~as well as numerous NE-striking pegmatite and mafic dykes crosscut and thus post-date the metamorphic belt (~~Figs. 2b and 2-c); (~~Wang et al., 2009c; Chen and Shu., 2010; Song et al., 2018; Zhu et al., 2018). In addition, the meta-sedimentary rocks yielded ~~early~~ Early Permian ~~mica~~ muscovite and biotite $^{40}Ar/^{39}Ar$ cooling ages ranging from 301 to 277 Ma (Sun, 2007).

In order to ~~further~~ constrain the ages and provenances of the meta-sedimentary rocks, and the timing of the migmatization, six representative samples were collected

289 from the ~~metamorphic belt~~JMC ~~and were further analyzed~~. Three mica-schist samples
290 (12TS119A, B, E) were taken from the migmatite zone (Fig. 2c). The sample
291 12TS119A is ~~mainly~~ composed of quartz (45-50 vol. %), biotite (20-25 vol. %),
292 plagioclase (10-15 vol. %), muscovite (5-10 vol. %) and a small amount of sillimanite.
293 The sample 12TS119B is a mylonitized mica-schist and main~~ost~~ly consists of quartz
294 (30-35 vol. %), biotite (20-25 vol. %), muscovite (30-35 vol. %) and plagioclase (5-10
295 vol. %). Another slightly altered sample 12TS119E is ~~primarily made up~~composed of
296 quartz (30-35 vol. %), chloritized biotite (20-25 vol. %), muscovite (10-15 vol. %),
297 sericite (20-25 vol. %) and minor sillimanite (< 5 vol. %). In these mica-schists, the
298 preferred orientation of biotite and/or muscovite and elongated quartz grains define ~~a~~
299 well-developed foliations (Fig~~s~~. 4a-~~4~~c).

300 One sample (12TS119F; Fig. 2c) was collected from the meta-sandstones that
301 are in fault contact with the migmatites (Fig. 3e). This meta-sandstone is mainly
302 composed of quartz (60-70 vol. %), chloritized mica (10-15 vol. %) and plagioclase
303 (15-20 vol. %). The chloritized micas are weakly oriented ~~to form~~and define an
304 almost unnoticeable foliation~~s that are sometimes unremarkable~~ due to ~~mostly~~ the
305 fine-grain~~ed,~~ and ~~angular~~ equidimensional shape of quartz and plagioclase (Fig. 4d).
306 ~~Intensive~~ U~~u~~ndulose extinction and bulging dynamic recrystallization of quartz ~~can be~~
307 ~~commonly observed under~~in ~~thin sections~~ (Fig~~s~~. 4a-~~4~~d)~~,~~ indicat~~e~~ing ~~a~~ ductile
308 deformation of these meta-sedimentary rocks under moderate temperature conditions.

309 ~~Additional t~~Two ~~more~~ samples were taken from ~~migmatitic gneissic~~

~~granite~~migmatitic gneissic-granite ~~—~~(12TS119G) and migmatite leucosome (12TS119H) (Fig. 3d). Both of them are mainly composed of quartz (40-45 vol. %), K-feldspar (25-30 vol. %), plagioclase (20-25 vol. %) and minor muscovite and biotite (Fig~~s~~. 4e-~~4~~f). The ~~migmatitic gneissic granite~~migmatitic gneissic-granite shows a clear foliation~~s~~ defined by the preferred orientation of mica~~s~~ and elongated quartz ribbons (Fig. 3c). The feldspar and quartz exhibit lattice bending, subgrains, undulose extinction and deformation bands, suggesting that these grains accommodated intracrystalline plastic deformation by dislocation creep (Fig. 4e; Gower and Simpson, 1992; Hirth and Tullis, 1992; Passchier and Trouw, 2005). In addition, typical chessboard subgrains in quartz and lobate grain boundaries between quartz and feldspar ~~were~~are ~~interpreted to~~ indicate high-temperature ductile deformation ~~under high-temperature conditions~~ (Gower and Simpson, 1992; Kruhl, 1996~~;~~ Stipp et al., 2002~~; Rosenberg and Stünitz, 2003; Zibra et al., 2012~~). By contrast, the migmatite leucosome (12TS119H) shows nearly equant and diamond-shaped quartz crystals enclosed by optically continuous K-feldspar (Fig. 4f), indicating that ~~the~~ quartz ~~likely~~ crystallized from ~~the anatectic~~ anatexic melt~~s~~ before K-feldspar crystallized from the remaining melt~~s~~ (Sawyer, 2008). Undulose extinction and recrystallization by grain boundary migration of quartz (Fig. 4f) suggest localized high-temperature ductile deformation ~~under high-temperature~~.

4. **Analytical methods**

All samples were crushed and milled into powders, from which zircon grains were separated by ~~using~~ heavy liquid and magnetic separation~~or~~, and finally handpicked under a binocular microscope fitted with a UV light. Selected zircon grains were mounted in epoxy, polished to about half of their thickness, and then coated with gold. Cathodoluminescence (CL) images of zircons were ~~conducted~~ obtained at the State Key Laboratory for Mineral Deposits Research (SKL-MDR), Nanjing University, using a Quanta 400 FEG scanning electron microscope equipped with a Gatan mini-CL detector (Mono CL3+).

~~The analyses of~~ U-Pb dating and trace elements analysis of representative zircons were conducted in two laboratories. The samples 12TS119A and 12TS119B were dated at the SKL-MDR of Nanjing University using Agilent 7500a inductively coupled plasma mass spectrometry (ICP-MS) coupled to a New Wave 193 nm laser ablation system with an in-house sample cell. The detailed analytical procedures are similar to those described in Jackson et al. (2004) and Liu et al. (2014). The U-Pb dating and trace elements analyses of zircons from samples 12TS119E, 12TS119F, 12TS119G and 12TS119H were carried out at the State Key Laboratory of Geological Processes and Mineral Resources, China University of Geosciences (Wuhan), where laser sampling was performed using a GeoLas 2005 System and an Agilent 7500a ICP-MS instrument was used to acquire ion-signal intensities. The detailed operating

conditions and analytical procedures are described in Liu et al. (2008, 2010a, 2010b).

For zircon crystals older than 1000 Ma, $^{207}Pb/^{206}Pb$ apparent ages were used to plot relative probability diagrams considering large amounts of radiogenic Pb. For zircon grains younger than 1000 Ma, $^{206}Pb/^{238}U$ apparent ages are more reliable due to the low content of radiogenic Pb and low uncertainty of common Pb correction. Uncertainties are quoted at 1σ for individual analysis and 2σ (with 95% confidence level) for weighted mean ages, respectively. The results of U-Pb isotopic dating and trace element compositions are listed in Supplementary Table S1 and Table S2, respectively.

5. Results

5.1. Meta-sandstone

A total of 55 zircon grains were chosen for U-Pb dating from the weakly metamorphosed sandstone sample 12TS119F. The CL images of all dated zircons together with their ages are shown in Supplementary Fig. S1 and those of the representative grains are presented in Fig. 5a. Most zircons have euhedral to sub-euhedral shapes and show clear oscillatory zoning without or with narrow dark rims, indicating original magmatic sources (Connelly, 2000; Corfu et al., 2003; Hoskin and Schaltegger, 2003). A small group of zircons show stubby or sub-rounded shapes and have complex core-rim textures, comprising irregular cores with blurry or

patchy zoning and structureless rims. This kind of zircons may have been produced by modification of primary igneous zircons in response to metamorphism (Corfu et al., 2003; Hoskin and Schaltegger, 2003; Rubatto, 2017). The rest few zircons are rounded and ~~unzoned or~~ sector zoned or without zoning, indicative of metamorphic origin (Figs. 5a and S1; Corfu et al., 2003; Hoskin and Schaltegger, 2003).

Forty-five out of fifty-five grains yielded concordant ages, a large majority of which have ages < 540 Ma, with two major age peaks at 425 Ma (n = 14; 31.1%) and 445 Ma (n = 10; 22.2%), as well as a minor age peak at ca. 490 Ma. The Precambrian zircons show sub-peaks at ~580 Ma, ~780 Ma, and in a range of 850-1000 Ma; only two Mesoproterozoic grains (1280 Ma and 1372 Ma) were ~~found~~identified (Fig~~s~~. 6a-~~6~~b; Table S1). The remaining ten analyses yielded discordant ages (Fig. 6a) probably due to Pb loss or disequilibrium of their isotopic systems (Connelly, 2000).

Twenty-three zircons with ages around 445-425 Ma were analyzed for rare earth element (REE) compositions. Most grains are characterized by steeply-rising REE patterns with remarkable positive Ce and negative Eu anomalies (Fig. 7a), together with ~~their~~ high Th/U ratios (mostly > 0.4) (Fig. 6b; Table S1), generally consistent with typical magmatic zircons (Hoskin and Schaltegger, 2003; Rubatto, 2017). Only two zircons (No~~s~~. 38 and 51) display relatively higher LREE values and weaker Ce anomalies in comparison to the other zircons, and their REE patterns (Fig. 7a) are similar to those of hydrothermal ~~related~~ zircons (Hoskin, 2005).

5.2. Mica-schists

From three mica-schist samples, a total of 192 zircon grains were analyzed, which show various sizes, sub-rounded to sub-euhedral shapes and complicated internal textures (Figs. 5 and S1). According to their CL images, four types of zirconss can be recognized. (1) Type 1 zircons have core-rim textures in which the cores are bright with oscillatory zoning and the rims are relatively dark and un-zoned, corresponding to originally magmatic zircons surrounded by metamorphic overgrowths (Hoskin and Schaltegger, 2003). (2) Type 2 zircons also show core-rim textures with bright un-zoned cores, which were eithercould be originally metamorphic and then subjected to secondary metamorphic or hydrothermal overgrowth., or aAlternatively, they could also be originally magmatic but were intensively "reworked" (via solid-state recrystallization or local dissolution-reprecipitation) by the subsequent metamorphism or alteration so that the original magmatic oscillatory zoning were was totally erased. In the latter case, the overgrowth rims may have formed synchronously with the reworking of the cores or even reflect a later metamorphic and/or hydrothermal event (Hoskin and Schaltegger, 2003). (3) Type 3 zircons have homogeneous dark to black CL images without visible oscillatory zoning, likely formed by metamorphism or hydrothermal alteration activities (Connelly, 2000; Corfu et al., 2003; Hoskin and Schaltegger, 2003). (4) Type 4 zircons are characterized by prismatic shapes and moderately bright CL images with

clearly concentric magmatic oscillatory zoning, ~~and no~~without visible overgrowths. ~~–~~

In order to obtain sufficiently representative zircon populations, all four types of zircons from each sample were analyzed. Most analyses plot on or close to the Concordia, but a few zircons show remarkable discordance, especially for the sample 12TS119E (Fig~~s~~. 6c, ~~6~~e and ~~6~~g). One reason for discordant ages can be Pb loss due to metamorphic or hydrothermal alteration. In addition, ~~physical~~ analytical mixing between two parts of zircons with different origins (e.g., older cores and younger rims) is also highly possible as some of the discordant zircons ~~are quite small~~ with core-rim texture are quite small (Fig. S1). The geological meaning of the discordant ages is ambiguous~~;~~, ~~thus these~~therefore, ~~discordant zircon~~ ages~~es~~they are excluded from further discussion and only concordant ages (concordance > 90%) are considered~~in further discussion~~. ~~In the following, only concordant ages (concordance > 90%) are considered.~~

For the mica~~-~~schist sample 12TS119A, fifty-eight out of sixty dated zircons yielded concordant ages (Fig. 6c) ranging from 313 to 2175 Ma. They show ~~showing~~ a dominant age peak at 477 Ma (n = 19; 32.8%), two younger age peaks at 322 Ma (n = 4; 6.9%) and 414 Ma (n = 4; 6.9%), and other populations of 500-550, 600-750, 850-1000,1100-1500, 1600-1800 and 2175 Ma (Fig. 6d). The youngest nine ages (peaked at 322 and 414 Ma) (Fig. 6d; Table S1) are obtained exclusively from type 2 zircons with Th/U ratios mostly lower than or near 0.4 (Table S1; Fig. 6d), showing bright or dark cores characterized by surface-controlled alteration (Corfu et al., 2003)

and encircled by thin and dark rims (Figs. 5b and S1). Zircons defining the major age peak of 477 Ma mainly belong to the ~~type 1, type 2 and minor type 4~~ type 1 and type 2, and show Th/U ratios higher than 0.4 (Table S1; Figs. 5b, 6d and S1). The other older zircons cover ~~all four types~~ types 1 and 2, and have variable Th/U ratios mostly higher than 0.4 (Figs. 6d and S1).

Sixty zircons were dated ~~from~~ for the mica-schist sample 12TS119B and all of them yielded concordant ages (Fig. 6e). Their age~~s ranges and~~ populations are very similar to those of the sample 12TS119A (Fig. 6f). Therein, ~~the~~ three youngest zircons (380-413 Ma) belong to the type 3 displaying homogeneous dark to black CL images (Figs. 5c and S1) and Th/U ratios around 0.4 (Table S1; Fig. 6f). Twenty zircons (33.3%) of type 1 and minor ~~types 3 and 4~~type 2 and type 4 (Figs. 5c and S1) define an age peak at 477 Ma and show Th/U ratios mostly higher than 0.4 (Fig. 6f; Table S1). Other ages around 500-550, 600-750, 850-1000, 1100-1500, 1600-1800 and 2200-2500 Ma (Fig. 6f) were obtained from zircons of all four types, most of which show Th/U ratios higher than 0.4 (Table S1).

As for the sample 12TS119E, sixty-one out of seventy-two zircons provided concordant ages ranging from 346 to 1765 Ma (Fig. 6g-6h). A major age peak at 475 Ma (n = 11; 18.0%) and a minor age peak at 425 Ma (n = 5; 8.2%) are mainly defined by types 1 and 2 zircons (Figs. 5d and S1), which mostly show Th/U ratios higher than 0.4 (Fig. 6h; Table S1). These zircons show steeply-rising REE patterns, remarkable positive Ce anomalies and negative Eu anomalies (Fig. 7b). Thus, these

ages are indicative of magmatic events (Hoskin and Schaltegger, 2003; Hoskin, 2005). One exceptional zircon (No. 57; ~424 Ma) shows a quite high Th/U ratio (2.93; Table S1). and fFor some unclear reasons, a UV-shaped REE pattern due to its high LREE content is similar to that of some "hydrothermal" zircons (Fig. 7b). Five zircons of types 2 and 3 with dark, homogenous CL images (Figs. 5d and S1) yielded ages offrom 346 to 402 Ma, they display gently-rising REE patterns with weak Ce anomalies and Th/U ratios mostly lower than 0.4 (Figs. 6h and 7b), similar to zircons of hydrothermal origin (Fig. 7b). With only a few exceptions, the other age populations (500-550, 600-800, 850-1000, 1100-1400 and 1600-1800 Ma) correspond to all four zircon types (Figs. 6g-6h) with Th/U ratios mostly >higher than 0.4 (Fig. 6h; Table S1).

5.3. Migmatites

For two migmatite samples, a total of 38 analyses were conducted on 36 zircons. Their CL images and ages are shown in Figs. 8a-8f. Almost all the dated zircons are sub-euhedral to euhedral with prismatic shapes, they have clear oscillatory zoning (Fig. 8) and their Th/U ratios are mostly higher than or close to 0.4 (Table S1), suggesting a magmatic origin.

Out of twenty analyses on zircons offrom the migmatitic gneissic-granite migmatitic gneissic granite 12TS119G, thirteen concordant ages form two age peaks or mean ages at 297.4 ± 2.1 Ma (n = 8; 61.5%; MSWD = 0.26) and 322.2 ± 2.3 Ma (n

= 5; 38.5%; MSWD = 0.066) (Fig~~s~~. 8c and 8e). Seven zircons yielded discordant ages (Fig. 8c; Table S1)~~,~~ that are ~~whichthat are geologically meaningless and they are~~ not considered in the following discussion.

Eighteen zircons were dated for the migmatite leucosome sample 12TS119H and fifteen analyses yielded concordant ages (Fig. 8d), ~~which also~~ define~~d~~ing comparable two age groups ~~peaks or mean ages~~ of 297.1 ± 2.7 Ma (n = 4; 26.7%; MSWD = 0.13) and 322.5 ± 2.1 Ma (n = 8; 53.3%; MSWD = 0.13) (Fig. 8f). Three zircons (Nos. 6, 10 and 16) yielded older~~,~~ and probably inherited~~,~~ ages of 338-365 Ma (Fig. 8d). The remaining three zircons (Nos. 2, 5 and 15) with discordant ages have been rejected.

The dated concordant zircons from these two samples were further analyzed for REE compositions. The results show steeply-rising Chondrite-normalized REE patterns characterized by enrichment of HREE relative to LREE, mostly positive Ce anomalies and negative Eu anomalies (Fig~~s~~. 7c and 7d), in accord with an igneous origin. Only two zircons (Nos. 15 and 16) in sample 12TS119G ~~are~~ have slightly different ~~in~~ REE patterns with relatively higher LREE values and weaker Ce anomalies than typical magmatic zircons (Fig. 7c).

6. Discussion

6.1. ~~Depositional~~ Protoliths depositional and metamorphic ages of the meta-sedimentary rocks

The most remarkable age population of detrital zircons from the meta-sandstone and mica~~-~~schists lies in the 540-420 Ma interval. The mica~~-~~schists have dominant peaks of 477-475 Ma, while the meta-sandstone shows a peak at 425 Ma ~~which~~that resembles a minor peak of the mica~~-~~schist 12TS119E (Fig. 6). Since these detrital zircons are mostly of magmatic origins, their ages ~~allow constraining~~constrain the maximum depositional ages~~ of~~for the~~ir~~ protoliths of meta-sedimentary rocks~~of the meta-sedimentary rocks~~.~~ The meta-sedimentary rocks are crosscut by granite dated at 320 ± 3 Ma (Song et al., 2018), thus, the deposition of meta-sedimentary rocks occurred between 425 Ma and 320 Ma.~~ The metamorphic ages ~~of the meta-sedimentary rocks is~~are ~~constrained to be~~ at 322 Ma and 297 Ma provide a constraint on the minimum sedimentary age (see discussion below).~~,~~ ~~T~~thusThus, the deposition of ~~detrital~~ protoliths of the meta-sedimentary rocks may have occurred between 425 Ma and 322 Ma. The maximum deposition age is ~~is consistent with~~also ~~constrained~~defined as >320 Ma by the ~~latter~~ crosscutting granite dated at 320 ± 3 Ma (Song et al., 2018).

Zircons ~~at~~ of ~480-420 Ma from sillimanite mica~~-~~schists generally exhibit dark rims, whereas detrital zircons of ~425 Ma from the meta-sandstone usually ~~do not~~

show no ~~such~~ overgrowth~~s~~ (Figs. 5 and S1). This indicates that zircons from high-grade mica~~-~~schists were ~~subjected to important~~significantly reworked~~ing~~ ~~in various degrees~~ by metamorphism, in contrast to the ~~lower~~ low-grade meta-sandstone. Such reworking may also account for the occurrence of discordant detrital zircons in the meta-sedimentary rocks (Fig. 6), most likely due to incomplete metamorphic reset.

The youngest zircon group (~420-320 Ma) from the mica~~-~~schists~~, which~~ ha~~ve~~s no equivalent in the meta-sandstone, displaying diagnostic features of metamorphic~~/~~ and/or hydrothermal zircons. Therefore, the younger~~se~~ ages suggest partial or total ~~youngest ones were partially or completely~~ reworking~~ed~~ ~~by~~ during amphibolite facies metamorphism, although it cannot be excluded that some of them were originally (pre-sedimentation) metamorphic. ~~As the youngest age peak of the metamorphic zircons is ~322 Ma, it is suggested that the~~ The ~~high temperature~~ metamorphism likely occurred at ~322 Ma, which is the youngest age peak of metamorphic zircons. The ~~other~~ older ages (420-322 Ma) possibly result~~ed~~ from age mixing between primary cores ~~(growth zoning)~~ and recrystallized areas or overgrowths (Corfu et al., 2003).

The two migmatite samples yielded exactly identical age peaks at 322 Ma and 297 Ma (Fig. 8). Both zircon groups ~~of zircons~~ show clear concentric oscillatory zonings, high Th/U ratios and steeply-rising REE patterns, ~~indicating~~ ~~diagnostic~~indicative of magmatic origin~~s~~ (Fig. 8; Table S1). Thus, these two ages ~~likely~~ represent two distinct episodes of zircon crystallization. Although ~~both groups~~

of zircons from both groups generally show similar morphologies and internal textures, some zircons of 322 Ma grains have vague thin dark rims (Figs. 8a-8b), which may have resulted from slightcorrespond to overgrowth during the second episode of crystallization at ~297 Ma. This is also confirmed by (1) the occurrence of thin dark rims surrounding the inherited zircons of 338 Ma, 342 Ma and 365 Ma (Fig. 8a-8b), whichthat were probably inherited from the protoliths of the migmatites, and (2) clear conspicuous dark rims and zoning-controlled alterations developed in discordant zircons (Figs. 8a-8b).

Regional tectonics, metamorphism, and miagmatiszation and deformation are known to be inhas close spatial and temporal relationships with peraluminous leucogranitoid emplacement genesis (e.g., Barrow, 1893; Vernon, 1982; Barton and Hanson, 1989; Keay et al., 2001; Okay et al., 2014). A comparison betweenof the new zircon U-Pb ages of the meta-sedimentary rocks and migmatites (from this study) withand the published zircon U-Pb agesones of the crosscutting granitic plutons (Figs. 2b and 9) shows that the Late PaleozoicCarboniferous to eEarly Permian crosscutting granite plutons (Figs. 2b and 9) magmatism occurred in two episodes at 330-310 Ma and 305-290 Ma (Sun et al., 2007b; Wang et al., 2009c; Chen and Shu, 2010; Chen et al., 2016; Song et al., 2018reference); (Fig. 9a), which fit the two zircon peak ages peaks of zircons from migmatites (322 Ma and 297 Ma); of zircons inin the migmatites (Figs. 8 and 9b). Moreover, the age of the first episode of granitic magmatism is also consistent with the youngest peak age peak (322 Ma) for of

548 “metamorphic” zircons of the mica-schists (Fig. 9b). Therefore, ~322 Ma can be
549 reasonably interpreted as the timing of amphibolite facies metamorphism, in
550 connection with the migmatization and the first episode of magmatism. As the
551 migmatitic leucosomees also contains zircon grains of zircons at ~297 Ma zircon
552 grains, it is likely that the migmatites remelted againanatexic melts were not totally
553 crystallized at ~322 Ma probably due to high thermal gradient or continuous addition
554 of melts atuntil ~297 Ma, associated in connexction with the second episode of
555 granitic magmatism, leading giving birth to the zircon crystallization of the younger
556 zircons, while some inherited zircons atof ~322 Ma were preserved. This hypothesis
557 Finally, is supported by the occurrence of ~308 Ma leucogranitcic dykes of ~308 Ma
558 containing a few inherited zircons atwith 320-330 Ma ages (Zhu et al., 2018)., Such a
559 genetic relationship between migmatites and granites and will needs verification to be
560 comfortedconfirmed with through detailed geochemical investigations.
561 further studies on geochemical balance between migmatites and granites.
562 It is also worth noting that mica $^{40}Ar/^{39}Ar$ apparent ages of the metamorphic
563 rocks range from 301 to 277 Ma and were considered as the timing of the
564 metamorphism in the Harlik domain (Sun, 2007). However, considering: that (1) the
565 relatively low closure temperature of argon isotopic system of micas (Harrison et al.,
566 1985, 2009), (2) the occurrence of extensive Permian granitic plutons and their close
567 spatial relationships with meta-sedimentary rocks and migmatites, and (3) the good
568 match between the mica $^{40}Ar/^{39}Ar$ apparent ages (301-277 Ma) and zircon U-Pb ages

of granites (305-290 Ma), we consider the mica $^{40}Ar/^{39}Ar$ apparent ages of meta-sedimentary rocks ~~as to be~~are most likely the timing of thermal reset and final cooling event ~~associated with~~related to the second episode of magmatism.

6.2. Provenances of the meta-sedimentary rocks

The studied meta-sedimentary rocks contain both Paleozoic and Proterozoic detrital zircons (Fig. 6). Among overall 224 concordant detrital zircons, 126 grains (56%) yielded Paleozoic ages and 98 zircons (44%) yielded Proterozoic ages. For the Paleozoic ages, as aforementioned, the U-Pb system of detrital zircons younger than 420 Ma was likely affected by post-depositional metamorphism. Thus, these zircons and their ages should be rejected for provenance investigation. The Ordovician to Silurian detrital zircons (~480-420 Ma with peaks at ~475, ~445 and ~425 Ma) are dominant constituents in the meta-sedimentary rocks (Fig. 9b). This is consistent with the ~~previous~~ study of Sun et al. (2007a)~~that~~ who found a predominant Ordovician to Silurian zircon population (482-418 Ma) in low-grade sandstones from the study area ~~(Sun et al., 2007a)~~.

As discussed above, the early Paleozoic zircons are mainly derived from magmatic rocks. Numerous early Paleozoic magmatic rocks ~~at~~of 440-450 Ma ~~have been~~were previously reported both in the Harlik and Dananhu arcs, while magmatic rocks of 420-430 Ma ~~occur~~ crop out ~~only~~ in the Dananhu area only (Cao et al., 2006; Ma et al., 2015; Wang et al., 2016; Zhang et al., 2016a; Chen et al., 2017; Liu et al.,

2017; Du et al., 2018a; Wang et al., 2018b; Zheng et al., 2018; Chai et al., 2019). In addition, very few ~475 Ma magmatic rocks ~~at ~475 Ma~~ have been reported so far in the North Tianshan, and only rhyolites ~~at~~of 469 ± 9 Ma were documented ~~from~~in the Harlik area (Li et al., 2017). The angular to sub-angular early Paleozoic detrital zircons indicate short distances of transportation (Sun et al., 2007a), while these samples ~~come~~are from the Qincheng area ~~which~~that is situated between the Harlik Arc and Dananhu Arc~~. As a consequence~~, thus, it can be suggested that these early Paleozoic detrital zircons (~480-420 Ma) likely came from magmatic rocks of the Harlik and Dananhu arcs.

Ordovician to Silurian arc-type magmatic rocks are also ~~occur~~exposed in the Central Tianshan and East Junggar-Altai belts (Fig. 10), which ~~could be~~are ~~the~~ potential sources for the meta-sedimentary rocks. However, the ~~separation of~~ North Tianshan was separation ~~is regarded~~proposed ~~to be separated~~ from ~~the~~ East Junggar-Altai belts ~~is thought to have occurred~~ before the early Carboniferous (>340 Ma) by the ~~opening of~~ Kalamaili oceanic basin (Li et al., 2009; Huang et al., 2012; Zhang et al., 2013; Xu et al., 2015a; Du et al., 2018b; Han and Zhao, 2018; Wang et al., 2019), ~~and~~ while the depositional age of protoliths of the meta-sedimentary rocks ~~the Julideneng Formation~~ is roughly constrained ~~as~~~~at~~between ~~~420-320~~~425~ to ~322 Ma. Therefore, the available data cannot sufficiently prove or disprove that the East Junggar-Altai magmatic arcs ~~are were~~might be ~~the~~ possible sources for the Ordovician~ to Silurian detrital zircons of the meta-sedimentary rocks in the Qincheng

area.

In addition, it is suggested that the North Tianshan (Harlik-Dananhu ~~Arc~~arcs) was amalgamated with the Yamansu Arc and Central Tianshan Block at ~320-300 Ma along the Kangguer shear zone after the closure of the Kangguer Ocean (e.g., Li, 2004; Li et al., 2006; Zhang et al., ~~2015b,~~ 2016b, 2020; Zhao et al., 2019). However, the rock sequences on both sides of this shear zone are comparable and it ~~may be~~might have been ~~actually~~ located within the North Tianshan belt (Wang et al., 2008, 2014a; Branquet et al., 2012). According to the studies on ophiolites of the North Tianshan Suture zone and Kangguer belt (Xu et al., 2006a, 2006b; Chen et al., 2019), the North Tianshan (or Kangguer) Ocean ~~was opening~~opened during the mid-late Carboniferous. Considering that the Precambrian zircons most likely came from the Central Tianshan Block (see discussion ~~blew~~below), it is possible that the Central Tianshan Block ~~also~~ have also provided ~~some~~certain early Paleozoic detritus for the ~~meta-~~sediments in the Qincheng area.~~Due to the uncertainty about the nature and the timing of the closure of the Kangguer Ocean, it is not certain that the Central Tianshan Block is the source area for the early Paleozoic zircons of the meta-sediments in the Qincheng area.~~

The main population of Proterozoic zircons in the meta-sedimentary rocks is the Neoproterozoic group (550-1000 Ma) showing a peak at ~870 Ma and a subordinate peak at ~780 Ma. Minor zircon populations of 1.1-1.5 Ga, 1.6-2.0 Ga, 2.1-2.3 Ga and ~2.5 Ga with peaks at ~1.45 Ga and ~1.7 Ga ~~can~~ are also ~~be found~~recognized (Fig. 10a). However, there is no ~~record for~~of a Precambrian basement exposed in the NTB

(Xiao et al., 2004; Zhang et al., 2016a). ~~Thus, t~~These Proterozoic zircons were thus most likely transported from nearby ~~Precambrian~~ Precambrian-based continental blocks. Chen et al. (2014) suggested that the Harlik Range ~~belongs to~~is a part of the Tuva-Mongol-Altai Arc. Nevertheless, the available data indicate that the Tuva-Mongol-Altai Arc and the East Junggar Belt ~~are~~ lack ~~of~~ both magmatic events and detrital records ~~of~~in ~1.35-1.45 Ga (Fig. 10d-~~10~~e; Jiang et al., 2011), which are common in the North Tianshan (Fig~~s~~. 10a-~~10~~b; Chen et al., 2014). In contrast, a lot of Mesoproterozoic granitic rocks ~~with ages from ca.~~of ~1.40 ~~to~~ -1.45 Ga have been documented in the Central Tianshan Block (Fig. 10c; Ma et al., 2012a; He et al., 2014, 2015; Wang et al., 2014b, 2017; Huang et al., 2015b). Moreover, the Central Tianshan Block has a detrital zircon age spectrum similar to that of the Harlik Range and the entire North Tianshan, they all display zircon populations of 750-800 Ma, 850-1000 Ma, ~1.45 Ga, 1.6-1.8 Ga and ~2.5 Ga. More importantly, the igneous rocks in the Central Tianshan Block formed during ~800, ~900 Ma and ~1.45 Ga episodes, identical with the detrital zircon age peaks of the meta-sedimentary rocks from the Harlik Range, which are absent~~, however, lacking~~ in the other neighboring units (Fig. 10). Therefore, the Central Tianshan Block is the most probable provenance area for the Precambrian detrital zircons in the studied meta-sedimentary rocks.

The Precambrian zircons in the meta-sedimentary rocks are ~~an~~euhedral in shape and show complex core-rim textures (Figs. 5 and S1), indicating that they ~~are~~were multiple-cycled. Thus, these Precambrian zircons were probably ~~were~~ transported

from the Central Tianshan Block to the North Tianshan Belt (Dananhu Arc) before the opening of the ~~the~~ North Tianshan (or Kangguer) Ocean, and ~~then were~~thereafter re-transported into the ~~the~~ Harlik area. This is ~~consistent~~in agreement with the fact that zircon populations of Devonian flysch ~~sediments from~~in the Dananhu Arc are comparable with that of the Central Tianshan Block (Wang et al., 2019). However, due to uncertainty on their deposition age, these zircons could ~~be also~~have been ~~directly be~~ transported directly from the Central Tianshan Block as well.~~to the Harlik because of the rough constraints on their depositional age.~~

Clastic sediments derived from orogens are generally a mixture of multifarious detritus from metamorphic, sedimentary and igneous rocks (e.g., Han et al., 2017). Mixing and preferential elimination of certain zircons during transport can significantly modify zircon populations in sediments, especially in old multiple-cycled populations (Hay and Dempster, 2009; Han et al., 2017). Therefore, comparison of detrital zircon populations must be undertaken with much care. In the present case, provenance from the Central Tianshan B~~b~~lock is most likely, but considering the limited size of the database, other provenances cannot be completely excluded.

6.3. Implications for the late Paleozoic tectonic evolution of the North Tianshan belt

Our new zircon U-Pb data indicate that the meta-sediments from the ~~Julideneng Formation~~JMC were deposited in the interval between l~~L~~ate Silurian and ~~early L~~late

Carboniferous. The predominant early Paleozoic detrital zircons were potentially derived from both the Harlik and Dananhu aArcs. In combination with the low maturity of the meta-sandstone that suggests a near-source deposition (Sun et al., 2007a), an intra-arc basin (Qincheng or Xiaopu basin; Zhao et al., 1997) located between these arcs can be suggested (Fig. 11A). The low maturity of the meta-sandstone suggests near-source deposition (Sun et al., 2007a) and the predominant early Paleozoic detrital zircons were potentially derived from the Harlik and Dananhu Aarcs, thus, an intra-arc basin (Qincheng or Xiaopu basin) was suggested (Zhao et al., 1997). In addition, the Precambrian zircons in the Julideneng Formation meta-sedimentary rocks were probably derived from the Central Tianshan Block. As a consequence result, the North Tianshan was likely connected with the northern margin of the Central Tianshan Block before the lLate Carboniferous. The North Tianshan was rifted from the Central Tianshan Block in the mid-late Carboniferous (Xu et al., 2006a, 2006b; Chen et al., 2019) due to the opening of the North Tianshan (or Kangguer) Ocean, and was thereafter re-amalgamated to the Central Tianshan Block during the latest Carboniferous (Han et al., 2010; Zhang et al., 2015b, 2016a, 2016b, 2020) (Fig. 11AB-BD).

As discussed above, the amphibolite-facies metamorphism and migmatization occurred at ~322 Ma. According to Sun (2007) and our field observations, the garnet-sillimanite-bearing meta-sedimentary rocks are most likely likely the protolith source rocks of the migmatites and associated felsic bodiesdykes. The generally

N-dipping foliations that bearing ~NW-SE stretching lineations were likely resulted from sinistral transtension (Sun, 2007). In addition, the HT-LP metamorphism (Zhao et al., 1997) and migmatization are coeval with the co-emplacement of undeformed high-K calc-alkaline undeformed I- and A-type granites (320-316 Ma) that formed probably by with positive whole-rock $\varepsilon_{Nd}(t)$ and zircon $\varepsilon_{Hf}(t)$ values, both of which are diagnostic of decompression melting of juvenile crustal sources in an extensional setting (Song et al., 2018). Similarly, in the nearby Bogda Beltarea, Carboniferous (350-315 Ma) volcanic rocks are thought to have formed in an intra-arc (Zhang et al., 2017; Wali et al., 2018) or back-arc extensional setting (Chen et al., 2013; Xie et al., 2016a, 2016b, 2016c). Taking all these arguments into consideration, we suggest that the meta-sedimentary rocks and migmatites are likely parts of the Harlik arc root, and the migmatization probably occurred due to decompression partial melting in a late-orogenic extensional setting a continent-basedn intra-arc or back-arc extensionalriftextensional setting (Fig. 11C).

The migmatites in the Harlik Range also recorded an event at ~297 Ma, which is coeval with the widespread emplacement of undeformed post-collisional orogenic K-feldspar granites and leucocratic two-mica granites at 298-295 Ma (Wang et al., 2009c; Chen and Shu, 2010). The occurrence of ductilely deformed granites ofwith the same age along the northern boundary of the metamorphic units belt (Fig. 2b-2c), and down dip-slip (normal) stretching lineation with normal fault motion along the north-dipping mylonite zone (see section 3) indicate syn-tectonic kinematic

emplacement of granites. Therefore, the development of a large volume of latest Carboniferous to earliest Permian post-~~collisional~~ orogenic granitoids (Wang et al., 2009c, 2009d; Chen and Shu, 2010; Yuan et al., 2010; Chen et al., 2016), bimodal dyke swarms (Gu et al., 1999) and nearly synchronous ductile normal faults correspond to the exhumation of the metamorphic units under a regional post-orogenic extensional regime and thus prominent crustal thinning (Fig. 11D). Final cooling at 301-277 Ma revealed by mica $^{40}Ar/^{39}Ar$ apparent ages (Sun, 2007) indicates that these events terminated during the Ee~~E~~arly Permian.

7. **Conclusions**

(1) ~~The~~ Protoliths of the meta-sedimentary rocks ~~of~~ from the Julideneng Metamorphic Complex~~Julideneng Formation~~ in the southern Harlik Range were originally deposited between the latest Silurian and ~~early L~~late Carboniferous (425-322 Ma).

(2) The Harlik-Dananhu magmatic arcs were likely the major sources for the Ordovician to Silurian detrital zircons in the meta-sedimentary rocks, while the Precambrian detrital zircons were most likely derived from the Central Tianshan Block, although possible provenances from the East Junggar and Chinese Altai cannot be excluded.

(3) ~~The HT-LP~~High-grade metamorphism and ~~migmatisation~~ migmatization occurred at ~322 Ma in the southern Harlik Range ~~occurred in a~~were probably related to continent-based~~n~~ intra-arc or back-arc crust thinning~~extensional setting~~a

late orogenic extensional setting. The orogenic events in the Harlik Range terminated in before the eEEarly Permian.

Acknowledgments

We appreciate the kind helps of Mr. B. Wu for LA-ICP-MS zircon U-Pb dating. Dr. K. de Jong reviewed the first version of the manuscript and provided constructive suggestions. We are very grateful to two anonymous reviewers for their constructive comments and, the Editor-in-Chief Prof. Mei-Fu Zhou and Editor Dr. Ibrahim Uysal are appreciated for histheir editorial handling. This study was co-sponsored by the National Nature Science Foundation of China (41772225, 42011530146, 41390445, and 41311120069), the Fundamental Research Funds for the Central Universities, and by the Open Fund of State Key Laboratory for Mineral Deposits Research (ZZKT-201603).

References

Ao, S.J., Xiao, W.J., Han, C.M., Li, X.H., Qu, J.F., Zhang, J.E., Guo, Q.Q., Tian, Z.H., 2012. Cambrian to early Silurian ophiolite and accretionary processes in the Beishan collage, NW China: implications for the architecture of the Southern Altaids. Geol. Mag. 149, 606-625.

Ao, S.J., Xiao, W.J., Windley, B.F., Mao, Q.G., Han, C.M., Zhang, J.E., Yang, L.K., Geng, J.Z., 2016. Paleozoic accretionary orogenesis in the eastern Beishan

753 orogen: Constraints from zircon U-Pb and $^{40}Ar/^{39}Ar$ geochronology. Gondwana
754 Res. 30, 224-235.
755 Barrow, G., 1893. On an intrusion of muscovite-biotite gneiss in the southeastern
756 Highlands of Scotland, and its accompanying metamorphism. Q. J. Geol. Soc. 49,
757 330-358.
758 Barton, M.D., Hanson, R.B., 1989. Magmatism and the development of low-pressure
759 metamorphic belts: Implications from the western United States and thermal
760 modeling. Geol. Soc. Am. Bull. 101, 1051-1065.
761 Branquet, Y., Gumiaux, C., Sizaret, S., Barbanson, L., Wang, B., Cluzel, D., Li, G.R.,
762 Delaunay, A., 2012. Synkinematic mafic/ultramafic sheeted intrusions:
763 Emplacement mechanism and strain restoration of the Permian Huangshan
764 Ni-Cu ore belt (Eastern Tianshan, NW China). J. Asian Earth Sci. 56, 240-257.
765 Belousova, E., Griffin, W. L., O'Reilly, S. Y., Fisher, N. L., 2002. Igneous zircon: trace
766 element composition as an indicator of source rock type. Contrib. Mineral. Petrol.
767 143, 602-622.
768 Cai, K.D., Sun, M., Yuan, C., Zhao, G.C., Xiao, W.J., Long, X.P., Wu, F.Y., 2011.
769 Prolonged magmatism, juvenile nature and tectonic evolution of the Chinese
770 Altai, NW China: Evidence from zircon U-Pb and Hf isotopic study of Paleozoic
771 granitoids. J. Asian Earth Sci. 42, 949-968.
772 Cai, K.D., Sun, M., Jahn, B.-M., Xiao, W., Yuan, C., Long, X., Chen, H., Tumurkhuu,
773 D., 2015. A synthesis of zircon U-Pb ages and Hf isotopic compositions of

granitoids from Southwest Mongolia: Implications for crustal nature and tectonic evolution of the Altai Superterrane. Lithos 232, 131-142.

Cao, F.G., Tu, Q.J., Zhang, X.M., Ren, Y., Li, S.L., Dong, F.R., 2006. Preliminary determination of the Early Paleozoic magmatic arc in the Karlik Mountains, East Tianshan, Xinjiang, China-Evidence from zircon SHRIMP U-Pb dating of granite bodies in the Tashuihe area. Geol. Bullet. China 25, 923-927 (in Chinese with English abstract).

Cao, F.G., Zhang, Y.P., Li, Y., Guan, W., Ren, Y., Dong, F.R., Guo, L., 2009. The geological daracter of Nanhua system Qingshixia formation in Qincheng Hami, Xinjiang. Xinjiang Geol. 27, 303-307 (in Chinese with English abstract).

Chai, F.M., Zhang, Z.C., Li, W.H., Santosh, M., Wang, H.P., Wang, W., Xu, Q.F., 2019. The early Paleozoic Huangtupo VMS Cu-Zn deposit in Kalatag, Eastern Tianshan: Implications from geochemistry and zircon U-Pb geochronology of volcanic host rocks. Lithos 342, 97-113.

Charvet, J., Shu, L.S., Laurent-Charvet, S., 2007. Paleozoic structural and geodynamic evolution of eastern Tianshan (NW China): welding of the Tarim and Junggar plates. Episodes 30, 162-186.

Charvet, J., Shu, L.S., Laurent-Charvet, S., Wang, B., Faure, M., Cluzel, D., Chen, Y., de Jong, K., 2011. Palaeozoic tectonic evolution of the Tianshan belt, NW China. Sci. China Earth Sci. 54, 166-184.

Chen, L., Wang, J.B., Bagas, L., Wu, X.B., Zou, H.Y., Zhang, H.Q., Sun, Y., Lv, X.Q.,

795 Deng, X.H., 2017. Significance of adakites in petrogenesis of Early Silurian
796 magmatism at the Yudai copper deposit in the Kalatag district, NW China. Ore
797 Geol. Rev. 91, 780-794.
798 Chen, X.J., Shu, L.S., 2010. Features of the post-collisional tectono-magmatism and
799 geochronological evidence in the Karlik Mt., Xinjiang. Acta Petrol. Sin. 26,
800 3057-3064 (in Chinese with English abstract).
801 Chen, X.J., Shu, L.S., Santosh, M., 2011. Late Paleozoic post-collisional magmatism
802 in the Eastern Tianshan Belt, Northwest China: New insights from geochemistry,
803 geochronology and petrology of bimodal volcanic rocks. Lithos 127, 581-598.
804 Chen, X.J., Shu, L.S., Santosh, M., Zhao, X.X., 2013. Island arc bimodal magmatism
805 in the eastern Tianshan Belt, Northwest China: Geochemistry, zircon U-Pb
806 geochronology and implications for the Paleozoic crustal evolution in Central
807 Asia. Lithos 168-169, 48-66.
808 Chen, X.J., Shu, L.S., Santosh, M., Xu, Z.Q., 2014. The provenance and tectonic
809 affinity of the Paleozoic meta-sedimentary rocks in the Chinese Tianshan belt:
810 New insights from detrital zircon U-Pb geochronology and Hf-isotope analysis. J.
811 Asian Earth Sci. 94, 12-27.
812 Chen, X.J., Zhang, K.H., Zhang, G.L., Zhou, J., 2016. Characteristics, petrogenesis
813 and tectonic implications of the Permian Omoertage alkaline granites in Harlik
814 area, Xinjiang. Acta Petrol. Mineral. 35, 929-946 (in Chinese with English
815 abstract).

816 Chen, Z.Y., Xiao, W.J., Windley, B.F., Schulmann, K., Mao, Q.G., Zhang, Z.Y., Zhang,
817 J.E., Deng, C., Song, S.H., 2019. Composition, Provenance, and Tectonic Setting
818 of the Southern Kangurtag Accretionary Complex in the Eastern Tianshan, NW
819 China: Implications for the Late Paleozoic Evolution of the North Tianshan
820 Ocean. Tectonics 38, 2779-2802.
821 Chen, Z.Y., Xiao, W.J., Windley, B.F., Schulmann, K., Mao, Q.G., Zhang, Z.Y., Zhang,
822 J.E., Li, C.Y., Song, S.H., 2020. Latest Permian-early Triassic arc amalgamation
823 of the Eastern Tianshan (NW China): Constraints from detrital zircons and Hf
824 isotopes of Devonian–Triassic sediments. Geol. J. 55, 1708-1727.
825 Connelly J.N. 2000. Degree of preservation of igneous zonation in zircon as a
826 signpost for concordancy in U/Pb geochronology. Chem. Geol. 172, 25-39.
827 Corfu, F., Hanchar, J.M., Hoskin, P.W.O., Kinny, P., 2003. Altas of zircon textures.
828 Rev. Mineral. Geochem. 53, 469-500.
829 de Jong, K., Wang, B., Faure, M., Shu, L.S., Cluzel, D., Charvet, J., Ruffet, G., Chen,
830 Y., 2009. New $^{40}Ar/^{39}Ar$ age constraints on the Late Palaeozoic tectonic
831 evolution of the Western Tianshan (Xinjiang, northwestern China), with
832 emphasis on Permian fluid ingress. Int. J. Earth Sci. 98, 1239-1258.
833 Deng, X.H., Wang, J.B., Santosh, M., Wang, Y.W., Long, L.L., Zhang H.Q., Yang,
834 L.Y., Xu, J., Chen, X., Chen, L., 2018. Early Paleozoic volcanic rocks with VMS
835 mineralization from easternTianshan Orogen: Implication for tectonic evolution.
836 Geol. J. 53, 2178-2192.

~~Dong, Y.P., Zhang, G.W., Neubauer, F., Liu, X.M., Hauzenberger, C., Zhou, D.W., Li, W., 2011. Syn- and post-collisional granitoids in the Central Tianshan orogen: Geochemistry, geochronology and implications for tectonic evolution. Gondwana Res. 20, 568-581.~~

Dong, Y.P., Zhou, D.W., Zhang, G.W., Zhao, X., Luo, J.H., Xu, J.G., 2006. Geology and geochemistry of the Gangou ophiolitic melange at the northern margin of the Middle Tianshan Belt. Acta Petrol. Sin. 22, 49-56 (in Chinese with English abstract).

Du, L., Long, X.P., Yuan, C., Zhang, Y.Y., Huang, Z.Y., Sun, M., Zhao, G.C., Xiao, W.J., 2018a. Early Paleozoic dioritic and granitic plutons in the Eastern Tianshan Orogenic Belt, NW China: Constraints on the initiation of a magmatic arc in the southern Central Asian Orogenic Belt. J. Asian Earth Sci. 153, 139-153.

Du, Q.X., Han, Z.Z., Shen, X.L., Han, C., Han, M., Song, Z.G., Gao, L.H., Liu, H., Zhong, W.J., Yan, J.L., 2018b. Zircon U-Pb geochronology and geochemistry of the post-collisional volcanic rocks in eastern Xinjiang Province, NW China: implications for the tectonic evolution of the Junggar terrane. Int. Geol. Rev. 60, 339-364.

Gao, J., Li, M.S., Xiao, X.C., Tang, Y.Q., He, G.Q., 1998. Paleozoic tectonic evolution of the Tianshan Orogen, northern China. Tectonophysics 287, 213-231.

Gao, J., Long, L.L., Klemd, R., Qian, Q., Liu, D.Y., Xiong, X.M., Su, W., Liu, W., Wang, Y.T., Yang, F.Q., 2009. Tectonic evolution of the South Tianshan orogen

and adjacent regions, NW China: geochemical and age constraints of granitoid rocks. Int. J. Earth Sci. 98, 1221-1238.

Gao, J., Wang, X.S., Klemd, R., Jiang, T., Qian, Q., Mu, L.X., Ma, Y.Z., 2015. Record of assembly and breakup of Rodinia in the Southwestern Altaids: Evidence from Neoproterozoic magmatism in the Chinese Western Tianshan Orogen. J. Asian Earth Sci. 113, 173-193.

Glorie, S., De Grave, J., Buslov, M.M., Zhimulev, F.I., Izmer, A., Vandoorne, W., Ryabinin, A., Van den haute, P., Vanhaecke, F., Elburg, M.A., 2011. Formation and Palaeozoic evolution of the Gorny-Altai-Altai-Mongolia suture zone (South Siberia): Zircon U-Pb constraints on the igneous record. Gondwana Res. 20, 465-484.

Gower, R.J.W., Simpson, C., 1992. Phase boundary mobility in naturally deformed, high-grade quartzofeldspathic rocks: evidence for diffusional creep. J. Struct. Geol. 14, 301-314.

Gu, L.X., Hu, S.X., Chu, Q., Yu, C.S., Xiao, X.J., 1999. Pre-collision granites and post-collision intrusive assemblage of the Kelameili-Harlik Orogenic Belt. Acta Petrol. Sin. 73, 316-329.

Gu, L.X., Hu, S.X., Yu, C.S., Li, H.Y., Xiao, X.J., 2000. Carboniferous volcanites in the Bogda orogenic belt of eastern Tianshan: their tectonic implications. Acta Petrol. Sin. 16, 305-316.

Gu, L.X., Hu, S.X., Yu, C.S., Wu, C.Z., Yan, Z.F., 2001. Initiation and evolution of the

879 Bogda subduction-torn-type rift. Acta Petrol. Sin. 17, 585-597.
880 Han, B.F., Guo, Z.J., Zhang, Z.C., Zhang, L., Chen, J.F., Song, B., 2010. Age,
881 geochemistry, and tectonic implications of a late Paleozoic stitching pluton in the
882 North Tian Shan suture zone, western China. Geol. Soc. Am. Bull. 122, 627-640.
883 Han, B.F., He, G.Q., Wang, X.C., Guo, Z.J., 2011. Late Carboniferous collision
884 between the Tarim and Kazakhstan-Yili terranes in the western segment of the
885 South Tianshan Orogen, Central Asia, and implication for the Northern Xinjiang,
886 western China. Earth Sci. Rev. 109, 74-93.
887 Han, S.Y., de Jong, K., Yi, K., 2017. Detrital zircon ages in Korean mid-Paleozoic
888 meta-sandstones (Imjingang Belt and Taean Formation): Constraints on tectonic
889 and depositional setting, source regions and possible affinity with Chinese
890 terranes. J. Asian Earth Sci. 143, 191-217.
891 Han, Y.G., Zhao, G.C., 2018. Final amalgamation of the Tianshan and Junggar
892 orogenic collage in the southwestern Central Asian Orogenic Belt: Constraints on
893 the closure of the Paleo-Asian Ocean. Earth Sci. Rev. 186, 129-152.
894 Harrison, T.M., Duncan, I., McDougall, I., 1985. Diffusion of ^{40}Ar in biotite:
895 Temperature, pressure and compositional effects. Geochim. Cosmochim. Acta 49,
896 2461-2468.
897 Harrison, T.M., Célérier, J., Aikman, A.B., Hermann, J., Heizler, M.T., 2009.
898 Diffusion of ^{40}Ar in muscovite. Geochim. Cosmochim. Acta 73, 1039-1051.
899 Hay, D.C., Dempster, T.J., 2009. Zircon alteration, formation and preservation in

sandstones. Sedimentology 56, 2175-2191.

He, Z.Y., Klemd, R., Yan, L.L., Zhang, Z.M., 2018a. The origin and crustal evolution of microcontinents in the Beishan orogen of the southern Central Asian Orogenic Belt. Earth Sci. Rev. 185, 1-14.

He, Z.Y., Klemd, R., Zhang, Z.M., Zong, K.Q., Sun, L.X., Tian, Z.L., Huang, B.T., 2015. Mesoproterozoic continental arc magmatism and crustal growth in the eastern Central Tianshan Arc Terrane of the southern Central Asian Orogenic Belt: Geochronological and geochemical evidence. Lithos 236-237, 74-89.

He, Z.Y., Zhang, Z.M., Zong, K.Q., Xiang, H., Chen, X.J., Xia, M.J., 2014. Zircon U-Pb and Hf isotopic studies of the Xingxingxia Complex from Eastern Tianshan (NW China): Significance to the reconstruction and tectonics of the southern Central Asian Orogenic Belt. Lithos 190-191, 485-499.

He, Z.Y., Wang, B., Zhong, L.L., Zhu, X.Y., 2018b. Crustal evolution of the Central Tianshan Block: Insights from zircon U-Pb isotopic and structural data from meta-sedimentary and meta-igneous rocks along the Wulasitai-Wulanmoren shear zone. Precambrian Res. 314, 111-128.

He, Z.Y., Wang, B., Ni, X.H., De Grave, J., Scaillet, S., Chen, Y., Liu, J.S., Zhu, X., 2021. Structural and kinematic evolution of strike-slip shear zones around and in the Central Tianshan: insights for eastward tectonic wedging in the southwest Central Asian Orogenic Belt. J. Struct. Geol. 144, ~~In press.~~ https://doi.org/10.1016/j.jsg.2021.104279.

921 Hirth, G., Tullis, J.A.N., 1992. Dislocation creep regimes in quartz aggregates. J.
922 Struct. Geol. 14, 145-159.
923 Hoskin, P.W., Schaltegger, U., 2003. The composition of zircon and igneous and
924 metamorphic petrogenesis. Rev. Mineral. Geochem. 53, 27-62.
925 Hoskin, P.W.O., 2005. Trace-element composition of hydrothermal zircon and the
926 alteration of Hadean zircon from the Jack Hills, Australia. Geochim. Cosmochim.
927 Acta 69, 637-648.
928 Hu, A.Q., Jahn, B., Zhang, G.X., Chen, Y.B., Zhang, Q.F., 2000. Crustal evolution and
929 Phanerozoic crustal growth in northern Xinjiang: Nd isotopic evidence. Part I.
930 Isotopic characterization of basement rocks. Tectonophysics 328, 15-51.
931 Hu, A.Q., Wei, G.J., Jahn, B.M., Zhang, J.B., Deng, W.F., Chen, L.L., 2010.
932 Formation of the 0.9 Ga Neoproterozoic granitoids in the Tianshan Orogen, NW
933 China: constraints from the SHRIMP zircon age determination and its tectonic
934 significance. Geochimica 39, 197-212 (in Chinese with English abstract).
935 Huang, B., Fu, D., Kusky, T., Ruan, K.P., Zhou, W.X., Zhang, X.H., 2018.
936 Sedimentary provenance in response to Carboniferous arc-basin evolution of
937 East Junggar and North Tianshan belts in the southwestern Central Asian
938 Orogenic Belt. Tectonophysics 722, 324-341.
939 Huang, B.T., He, Z.Y., Zhang, Z.M., Klemd, R., Zong, K.Q., Zhao, Z.D., 2015a. Early
940 Neoproterozoic granitic gneisses in the Chinese Eastern Tianshan: Petrogenesis
941 and tectonic implications. J. Asian Earth Sci. 113, 339-352.

Huang, G., Niu, G.Z., Wang, X.L., Guo, J., Yu, F., 2012. Formation and emplacement age of Karamaili ophiolite: LA-ICP-MS zircon U-Pb age evidence from the diabase and tuff in eastern Junggar, Xinjiang. Geol. Bullet. China 31, 1267-1278 (in Chinese with English abstract).

Huang, H., Wang, T., Tong, Y., Qin, Q., Ma, X.X., Yin, J.Y., 2020. Rejuvenation of ancient micro-continents during accretionary orogenesis: Insights from the Yili Block and adjacent regions of the SW Central Asian Orogenic Belt. Earth Sci. Rev. 103255. https://doi.org/10.1016/j.earscirev.2020.103255

Huang, Z.Y., Long, X.P., Kröner, A., Yuan, C., Wang, Y.J., Chen, B., Zhang, Y.Y., 2015b. Neoproterozoic granitic gneisses in the Chinese Central Tianshan Block: Implications for tectonic affinity and Precambrian crustal evolution. Precambrian Res. 269, 73-89.

Huang, Z.Y., Long, X.P., Wang, X.C., Zhang, Y.Y., Du, L., Yuan, C., Xiao, W.J., 2017. Precambrian evolution of the Chinese Central Tianshan Block: Constraints on its tectonic affinity to the Tarim Craton and responses to supercontinental cycles. Precambrian Res. 295, 24-37.

Huang, Z.Y., Yuan, C., Long, X.P., Zhang, Y.Y., Du, L., 2019. From Breakup of Nuna to Assembly of Rodinia: A Link Between the Chinese Central Tianshan Block and Fennoscandia. Tectonics 38, 4378-4398.

Jackson, S.E., Pearson, N.J., Griffin, W.L., Belousova, E.A., 2004. The application of laser ablation-inductively coupled plasma-mass spectrometry to in situ U-Pb

zircon geochronology. Chem. Geol. 211, 47-69.

Jiang, T., Gao, J., Klemd, R., Qian, Q., Zhang, X., Xiong, X.M., Wang, X.S., Tan, Z., Chen, B.X., 2014. Paleozoic ophiolitic mélanges from the South Tianshan Orogen, NW China: geological, geochemical and geochronological implications for the geodynamic setting. Tectonophysics 612-613, 106-127.

Jiang, Y.D., Sun, M., Zhao, G.C., Yuan, C., Xiao, W.J., Xia, X.P., Long, X.P., Wu, F.Y., 2011. Precambrian detrital zircons in the Early Paleozoic Chinese Altai: Their provenance and implications for the crustal growth of central Asia. Precambrian Res. 189, 140-154.

Kruhl, J.H. 1996. Prism- and basal-plane parallel subgrain boundaries in quartz: A microstructural geothermobarometer. J. Metamorph. Geol. 14(5), 581-589.

~~Laurent-Charvet, S., Charvet, J., Shu, L.S., 2002. Palaeozoic late collisional strike-slip deformations in Tianshan and Altay, Eastern Xinjiang, NW China. Terra Nova 14, 249-256.~~

Laurent-Charvet, S., Charvet, J., Monié, P., Shu, L.S., 2003. Late Paleozoic strike-slip shear zones in eastern Central Asia (NW China): New structural and geochronological data. Tectonics 22(2), 1009, doi:10.1029/2001TC901047.

Lei, R.X., Wu, C.Z., Gu, L.X., Zhang, Z.Z., Chi, G.X., Jiang, Y.H., 2011. Zircon U-Pb chronology and Hf isotope of the Xingxingxia granodiorite from the Central Tianshan zone (NW China): Implications for the tectonic evolution of the southern Altaids. Gondwana Res. 20, 582-593.

Lei, R.X., Wu, C.Z., Feng, Y.G., Xia, M.Z., Jiao, J.G., 2018. Formation age and geodynamic setting of the Neoproterozoic Shalong iron formation in the Central Tianshan, NW China: Constraints from zircon U-Pb dating, geochemistry, and Hf-Nd isotopes of the host rocks. Geol. J. 53, 345-361.

Liang, P., Chen, H., Hollings, P., Xiao, B., Wu, C., Bao, Z., Cai, K., 2016a. The Paleozoic tectonic evolution and metallogenesis of the northern margin of East Junggar, Central Asia Orogenic Belt: Geochronological and geochemical constraints from igneous rocks of the Qiaoxiahala Fe-Cu deposit. J. Asian Earth Sci. 130, 23-45.

Liang, P., Chen, H.Y., Hollings, P., Wu, C., Xiao, B., Bao, Z.W., Xu, D., 2016b. Geochronology and geochemistry of igneous rocks from the Laoshankou district, north Xinjiang: Implications for the late Paleozoic tectonic evolution and metallogenesis of east Junggar. Lithos 266-267, 115-132.

Li, D.F., Zhang, L., Chen, H.Y., Hollings, P., Cao, M.J., Fang, J., Wang, C.M., Lu, W.J., 2016. Geochronology and geochemistry of the high Mg dioritic dikes in Eastern Tianshan, NW China: Geochemical features, petrogenesis and tectonic implications. J. Asian Earth Sci. 115, 442-454.

Li, J.T., He, X.F., Liu, L., Yang, P.T., Liang, B., Su, H., Yang, Y.D., Han, H.M., Liu, Y.Z., Dai, Z.H., 2017. Ordovician tectonic evolution of Harlik in Eastern Tianshan of Xinjiang: Constraints from LA-ICP-MS zircon U-Pb geochronology and geochemistry of volcanic rocks. Geoscience 31, 460-473 (in Chinese with

English abstract).

Li, J.Y., 2004. Late Neoproterozoic and Paleozoic tectonic framework and evolution of Eastern Xinjiang, NW China. Geol. Rev. 50, 304-322 (in Chinese with English abstract).

Li, J.Y., Wang, K.Z., Sun, G.H., Mo, S.G., Li, W.Q., Yang, T.N., Gao, L.M., 2006. Paleozoic active margin slices in the southern Turfan–Hami basin: geological records of subduction of the Paleo-Asian ocean plate in Central Asian regions. Acta Petrol. Sin. 22, 1087-1102 (in Chinese with English abstract).

Li, J.Y., Yang, T.N., Li, Y.P., Zhu, Z.X., 2009. Geological features of the Karamaili faulting belt, eastern Junggar region, Xinjiang, China and its constraints on the reconstruction of Late Paleozoic ocean-continental framework of the Central Asian region. Geol. Bullet. China 28, 1817-1826 (in Chinese with English abstract).

Li, W., Liu, Y.Q., Dong, Y.P., Zhou, X.H., Liu, X.M., Li, H., Fan, T.T., Zhou, D.W., Xu, X.Y., Chen, J.L., 2013. The geochemical characteristics, geochronology and tectonic significance of the Carboniferous volcanic rocks of the Santanghu area in northeastern Xinjiang, China. Sci. China Earth Sci. 56, 1318-1333.

Lin, W., Faure, M., Shi, Y.H, Wang, Q.C, Li, Z., 2009. Palaeozoic tectonics of the southwestern Chinese Tianshan: new insights from a structural study of the high-pressure/low-temperature metamorphic belt. Int. J. Earth Sci. 98, 1259-1274.

Liu, H.S., Wang, B., Shu, L.S., Jahn, B.M., Lizuka, Y., 2014. Detrital zircon ages of Proterozoic meta-sedimentary rocks and Paleozoic sedimentary cover of northern Yili Block: Implications for the tectonics of microcontinents in the Central Asian Orogenic Belt. Precambrian Res. 252, 209-222.

Liu, L., He, X.F., Li, J.T., Yang, P.T., Liang, B., Su, H., Yang, Y.D., Liu, Y.Z., Dai, Z.H., 2017. Petrogenesis and tectonic significances of the Qincheng Tianshengquan pluton in the Harlik Orogen of Eastern Xinjiang. Geol. Sci. Technol. Info. 36, 86-96 (in Chinese with English abstract).

Liu, S.W., Guo, Z.J., Zhang, Z.C., Li, Q.G., Zheng, H.F., 2004. Nature of Precambrian metamorphic blocks in eastern segment of the Central Tianshan: constraints from geochronology and Nd geochemistry. Sci. China Ser. D Earth Sci. 47, 1085-1094.

Liu, W., Liu, X.J., Liu, L.J., 2013. Underplating generated A- and I-type granitoids of the East Junggar from the lower and the upper oceanic crust with mixing of mafic magma: insights from integrated zircon U-Pb ages, petrography, geochemistry and Nd-Sr-Hf isotopes. Lithos 179, 293-319.

Liu, X.J., Liu, W., Si, C.Q., 2019. Petrogenesis and source rocks of the high-K calc-alkaline and shoshonitic I-type granitoids in the northwestern part of East Junggar, NW China. Lithos 326-327, 298-312.

Liu, Y.S., Gao, S., Hu, Z.C., Gao, C.G., Zong, K.Q., Wang, D.B., 2010a. Continental and oceanic crust recycling-induced melt-peridotite interactions in the

1047 Trans-North China Orogen: U-Pb dating, Hf isotopes and trace elements in
1048 zircons from mantle xenoliths. J. Petrol. 51, 537-571.
1049 Liu, Y.S., Hu, Z.C., Gao, S., Günther, D., Xu, J., Gao, C.G., Chen, H.H., 2008. In situ
1050 analysis of major and trace elements of anhydrous minerals by LA-ICP-MS
1051 without applying an internal standard. Chem. Geol. 257, 34-43.
1052 Liu, Y.S., Hu, Z.C., Zong, K.Q., Gao, C.G., Gao, S., Xu, J., Chen, H.H., 2010b.
1053 Reappraisement and refinement of zircon U-Pb isotope and trace element
1054 analyses by LA-ICP-MS. Chin. Sci. Bull. 55, 1535-1546.
1055 Long, L.L., Wang, J.B., Wang, Y.W., Mao, Q.G., Deng, X.H., Zhao, L.T., Sun, Z.Y.,
1056 Sun, Y., Gao, Y. H., 2016. Discussion on the age of ore-host volcanic strata in the
1057 Kalatage ore concentration area, Eastern Tianshan: Evidence from shrimp zircon
1058 U-Pb dating. Miner. Explor. 7, 31-37 (in Chinese with English abstract).
1059 Long, X.P., Sun, M., Yuan, C., Xiao, W.J., Lin, S.F., Wu, F.Y., Xia, X.P., Cai, K.D.,
1060 2007. Detrital zircon age and Hf isotopic studies for metasedimentary rocks from
1061 the Chinese Altai: Implications for the Early Paleozoic tectonic evolution of the
1062 Central Asian Orogenic Belt. Tectonics 26, TC5015.
1063 Long, X.P., Yuan, C., Sun, M., Xiao, W.J., Zhao, G.C., Wang, Y.J., Cai, K.D., 2010.
1064 Detrital zircon ages and Hf isotopes of the early Paleozoic flysch sequence in the
1065 Chinese Altai, NW China: New constraints on depositional age, provenance and
1066 tectonic evolution. Tectonophysics 480, 213-231.
1067 Long, X.P., Sun, M., Yuan, C., Kröner, A., Hu, A.Q., 2012a. Zircon REE patterns and

1068 geochemical characteristics of Paleoproterozoic anatectic granite in the northern
1069 Tarim Craton, NW China: Implications for the reconstruction of the Columbia
1070 supercontinent. Precambrian Res. 222, 474-487.
1071 Long, X.P., Yuan, C., Sun, M., Safonova, I., Xiao, W.J., Wang, Y.J., 2012b.
1072 Geochemistry and U-Pb detrital zircon dating of Paleozoic graywackes in East
1073 Junggar, NW China: Insights into subduction-accretion processes in the southern
1074 Central Asian Orogenic Belt. Gondwana Res. 21, 637-653.
1075 Luo, J., Xiao, W.J., Wakabayashi, J., Han, C.M., Zhang, J.E., Wan, B., Ao, S.J., Zhang,
1076 Z.Y., Tian, Z.H., Song, D.F., Chen, Y.C., 2017. The Zhaheba ophiolite complex
1077 in Eastern Junggar (NW China): Long lived supra-subduction zone ocean crust
1078 formation and its implications for the tectonic evolution in southern Altaids.
1079 Gondwana Res. 43, 17-40.
1080 Ma, R.S., Shu, L.S., Sun, J.Q., 1997. Tectonic Evolution and Metallogeny of Eastern
1081 Tianshan Mountains. Geological Publishing House, Beijing, pp. 1-202.
1082 Ma, X.X., Shu, L.S., Jahn, B.M., Zhu, W.B., Faure, M., 2012a. Precambrian tectonic
1083 evolution of Central Tianshan, NW China: Constraints from U-Pb dating and in
1084 site Hf isotopic analysis of detrital zircons. Precambrian Res. 222-223, 450-473.
1085 Ma, X.X., Shu, L.S., Santosh, M., Li, J.Y., 2012b. Detrital zircon U-Pb geochronology
1086 and Hf isotope data from Central Tianshan suggesting a link with the Tarim
1087 Block: Implications on Proterozoic supercontinent history. Precambrian Res. 206,
1088 1-16.

1089 Ma, X.X., Shu, L.S., Santosh, M., Li, J.Y., 2013. Petrogenesis and tectonic
1090 significance of an early Palaeozoic mafic-intermediate suite of rocks from the
1091 Central Tianshan, northwest China. Int. Geol. Rev. 55, 548-573.
1092 Ma, X.X., Shu, L.S., Meert, J.G., Li, J.Y., 2014. The Paleozoic evolution of Central
1093 Tianshan: Geochemical and geochronological evidence. Gondwana Res. 25,
1094 797-819.
1095 Ma, X.H., Chen, B., Wang, C., Yan, X.L., 2015. Early Paleozoic subduction of the
1096 Paleo-Asian Ocean: Zircon U-Pb geochronological, geochemical and Sr-Nd
1097 isotopic evidence from the Harlik pluton, Xinjiang. Acta Petrol. Sin. 31, 89-104
1098 (in Chinese with English abstract).
1099 Mao, Q.G., Yu, M.J., Xiao, W.J., Windley, B.F., Li, Y.C., Wei, X.F., Zhu, J.J., Lv, X.Q.,
1100 2018. Skarn-mineralized porphyry adakites in the Harlik arc at Kalatage, E.
1101 Tianshan (NW China): Slab melting in the Devonian-early Carboniferous in the
1102 southern Central Asian Orogenic Belt. J. Asian Earth Sci. 153, 365-378.
1103 Muhtar, M.N., Wu, C.Z., Santosh, M., Lei, R.X., Gu, L.X., Wang, S.M., Gan, K.,
1104 2020. Late Paleozoic tectonic transition from subduction to post-collisional
1105 extension in Eastern Tianshan, Central Asian Orogenic Belt. Geol. Soc. Am. Bull.
1106 132, 1756-1774.
1107 Okay, A.I., Sunal, G., Tüysüz, O., Sherlock, S., Keskin, M., Kylander-Clark, A.R.C.,
1108 2014. Low-pressure–high-temperature metamorphism during extension in a
1109 Jurassic magmatic arc, Central Pontides, Turkey. J. Metamorph. Geol. 32,

49-69.

Passchier, C.W., Trouw, R.A.J., 2005. Microtectonics, second ed. Springer, Berlin, Heidelberg, pp. 1-306.

Rubatto, D., 2017. Zircon: The metamorphic mineral. Rev. Mineral. Geochem. 83, 261-295.

Safonova, I., 2017. Juvenile versus recycled crust in the Central Asian Orogenic Belt: Implications from ocean plate stratigraphy, blueschist belts and intra-oceanic arcs. Gondwana Res. 47, 6-27.

Sawyer, E.W., 2008. Atlas of migmatites. The Canadian Mineralogist Special Publication 9. NRC Research Press, Ottawa, pp. 1-371.

Şengör, A.M.C., Natal'in, B.A., Burtman, V.S., 1993. Evolution of the Altaid tectonic collage and Paleozoic crustal growth in Eurasia. Nature 364, 209-304.

She, J.Z., Yang, W.Z., Xun, Q.U., Jia, J., Di, X.C., 2017. Geochemistry and zircon U-Pb dating of the Dacaotanbei mafic-ultramafic complex, eastern Tianshan and its geological significance. Bull. Mineral. Petrol. Geochem. 36, 82-91 (in Chinese with English abstract).

Shi, Y.R., Liu, D.Y., Zhang, Q., Jian, P., Zhang, F.Q., Miao, L.C., 2007. SHRIMP zircon U-Pb dating of the Gangou granitoids, Central Tianshan Mountains, Northwest China and tectonic significances. Chin. Sci. Bull. 52, 1507-1516.

Shi, Y.R., Zhang, W., Kröner, A., Li, L.L., Jian, P., 2018. Cambrian ophiolite complexes in the Beishan area, China, southern margin of the Central Asian

Orogenic Belt. J. Asian Earth Sci. 153, 193-205.

Shu, L.S., Wang, B., Zhu, W.B., 2007. Age of radiolarian fossils from the Heiyingshan ophiolitic mélange, Southern Tianshan Belt, NW China, and its tectonic significance. Acta Petrol. Sin. 81, 1161-1168 (in Chinese with English abstract).

Shu, L.S., Wang, B., Zhu, W.B., Guo, Z.J., Charvet, J., Zhang, Y., 2011. Timing of initiation of extension in the Tianshan, based on structural, geochemical and geochronological analyses of bimodal volcanism and olistostrome in the Bogda Shan (NW China). Int. J. Earth Sci. 100, 1647-1663.

Shu, L.S., Wang, Y.J., 2003. Late Devonian-Early Carboniferous radiolarian fossils from siliceous rocks of the Kelameili ophiolite, Xinjiang. Geol. Rev. 49, 408-412 (in Chinese with English abstract).

Shu L.S., Zhu, W.B., Wang, B., Faure, M., Charvet, J., Cluzel, D., 2005. The post-collision intracontinental rifting and olistostrome on the southern slope of Bogda Mountains, Xinjiang. Acta Petrol. Sin. 21, 25-36 (in Chinese with English abstract).

Song, D.F., Xiao, W.J., Han, C.M., Li, J.L., Qu, J.F., Guo, Q.Q., Lin, L.N., Wang, Z.M., 2013. Progressive accretionary tectonics of the Beishan orogenic collage, Southern Altaids: Insights from zircon U-Pb and Hf isotopic data of high-grade complexes. Precambrian Res. 227, 368-388.

Song, D.F., Xiao, W.J., Windley, B.F., Han, C.M., Tian, Z.H., 2015. A Paleozoic Japan-type subduction-accretion system in the Beishan orogenic collage,

southern Central Asian Orogenic Belt. Lithos 224, 195-213.

Song, P., Tong, Y., Wang, T., Huang, H., Zhang, J.J., Huang, W., 2018. Zircon U-Pb ages, genetic evolution and geological significance of Carboniferous granites in the Harlik Mountain, East Tianshan, Xinjiang. Geol. Bullet. China 37, 790-804 (in Chinese with English abstract).

Stipp, M., Stünitz, H., Heilbronner, R., Schmid, S.M., 2002. The eastern Tonale fault zone: a 'natural laboratory' for crystal plastic deformation of quartz over a temperature range from 250 to 700 °C. J. Struct. Geol. 24, 1861-1884.

Sun, M., Yuan, C., Xiao, W., Long, X., Xia, X., Zhao, G., Lin, S., Wu, F., Kröner, A., 2008. Zircon U-Pb and Hf isotopic study of gneissic rocks from the Chinese Altai: Progressive accretionary history in the early to middle Paleozoic. Chem. Geol. 247, 352-383.

Sun, S.S., McDonough, W.F., 1989. Chemical and isotopic systematics of oceanic basalts: implications for mantle composition and processes. Geol. Soc. Lond., Spec. Publ. 42, 313-345.

Sun, G.H., Li, J.Y., Gao, L.M., Yang, T.N., 2005. Zircon SHRIMP U-Pb age of a dioritic pluton in the Harlik Mountains, eastern Xinjiang, and its tectonic implications. Geol. Rev. 51, 463-469 (in Chinese with English abstract).

Sun, G.H., Li, J.Y., Zhu, Z.X., Li, Y.P., Yang, Z.Q., 2007a. Detrital zircon SHRIMP U-Pb dating of Carboniferous sandstone from the southern foot of the Harlik Mountains, eastern Xinjiang, and its geological implications. Geol. China 34,

778-789 (in Chinese with English abstract).

Sun, G.H., Li, J.Y., Zhu, Z.X., Li, Y.P., Yang, Z.Q., 2007b. Zircons SHRIMP U-Pb dating of gneissoid-biotite granite in Harlik Mountains, eastern of Xinjiang and its geological implications. Xinjiang Geol. 25, 1-10 (in Chinesewith English abstract).

Sun, G.H., 2007. Structural deformation and tectonic evolution of Harlik Mountain, in Xinjiang since Paleozoic (in Chinese). Ph.D. thesis, Chinese Academy of Geological Science.

Takatsuka, K., Kawakami, T., Skrzypek, E., Sakata, S., Obayashi, H., Hirata, T., 2018. Spatiotemporal evolution of magmatic pulses and regional metamorphism during a Cretaceous flare-up event: Constraints from the Ryoke belt (Mikawa area, central Japan). Lithos 308, 428-445.

Vernon, R.H., 1982. Isobaric cooling of two regional metamorphic complexes related to igneous intrusions in southern Australia. Geology 10, 76-81.

Wali, G., Wang, B., Cluzel, D., Zhong, L.L., 2018. Carboniferous-Early Permian magmatic evolution of the Bogda Range (Xinjiang, NW China): Implications for the Late Paleozoic accretionary tectonics of the SW Central Asian Orogenic Belt. J. Asian Earth Sci. 153, 238-251.

Wang, B., Cluzel, D., Shu, L.S., Faure, M., Charvet, J., Chen, Y., Meffre, S., de Jong, K., 2009a. Evolution of calc-alkaline to alkaline magmatism through Carboniferous convergence to Permian transcurrent tectonics, western Chinese

Tianshan. Int. J. Earth Sci. 98, 1275-1298.

Wang, B., Cluzel, D., Jahn, B.M., Shu, L.S., Chen, Y., Zhai, Y.Z., Branquet, Y., Barbanson, L., Sizaret, S., 2014a. Late paleozoic pre- and syn-kinematic plutons of the Kangguer-Huangshan Shear zone: Inference on the tectonic evolution of the eastern Chinese north Tianshan. Am. J. Sci. 314, 43-79.

Wang, B., Faure, M., Shu, L.S., de Jong, K., Charvet, J., Cluzel, D., Jahn, B.M., Chen, Y., Ruffet, G., 2010. Structural and geochronological study of High-Pressure metamorphic rocks in the Kekesu section (Northwestern China): implications for the late Paleozoic tectonics of the southern Tainshan. J. Geol. 118, 59-77.

Wang, B., Shu, L.S., Faure, M., Jahn, B.M., Cluzel, D., Charvet, J., Chung, S.L., Meffre, S., 2011a. Paleozoic tectonics of the southern Chinese Tianshan: Insights from structural, chronological and geochemical studies of the Heiyingshan ophiolitic mélange (NW China). Tectonophysics 497, 85-104.

Wang, B.Y., Jiang, C.Y., Li, Y.J., Wu, H.E., Xia, Z.D., Lu, R.H., 2009b. Geochemistry and tectonic implications of Karamaili ophiolite in East Junggar of Xinjiang. J. Minearl. Petrol. 29, 74-82 (in Chinese with English abstract).

Wang, B., Zhai, Y.Z., Kapp, P., de Jong, K., Zhong, L.L., Liu, H.S., Ma, Y.Z., Gong, H.J., Geng, H.J., 2018a. Accretionary tectonics of back-arc oceanic basins in the South Tianshan: Insights from structural, geochronological, and geochemical studies of the Wuwamen ophiolite mélange. Geol. Soc. Am. Bull. 130, 284-306.

Wang, C., Chen, B., Ma, X.H., Yan, X.L., 2015. Petrogenesis of Early and Late

Paleozoic plutons in Sanchakou area of East Tianshan and their implications for evolution of Kangur suture zone. J. Earth Sci. Environ. 5, 52-70 (in Chinese with English abstract).

Wang, C.S., Gu, L.X., Zhang, Z.Z., Wu, C.Z., Tang, J.H., Tang, X.Q., 2009c. Petrogenesis and geological implications of the Permian high-k calc-alkaline granites in Harlik Mountains of eastern Tianshan, NW China. Acta Petrol. Sin. 25, 1499-1511 (in Chinese with English abstract).

Wang, C.S., Gu, L.X., Zhang, Z.Z., Wu, C.Z., Tang, J.H., San, J.Z., Li, G.R., Li, Z.H., 2009d. Petrogenesis and tectonic implications of the Permian alkaline granite and quartz-syenite assemblage in Harlik Mountains, Xinjiang. Acta Petrol. Sin. 25, 3182-3196 (in Chinese with English abstract).

Wang, G.C., Zhang, M., Feng, J.L., Liao, Q.A., Zhang, X.H., Kang, L., Guo, R.L., Xuan, Z.Y., Han, K.Y., 2019. New understanding of the tectonic framework and evolution during the Neoproterozoic-Paleozoic era in the East Tianshan Mountains. J. Geomech. 25, 798-819 (in Chinese with English abstract).

Wang, X.S., Gao, J., Klemd, R., Jiang, T., Li, J.L., Zhang, X., Tan, Z., Li, L., Zhu, Z.X., 2014b. Geochemistry and geochronology of the Precambrian high-grade metamorphic complex in the Southern Central Tianshan ophiolitic mélange, NW China. Precambrian Res. 254, 129-148.

Wang, X.S., Gao, J., Klemd, R., Jiang, T., Li, J.L., Zhang, X., Xue, S.C., 2017. The Central Tianshan Block: A microcontinent with a Neoarchean-Paleoproterozoic

basement in the southwestern Central Asian Orogenic Belt. Precambrian Res. 295, 130-150.

Wang, Y.F., Chen, H.Y., Han, J.S., Chen, S.B., Huang, B.Q., Li, C., Tian, Q.L., Wang, C., Wu, J.X., Chen, M.X., 2018b. Paleozoic tectonic evolution of the Dananhu-Tousuquan island arc belt, eastern Tianshan: Constraints from the magmatism of the Yuhai porphyry Cu deposit, Xinjiang, NW China. J. Asian Earth Sci. 153, 282-306.

Wang, Y.H., Zhang, F.F., Liu, J.J., 2016. The genesis of the ores and intrusions at the Yuhai Cu-Mo deposit in eastern Tianshan, NW China: Constraints from geology, geochronology, geochemistry, and Hf isotope systematics. Ore Geol. Rev. 77, 312-331.

Wang, Y.J., Yuan, C., Long, X.P., Sun, M., Xiao, W.J., Zhao, G.C., Cai, K.D., Jiang, Y.D., 2011b. Geochemistry, zircon U-Pb ages and Hf isotopes of the Paleozoic volcanic rocks in the northwestern Chinese Altai: Petrogenesis and tectonic implications. J. Asian Earth Sci. 42 (5), 969-985.

Wang, Y.J., Long, X.P., Wilde, S.A., Xu, H.L., Sun, M., Xiao, W.J., Yuan, C., Cai, K.D., 2014c. Provenance of Early Paleozoic metasediments in the central Chinese Altai: Implications for tectonic affinity of the Altai-Mongolia terrane in the Central Asian Orogenic Belt. Lithos 210-211, 57-68.

Wang, Y., Li, J.Y., Sun, G.H., 2008. Postcollisional eastward extrusion and tectonic exhumation along the Eastern Tianshan Orogen, Central Asia: Constraints from

dextral strike-slip motion and $^{40}Ar/^{39}Ar$ geochronological evidence. J. Geol. 116, 599-618.

~~Wang, Z.M., Han, C.M., Xiao, W.J., Su, B.X., Sakyi, P.A., Song, D.F., Lin, L.N., 2014d. The petrogenesis and tectonic implications of the granitoid gneisses from Xingxingxia in the eastern segment of Central Tianshan. J. Asian Earth Sci. 88, 277-292.~~

Windley, B.F., Alexeiev, D., Xiao, W., Kröner, A., Badarch, G., 2007. Tectonic models for accretion of the Central Asian Orogenic Belt. J. Geol. Soc. Lond. 164, 31-47.

XBGMR (Xinjiang Bureau of Geology and Mineralogy Resources), 1966. Geological Map 1: 200000, Yiwu sheet (K-46-XI).

XBGMR (Xinjiang Bureau of Geology and Mineral Resources), 1993. Regional Geology of Xinjiang Uygur Autonomy Region. Geology Publishing House, Beijing, pp. 1-841 (in Chinese).

XGSC (Xi'an Geological Survey Center), 2007. Geological Map of Tianshan and Adjacent region (1:1,000,000).

Xia, L.Q., Zhang, G.W., Xia, Z.C., Xu, X.Y., Dong, Y.P., Li, X.M., 2002. Constraints on the timing of opening and closing of the Tianshan Paleozoic ocenic basin: Evidence from Sinian and Carboniferous volcanic rocks. Geol. Bullet. China 21, 55-62 (in Chinese with English abstract).

Xia, L.Q., Xia, Z.C., Xu, X.Y., Li, X.M., Ma, Z.P., 2008. Relative contributions of crust and mantle to the generation of the Tianshan Carboniferous rift-related

basic lavas, northwestern China. J. Asian Earth Sci. 31, 357-378.

Xia, L.Q., Xu, X.Y., Li, X.M., Ma, Z.P., Xia, Z.C., 2012. Reassessment of petrogenesis of Carboniferous-early Permian rift-related volcanic rocks in the Chinese Tianshan and its neighboring areas. Geosci. Front. 3, 445-471.

Xiao, B., Chen, H.Y., Wang, Y.F., Yang, J.T., 2015. Discovery of the Late Silurian granodiorite and its tectonic significance in the Tuwu-Yandong porphyry copper deposits, Dananhu-Tousuquan island arc, Eastern Tianshan. Earth Sci. Front. 22, 251-266 (in Chinese with English abstract).

Xiao, W.J., Mao, Q.G., Windley, B.F., Han, C.M., Qu, J.F., Zhang, J.E., Ao, S.J., Guo, Q.Q., Cleven, N.R., Lin, S.F., Shan, Y.H., Li, J.L., 2010. Paleozoic multiple accretionary and collisional processes of the Beishan orogenic collage. Am. J. Sci. 310, 1553-1594.

Xiao, W.J., Windley, B.F., Allen, M.B., Han, C.M, 2013. Paleozoic multiple accretionary and collisional tectonics of the Chinese Tianshan orogenic collage. Gondwana Res. 23, 1316-1341.

Xiao, W.J., Windley, B.F., Huang, B.C., Han, C.M., Yuan, C., Chen, H.L., Sun, M., Sun, S., Li, J.L., 2009. End-Permian to mid-Triassic termination of the accretionary processes of the southern Altaids: implications for the geodynamic evolution, Phanerozoic continental growth, and metallogeny of Central Asia. Int. J. Earth Sci. 98, 1189-1217.

Xiao, W.J., Zhang, L.C., Qin, K.Z., Sun, S., Li, J.L., 2004. Paleozoic accretionary and

collisional tectonics of the Eastern Tianshan (China): Implications for the continental growth of Central Asia. Am. J. Sci. 304, 370-395.

Xiao, Y., Zhang, H.F., Shi, J.A., Su, B.X., Sakyi, P.A., Lu, X.C., Hu, Y., Zhang, Z., 2011. Late Paleozoic magmatic record of East Junggar, NW China and its significance: Implication from zircon U-Pb dating and Hf isotope. Gondwana Res. 20, 532-542.

Xie, W., Xu, Y.G., Chen, Y.B., Luo, Z.Y., Liu, H.Q., 2016a. High-alumina basalts from the Bogda Mountains suggest an arc setting for Chinese Northern Tianshan during the Late Carboniferous. Lithos 256, 165-181.

Xie, W., Xu, Y.G., Luo, Z.Y., Chen, Y.B., Hong, L.B., Ma, L., Ma, Q., 2016b. Petrogenesis and geochemistry of the Late Carboniferous rear-arc (or back-arc) pillow basaltic lava in the Bogda Mountains, Chinese North Tianshan. Lithos 244, 30-42.

Xie, W., Xu, Y.G., Luo, Z.Y., Liu, H.Q., Hong, L.B., Ma, L., 2016c. Petrogenesis and geodynamic implications of the Late Carboniferous felsic volcanics in the Bogda belt, Chinese Northern Tianshan. Gondwana Res. 39, 165-179.

Xu, X.W., Ma, T.L., Sun, L.Q., Cai, X.P., 2003. Characteristics and dynamic origin of the large-scale Jiaoluotage ductile compressional zone in the eastern Tianshan Mountains, China. J. Struct. Geol. 25, 1901-1915.

Xu, X.W., Jiang, N., Li, X.H., Qu, X., Yang, Y.H., Mao, Q., Wu, Q., Zhang, Y., Dong, L.H., 2013. Tectonic evolution of the East Junggar terrane: Evidence from the

Taheir tectonic window, Xinjiang, China. Gondwana Res. 24, 578-600.

Xu, X.W., Jiang, N., Li, X.H., Wu, C., Qu, X., Zhou, G., Dong, L.H., 2015a. Spatial-temporal framework for the closure of the Junggar Ocean in central Asia: New SIMS zircon U-Pb ages of the ophiolitic mélange and collisional igneous rocks in the Zhifang area, East Junggar. J. Asian Earth Sci. 111, 470-491.

Xu, X.W., Li, X.H., Jiang, N., Li, Q.L., Qu, X., Yang, Y.H., Dong, L.H., 2015b. Basement nature and origin of the Junggar terrane: New zircon U-Pb-Hf isotope evidence from Paleozoic rocks and their enclaves. Gondwana Res. 28, 288-310.

Xu, X.Y., Li, X.M., Ma, Z.P., Xia, L.Q., Xia, Z.C., Peng, S.X., 2006a. LA-ICP-MS zircon U-Pb dating of gabbro from the Bayingou ophiolite in the northern Tianshan Mountains. Acta Geol. Sin. 80, 1168-1176 (in Chinese with English abstract).

Xu, X.Y., Xia, L.Q., Ma, Z.P., Wang, Y.B., Xia, Z.C., Li, X.M., Wang, L.S., 2006b. SHRIMP zircon U-Pb geochronology of the plagiogranites from Bayingou ophiolite in North Tianshan Mountains and the petrogenesis of the ophiolite. Acta Petrol. Sin. 22, 83-94 (in Chinese with English abstract).

Yang, J.S., Xu, X.Z., Li, T.F., Chen, S.Y., Ren, Y.F., Li, J.Y., Liu, Z., 2011a. U-Pb ages of zircons from ophiolite and related rocks in the Kumishi region at the southern margin of Middle Tianshan, Xinjiang: Evidence of early Paleozoic oceanic basin. Acta Petrol. Sin. 27, 77-95 (in Chinese with English abstract).

Yang, M., Wang, J.L., Wang, J.Q., Dang, F.P., 2012a. Studies on geochemistry, zircon

U-Pb geochronology and Hf isotopes of granite in Wangfeng area at the northern margin of Middle Tianshan, Xinjiang. Acta Petrol. Sin. 28, 2121-2131 (in Chinese with English Abstract).

Yang, T.N., Li, J.Y., Zhang, J., Hou, K.J., 2011b. The Altai-Mongolia terrane in the Central Asian Orogenic Belt (CAOB): A peri-Gondwana one? Evidence from zircon U-Pb, Hf isotopes and REE abundance. Precambrian Res. 187, 79-98.

Yang, W.B., Niu, H.C., Shan, Q., Sun, W.D., Zhang, H., Li, N.B., Jiang, Y.H., Yu, X.Y., 2014. Geochemistry of magmatic and hydrothermal zircon from the highly evolved Baerzhe alkaline granite: Implications for Zr-REE-Nb mineralization. Miner. Deposita 49, 451-470.

Yang, X.F., He, D.F., Wang, Q.C., Tang, Y., Tao, H.F., Li, D., 2012b. Provenance and tectonic setting of the Carboniferous sedimentary rocks of the East Junggar Basin, China: Evidence from geochemistry and U-Pb zircon geochronology. Gondwana Res. 22, 567-584.

Yin, J.Y., Chen, W., Xiao, W.J., Yuan, C., Zhang, B., Cai, K.D., Long, X.P., 2017. Geochronology, petrogenesis and tectonic significance of the latest Devonian-early Carboniferous I-type granites in the Central Tianshan, NW China. Gondwana Res. 47, 188-199.

Yuan, C., Sun, M., Xiao, W.J., Li, X.H., Chen, H.L., Lin, S.F., Xia, X.P., Long, X.P., 2007. Accretionary orogenesis of the Chinese Altai: Insights from Paleozoic granitoids. Chem. Geol. 242, 22-39.

1362 Yuan, C., Sun, M., Wilde, S., Xiao, W.J., Xu, Y.G., Long, X.P., Zhao, G.C., 2010.
1363 Post-collisional plutons in the Balikun area, East Chinese Tianshan: Evolving
1364 magmatism in response to extension and slab break-off. Lithos 119, 269-288.
1365 Yuan, Y., Zong, K.Q., He, Z.Y., Klemd, R., Liu, Y.S., Hu, Z.C., Guo, J.L., Zhang,
1366 Z.M., 2015. Geochemical and geochronological evidence for a former early
1367 Neoproterozoic microcontinent in the South Beishan Orogenic Belt,
1368 southernmost Central Asian Orogenic Belt. Precambrian Res. 266, 409-424.
1369 Yu, J.Y., Guo, L., Li, J.X., Li, Y.G., Smithies, R.H., Wingate, M.T.D., Meng, Y., Chen,
1370 S.F., 2016. The petrogenesis of sodic granites in the Niujuanzi area and
1371 constraints on the Paleozoic tectonic evolution of the Beishan region, NW China.
1372 Lithos 256-257, 250-268.
1373 Zeng, L., Niu, H., Bao, Z., Shan, Z., Li, H., Yang, W., 2015. Petrogenesis and tectonic
1374 significance of the plagiogranites in the Zhaheba ophiolite, Eastern Junggar
1375 orogen, Xinjang, China. J. Asian Earth Sci. 113, 137-150.
1376 Zhang, J., Sun, M., Schulmann, K., Zhao, G.C., Wu, Q.H., Jiang, Y.D., Guy, A., Wang,
1377 Y.J., 2015a. Distinct deformational history of two contrasting tectonic domains in
1378 the Chinese Altai: Their significance in understanding accretionary orogenic
1379 process. J. Struct. Geol. 73, 64-82.
1380 Zhang, W.F., Chen, H.Y., Han, J.S., Zhao, L.D., Huang, J.H., Yang, J.T., Yan, X.L.,
1381 2016. Geochronology and geochemistry of igneous rocks in the Bailingshan area:
1382 Implications for the tectonic setting of late Paleozoic magmatism and iron skarn

mineralization in the eastern Tianshan, NW China. Gondwana Res. 38, 40-59.

Zhang, X.R., Zhao, G.C., Eizenhöfer, P.R., Sun, M., Han, Y.G., Hou, W.Z., Liu, D.X., Wang, B., Liu, Q., Xu, B., 2015b. Latest Carboniferous closure of the Junggar Ocean constrained by geochemical and zircon U-Pb-Hf isotopic data of granitic gneisses from the Central Tianshan block, NW China. Lithos 238, 26-36.

Zhang, X.R., Zhao, G.C., Sun, M., Eizenhöfer, P.R., Han, Y.G., Hou, W.Z., Liu, D.X., Wang, B., Liu, Q., Xu, B., 2016a. Tectonic evolution from subduction to arc-continent collision of the Junggar ocean: Constraints from U-Pb dating and Hf isotopes of detrital zircons from the North Tianshan belt, NW China. Geol. Soc. Am. Bull. 128, 644-660.

Zhang, X.R., Zhao, G.C., Eizenhöfer, P.R., Sun, M., Han, Y.G., Hou, W.Z., Liu, D.X., Wang, B., Liu, Q., Xu, B., 2016b. Tectonic transition from late carboniferous subduction to early Permian post-collisional extension in the eastern Tianshan, NW China: Insights from geochronology and geochemistry of mafic-intermediate intrusions. Lithos 256-257, 269-281.

Zhang, Y.Y., Pe-Piper, G., Piper, D.J.W., Guo, Z.J., 2013. Early Carboniferous collision of the Kalamaili orogenic belt, North Xinjiang, and its implications: Evidence from molasse deposits. Geol. Soc. Am. Bull. 125, 932-944.

Zhang, Y.Y., Sun, M., Yuan, C., Long, X.P., Jiang, Y.D., Li, P.F., Huang, Z., Du, L., 2018. Alternating trench advance and retreat: Insights from Paleozoic magmatism in the eastern Tianshan, Central Asian Orogenic Belt. Tectonics 37,

2142-2164.

Zhang, Y.Y., Yuan, C., Long, X.P., Sun, M., Huang, Z.Y., Du, L., Wang, X.Y., 2017. Carboniferous bimodal volcanic rocks in the Eastern Tianshan, NW China: Evidence for arc rifting. Gondwana Res. 43, 92-106.

Zhang, Y.Y., Yuan, C., Sun, M., Long, X.P., Huang, Z.Y., Jiang, Y.D., Li, P.F., Du, L., 2020. Two late Carboniferous belts of Nb-enriched mafic magmatism in the Eastern Tianshan: Heterogeneous mantle sources and geodynamic implications. Geol. Soc. Am. Bull. 132, 1404-1418.

Zhang, Z.W., Zang, Y.S., Wang, Y.L., Chen, S.B., 2016c. Zircon SHRIMP U-Pb age of the Yuhai prophyry copper deposit in Eastern Tianshan Mountains of Xinjiang and its tectonic implications. Acta Geosci. Sin. 37, 59-68 (in Chinese with English abstract).

Zhao, L.D., Chen, H.Y., Hollings, P., Han, J.S., 2019. Late Paleozoic magmatism and metallogenesis in the Aqishan-Yamansu belt, Eastern Tianshan: Constraints from the Bailingshan intrusive complex. Gondwana Res. 65, 68-85.

Zhao, M., Shu, L.S., Wang, C.Y., 1997. Characteristics of metamorphism in the Harlik Metamorphic Belt, east Xinjiang, and its tectonic envorionment. Geol. J. China Univ. 3, 40-50 (in Chinese with English abstract).

Zhao, M., Shu, L.S., Zhu, W.B., Wang, C.Y. Ma, R.S., 2002. Zircon U-Pb dating of the rocks from the Harlik Metamorphic Belt in eastern Xinjiang and its geological significance. Acta Geol. Sin. 76, 379-383 (in Chinese with English

abstract).

Zheng, J.H., Chai, F.M., Feng, W.Y., Yang, F.Q., Shen, P., 2018. Geochemistry and chronology of the early Paleozoic diorites and granites in the Huangtupo volcanogenic massive sulfide (VMS) deposit, Eastern Tianshan, NW China: Implications for petrogenesis and geodynamic setting. Lithos 302-303, 455-466.

Zhong, L.L., Wang, B., Alexeiev, D.V., Cao, Y.C., Biske, Y.S., Liu, H.S., Zhai, Y.Z., Xing, L.Z., 2017. Paleozoic multi-stage accretionary evolution of the SW Chinese Tianshan: New constraints from plutonic complex in the Nalati Range. Gondwana Res. 45, 254-274.

Zhong, L.L., Wang, B., Shu, L.S., Liu, H.S., Mu, L.X., Ma, Y.Z., Zhai, Y.Z., 2015. Structural overprints of early Paleozoic arc-related intrusive rocks in the Chinese Central Tianshan: Implications for Paleozoic accretionary tectonics in SW Central Asian Orogenic Belts. J. Asian Earth Sci. 113, 194-217.

Zhong, L.L., Wang, B., de Jong, K., Zhai, Y.Z., Liu, H.S., 2019. Deformed continental arc sequences in the South Tianshan: New constraintson the Early Paleozoic accretionary tectonics of the Central Asian Orogenic Belt. Tectonophysics 768, 228169.

Zhou, G.Q., 2004. The two-fold-contact metamorphic rocks occurring at Xiaopu, Hami, Eastern Xinjiang, their mineral paragenesis analysis and PTt path. Acta Mineral. Sin. 24, 290-300 (in Chinese with English abstract).

Zhu, X.H., Zhu, T., Zhang, X., Xi, R.G., Meng, Y., Wang, K., 2018. Petrogenesis and

geological implications of late Carboniferous leucogranites in Harlik aera, eastern Xinjiang. Earth Sci. 43, 179-194 (in Chinese with English abstract).

Zong, K.Q., Klemd, R., Yuan, Y., He, Z.Y., Guo, J.L., Shi, X.L., Liu, Y., Hu, Z., Zhang, Z., 2017. The assembly of Rodinia: The correlation of early Neoproterozoic (ca. 900 Ma) high-grade metamorphism and continental arc formation in the southern Beishan Orogen, southern Central Asian Orogenic Belt (CAOB). Precambrian Res. 290, 32-48.

Figure and Table captions:

Fig. 1. (a) Tectonic sketch map of Eurasia showing the location of the Central Asian Orogenic Belt (modified from Sengör et al., 1993). (b) Sketch map of the northern Xinjiang area, NW China, showing tectonic subdivisions of the Chinese Tianshan (modified from Wang et al., 2014a ~~and He et al., 2014~~). Abbreviations: NTB = North Tianshan Belt, CTB = Central Tianshan Belt, STB = South Tianshan Belt. (c) Geological map of the northeastern Tianshan Belt (modified from 1:1,000,000 scale geological map of the Chinese Tianshan and surrounding regions, after XGSC, 2007).

Fig. 2. (a) Geological map of the Harlik Range, North Tianshan (modified from 1:200,000 scale geological map No. K-46-XI by XBGMR, 1966). (b) Detailed geological map of the Qincheng area, North Tianshan showing the metamorphic zone

and sampling sites (modified from Sun, 2007). Dating results are from Sun, 2007; Chen and Shu, 2010. Abbreviations: Bt = Biotite Ar-Ar age, Mus = Muscovite Ar-Ar age, Zr = Zircon U-Pb age. (c) Cross-section of the ~~metamorphic belt~~Julideneng Metamorphic Complex (JMC) in the Qincheng area showing the occurrence of migmatites and sampling sites. Stereograms of the bedding and foliation are equal-area Schmidt net, lower hemisphere.

Fig. 3. Representative field photographs of meta-sedimentary rocks and migmatites in the Qincheng area, North Tianshan. (a) Weakly deformed and metamorphosed sandstone and siltstone. The cleavage S1 is steeper than the bedding S0 indicating a normal sequence. (b) Migmatite with leucosome (Leu), melanosome (Mel) and mesosome (Mes). (c) Parallel and consistent foliations in ~~gneissic~~ gneissic-granite and schist. (d) Migmatite with ~~unregular~~ irregular transition between leucosome and melanosome. (e) ~~The~~ F~~f~~aulted contact ~~zone~~ between meta-sandstones and migmatites.

Fig. 4. Photomicrographs of metamorphic rocks and migmatites from the Qincheng area, North Tianshan. (a-c) Mica-schists (12TS119A, B and E) showing preferred orientations of mica and sillimanite. (d) Meta-sandstone (12TS119F) with weak orientation of chloritized mica and tabular feldspar grains. (e) Cuspate and lobate grain boundaries between plagioclase and quartz with chessboard subgrains (12TS119G). (f) Optically continuous K-feldspar enclosing diamond-shaped quartz

crystals in leucosome (12TS119H). Mineral abbreviations: Kf = K-feldspar; Bt = biotite; Chl = chlorite; Mus = muscovite; Pl = plagioclase; Qz = quartz; Sil = sillimanite.

Fig. 5. Cathodoluminescence images for representative ~~detrital~~ zircons from meta-sandstone (12TS119F) and mica schists (12TS119A, B and E) showing their apparent $^{206}Pb/^{238}U$ ages (<1000 Ma) or $^{207}Pb/^{206}Pb$ ages (>1000 Ma). Four types of zircons can be recognized. See text for more explanations. The CL images of all the dated zircons can be found in Supplementary Fig. S1.

Fig. 6. Concordia diagrams (a, c, e and g) and U-Pb age probability diagrams (b, d, f and h), and insets are plots of Th/U ratios vs. U-Pb age for detrital zircons from the meta-sedimentary rocks, southern Harlik Range.

Fig. 7. Chondrite-normalized REE patterns for detrital zircons from meta-sandstone 12TS119F (a), mica schist 12TS119E (b), and two migmatites 12TS119G and 12TS119H (c-d). Only the Paleozoic detrital zircons with $^{206}Pb/^{238}U$ ages between 425 Ma and 475 Ma were analyzed for REE abundances. The grey shaded area is the REE composition of hydrothermal zircons (after Hoskin, 2005; Yang et al., 2014) and magmatic zircons of various igneous rocks (Belousova et al., 2002; Hoskin, 2005; Long et al., 2012a; Yang et al., 2014). Insets are plots of Th/U ratios against U-Pb age.

Chondrite normalization values are from Sun and McDonough (1989).

Fig. 8. (a-b) Cathodoluminescence images showing $^{206}Pb/^{238}U$ apparent ages, (c-d) Concordia diagrams, and (e-f) U-Pb age probability diagrams for the zircons from the migmatites, Qincheng area, North Tianshan.

Fig. 9. (a) Compilation of zircon U-Pb ages for granites ~~intruding in~~crosscuting the meta-sedimentary rocks of the Harlik area (data from Sun et al., 2007b; Wang et al., 2009c; Chen and Shu, 2010; Chen et al., 2016; Song et al., 2018). (b) U-Pb age spectra of Paleozoic zircons from the migmatites and meta-sedimentary rocks of the Qincheng area (this study), North Tianshan.

Fig. 10. Compilation of zircon U-Pb ages from the Qincheng area and neighboring tectonic units. The right columns show the age distributions of Precambrian zircons only. DZ: Detrital zircons from sedimentary rocks; IZ: Zircons from igneous rocks (Inherited zircons were excluded). All the reference data and corresponding literature~~s~~ are listed in Supplementary Table S2.

Fig. 11. Tentative cartoon model for the Paleozoic tectonic evolution of the North Tianshan Belt and adjacent areas.

Table 1. Sample description and analytical data summary.

Supplementary Fig. S1. Cathodoluminescence images for all the dated detrital zircons from the meta-sedimentary rocks, Qincheng area, North Tianshan.

Supplementary Fig. S2. Discrimination diagrams for magmatic and hydrothermal zircons of the meta-sedimentary rocks and migmatites (after Hoskin, 2005). (a, c, e and g) $(Sm/La)_N$ (chondrite-normalized Sm/La ratio) vs. La (ppm) plots. (b, d, f and h) Ce/Ce* (Ce anomaly) vs. $(Sm/La)_N$ plots. Chondrite normalization values are from Sun and McDonough (1989).

Supplementary Table S1. LA-ICP-MS zircon U-Pb analytical results of the meta-sedimentary rocks and migmatites from the Qincheng area, North Tianshan.

Supplementary Table S2. REE abundances of representative zircons of meta-sedimentary rocks and migmatites from the Qincheng area, North Tianshan.

Supplementary Table S3. Compilations of zircon U-Pb ages from the Qincheng area, North Tianshan and the neighboring Central Tianshan, East Junggar, and Chinese Altai.

Figure 1

Click here to access/download;Figure;Fig. 1. Map of North Tianshan.jpg

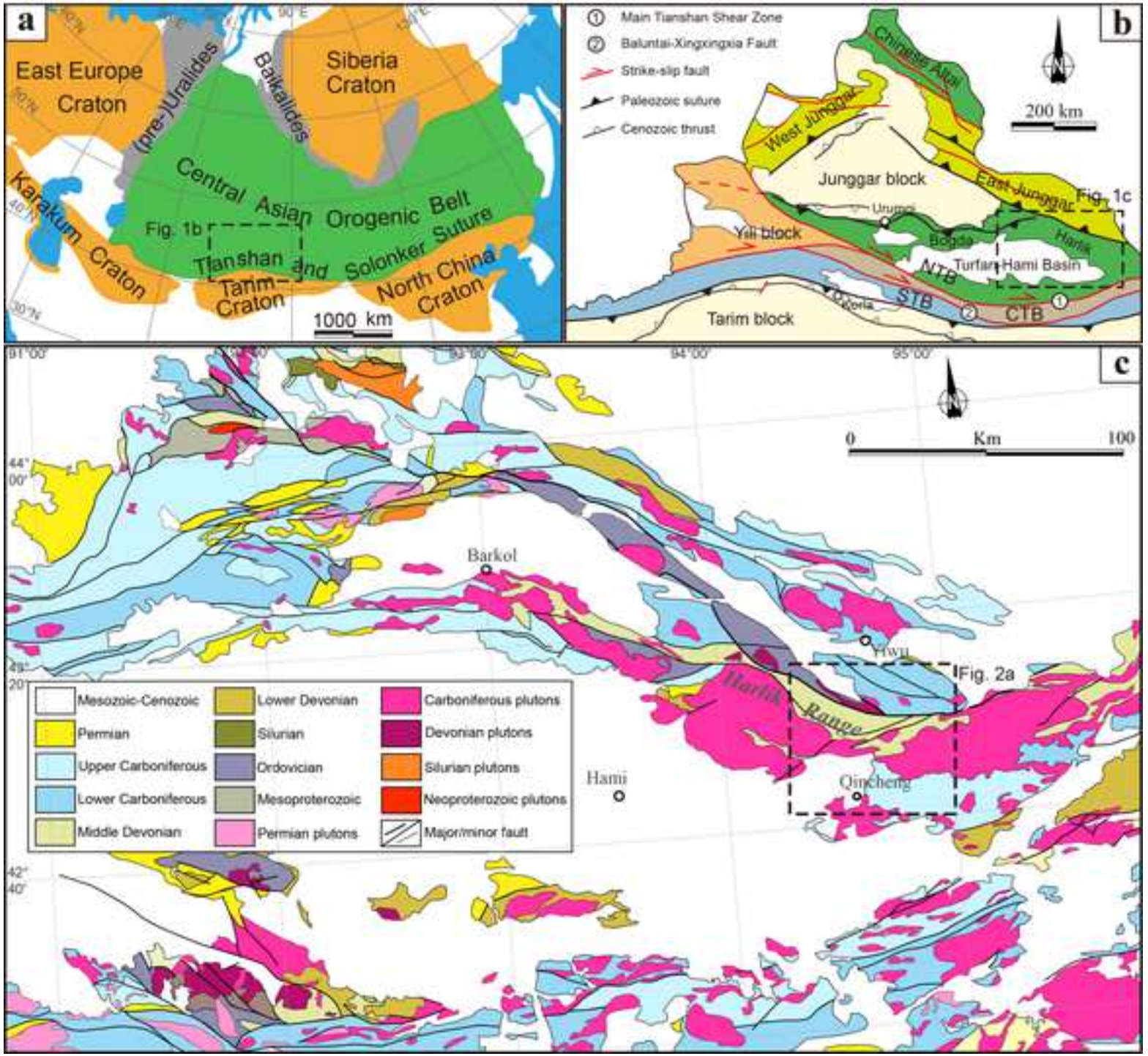

Figure 2

Click here to access/download;Figure;Fig. 2. Geological map of the Qincheng area.jpg

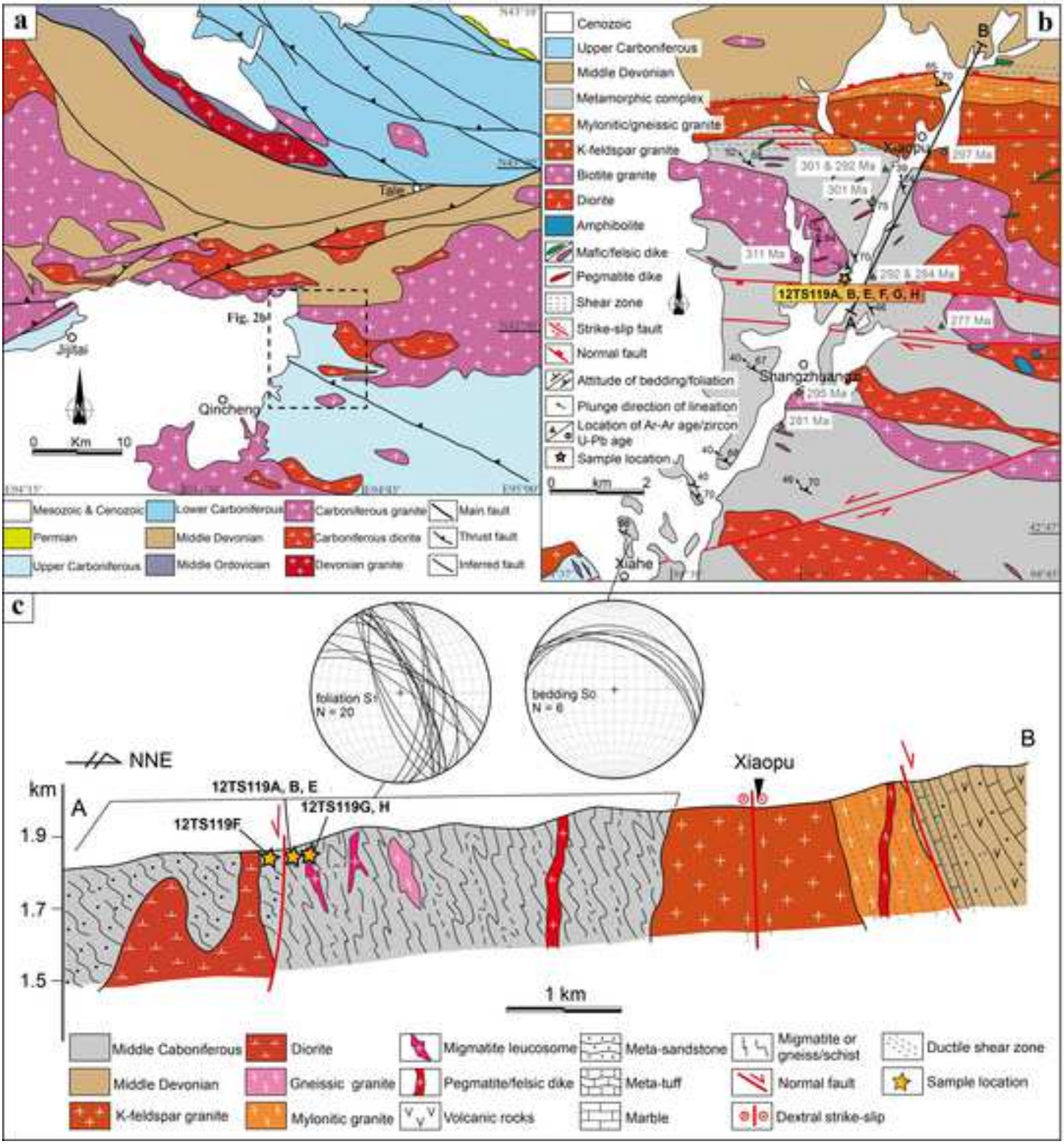

Figure 3

Click here to access/download;Figure;Fig. 3. Representative field photographs.jpg

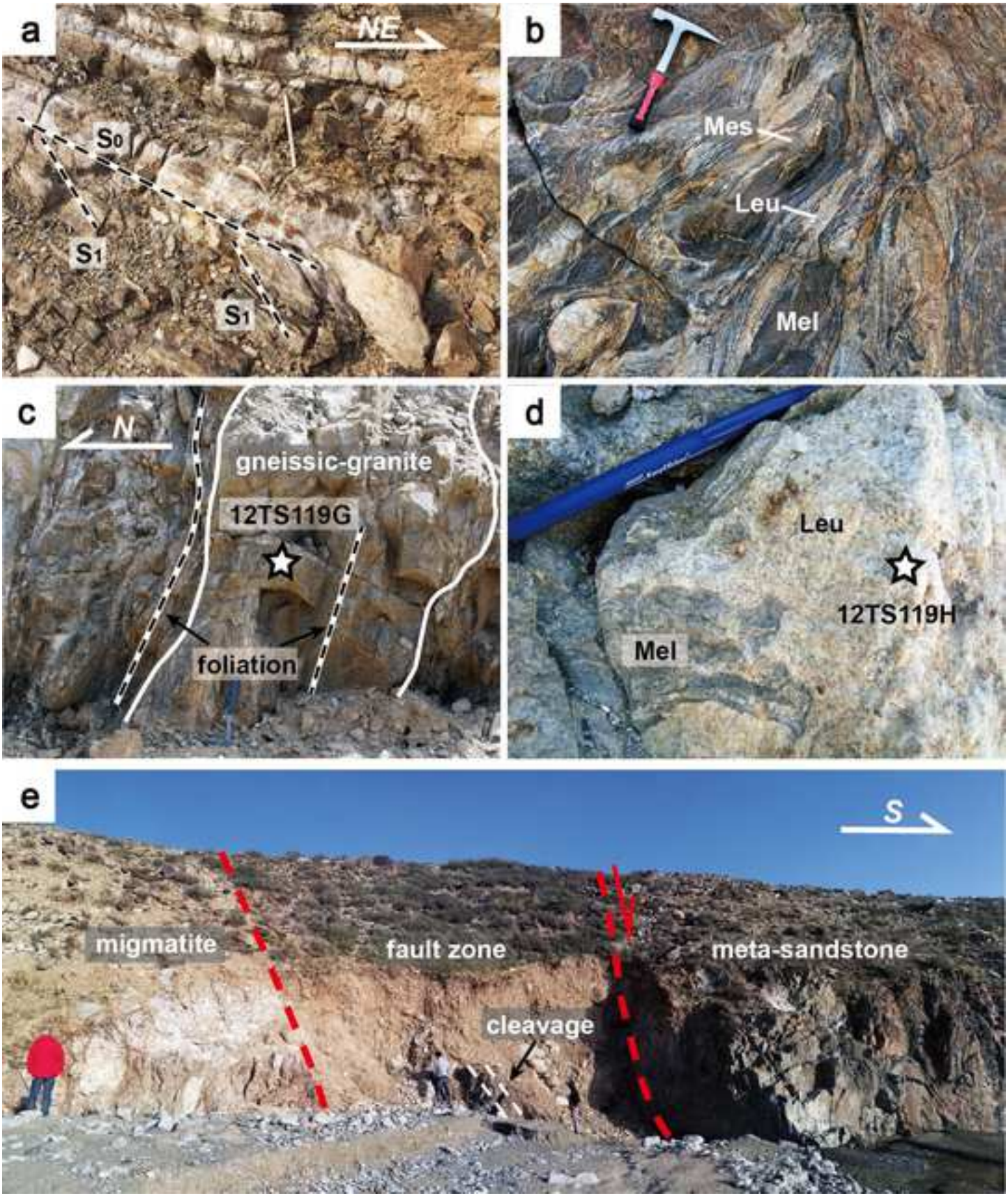

Figure 4

Click here to access/download;Figure;Fig. 4. Photomicrographs of metamorphic rocks and migmatites.jpg

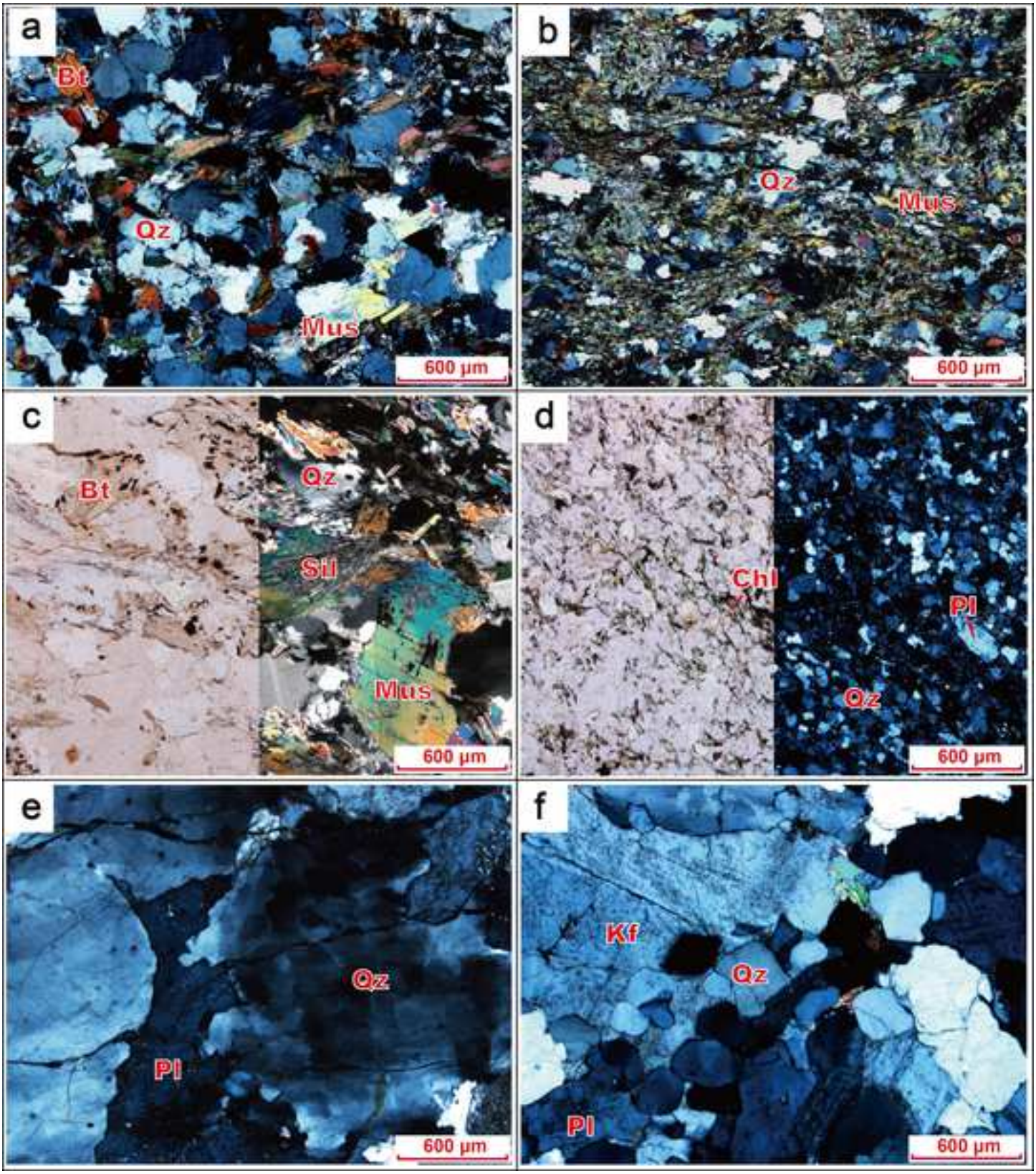

Figure 5

Click here to access/download;Figure;Fig. 5. CL images for representative detrital zircons.jpg

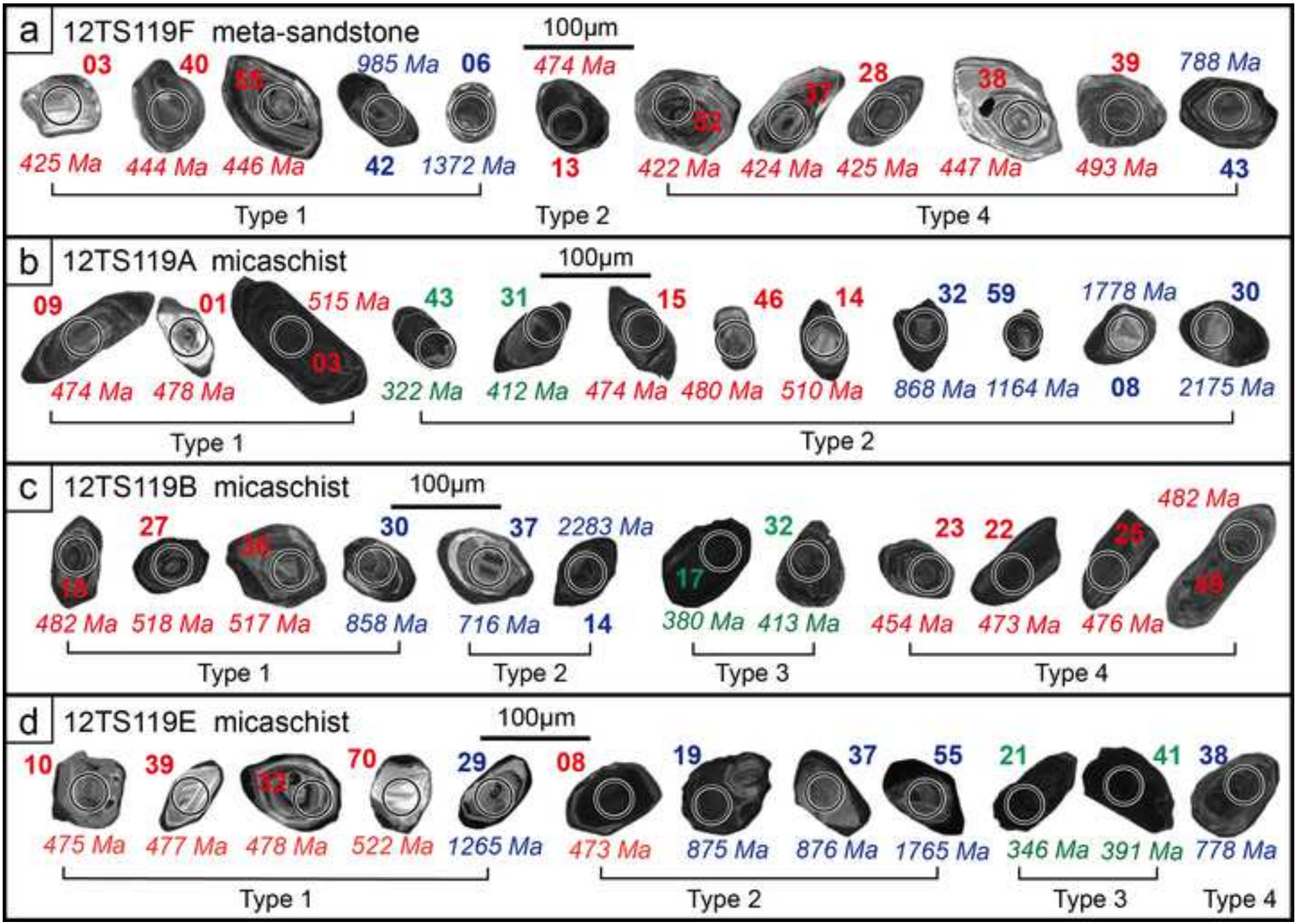

Figure 6

Click here to access/download;Figure;Fig. 6. Concordia diagrams and U-Pb age probability diagrams.jpg

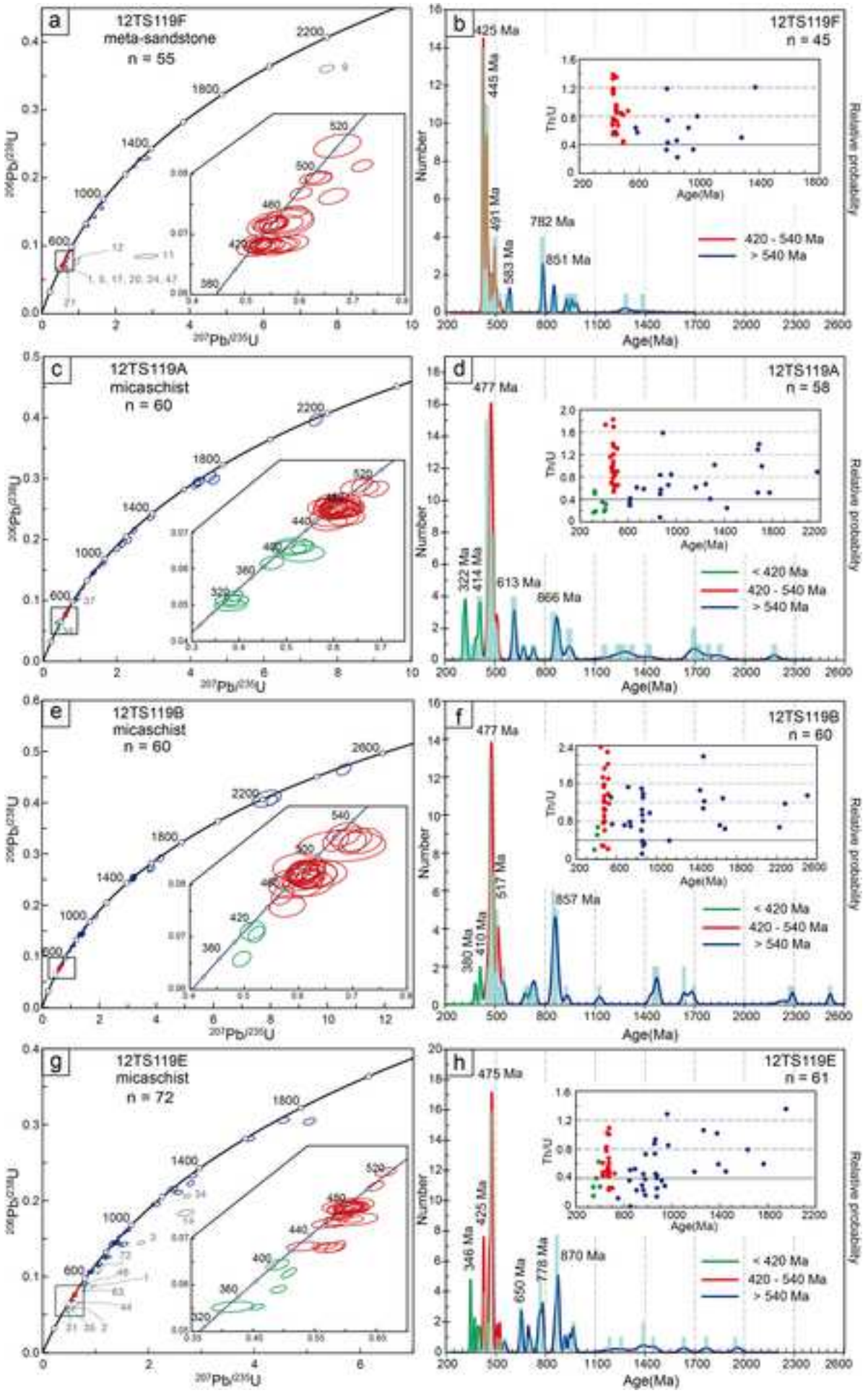

Figure 7

Click here to access/download;Figure;Fig. 7. Chondrite-normalized REE patterns.jpg

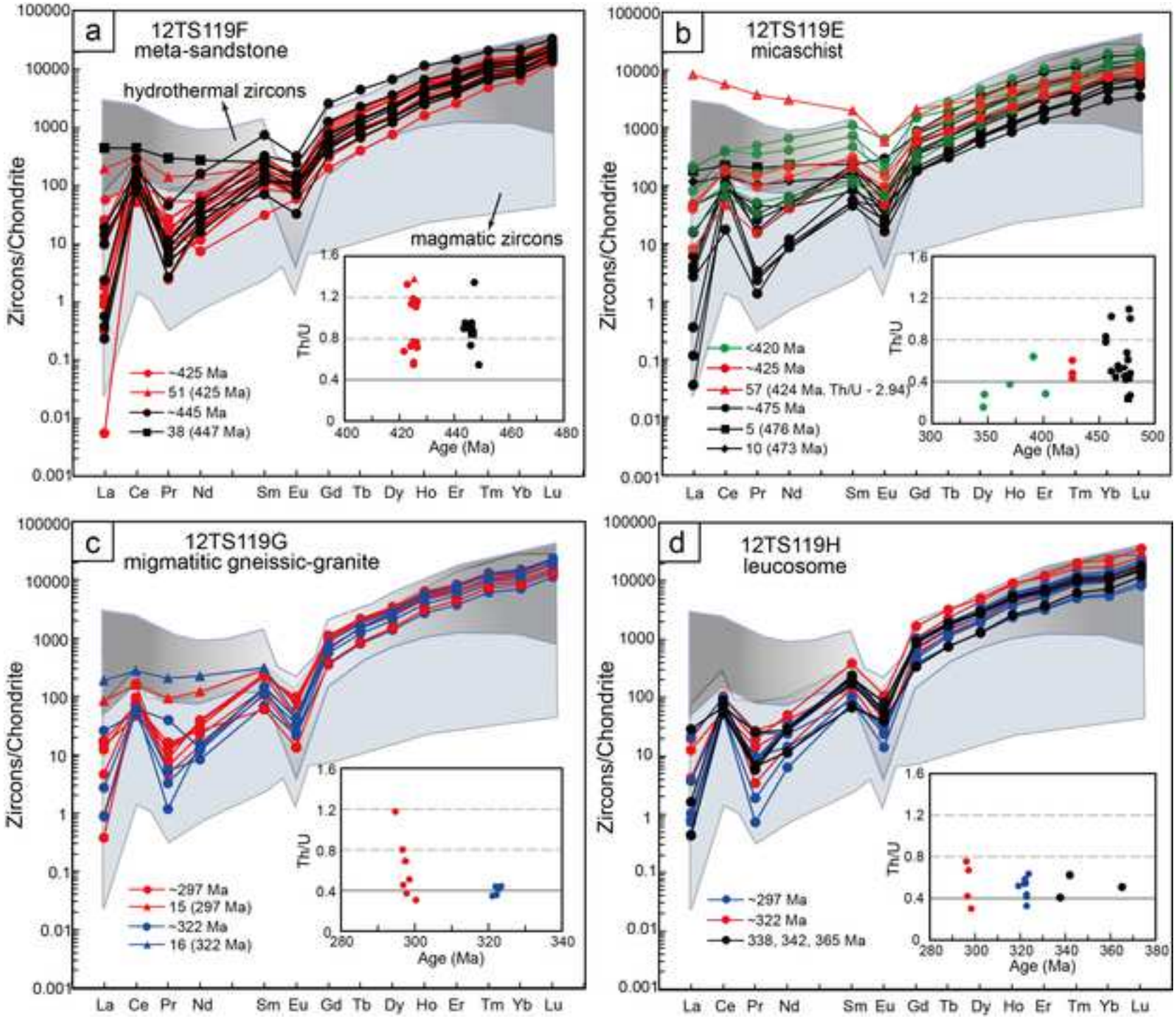

Figure 8

Click here to access/download;Figure;Fig. 8. CL images, concordia and U-Pb age.jpg

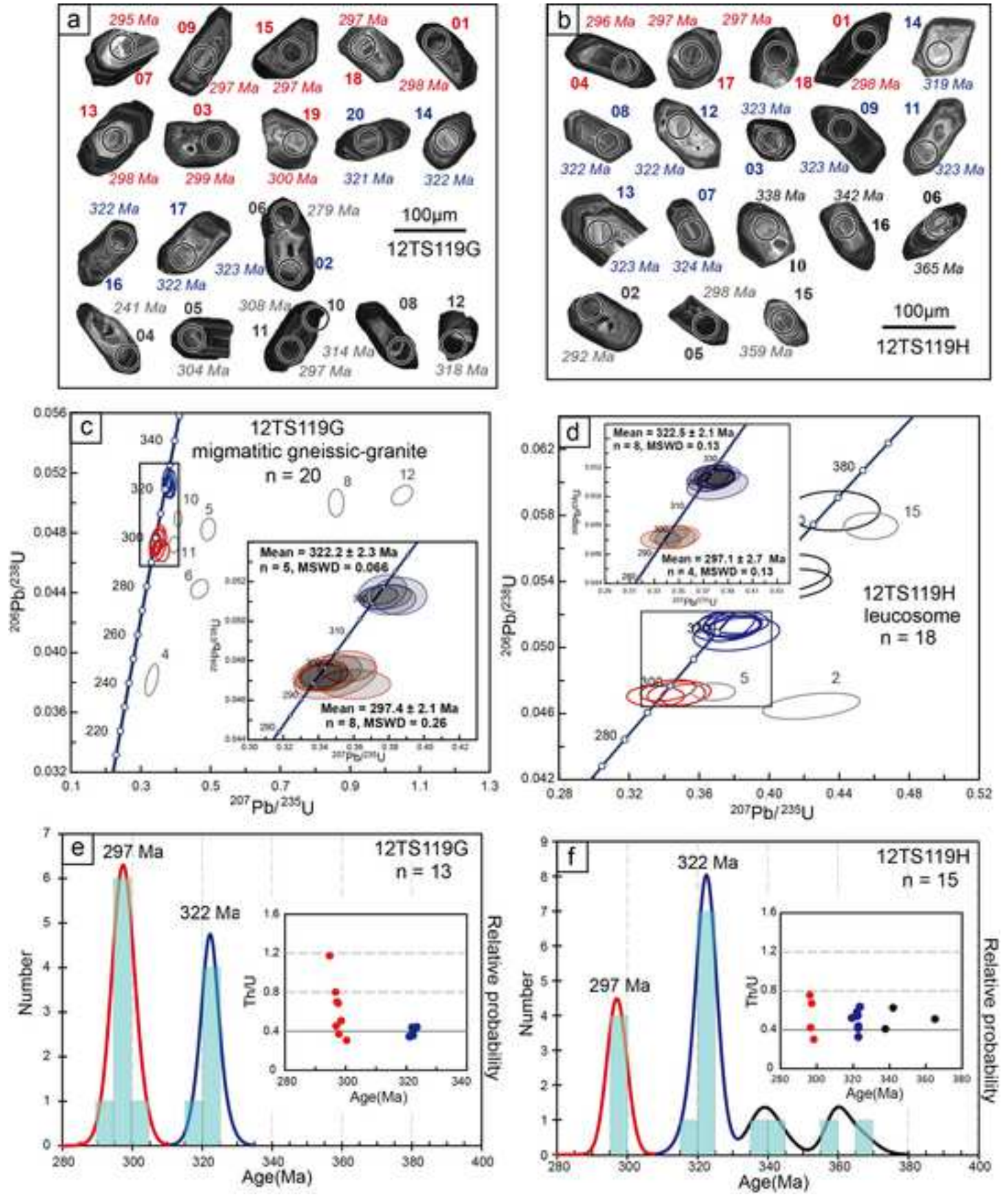

Figure 9

Click here to access/download;Figure;Fig. 9. Compilations of zircon U-Pb ages from Qincheng.jpg

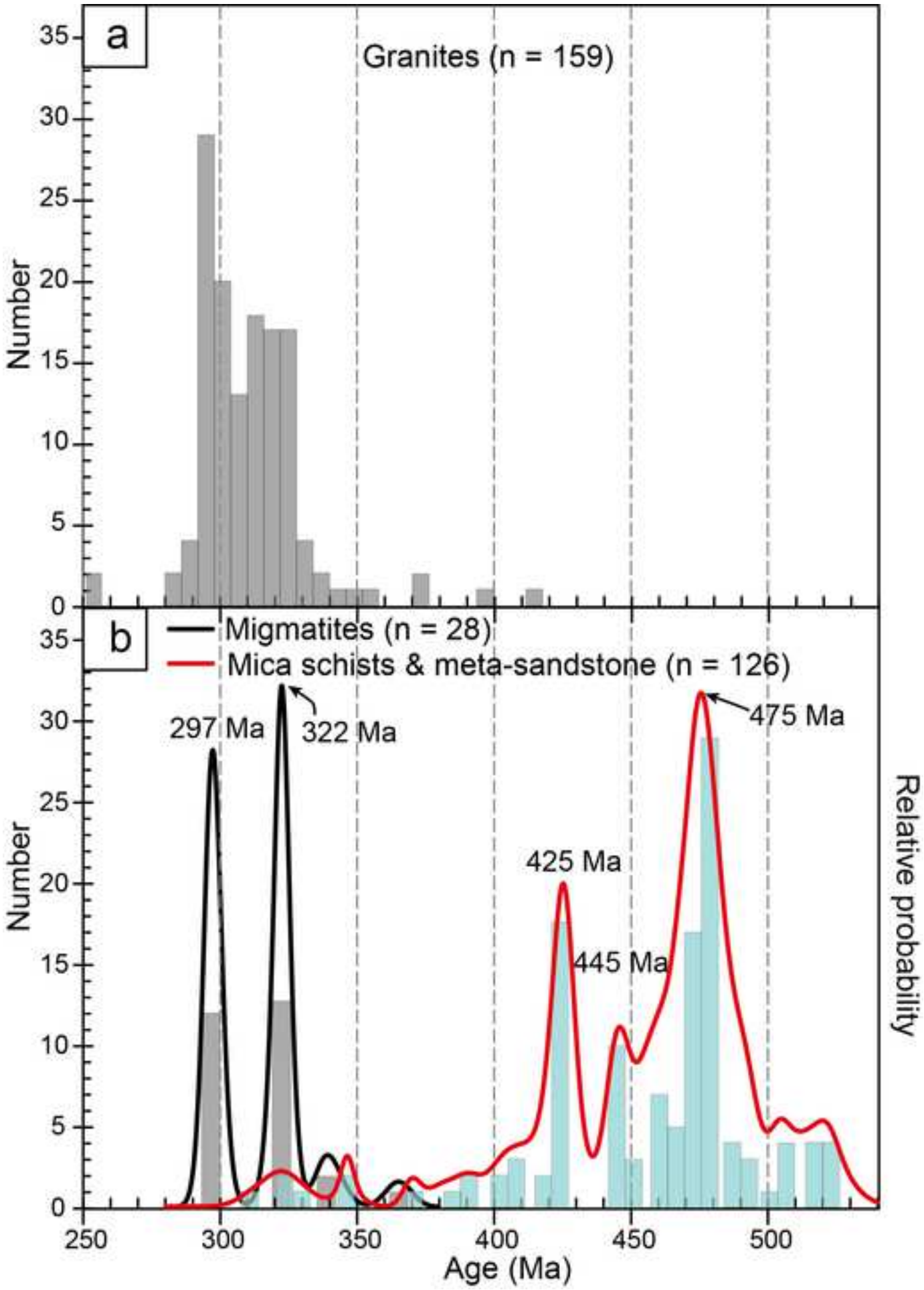

Figure 10

Click here to access/download;Figure;Fig. 10. Compilations of zircon U-Pb ages.jpg

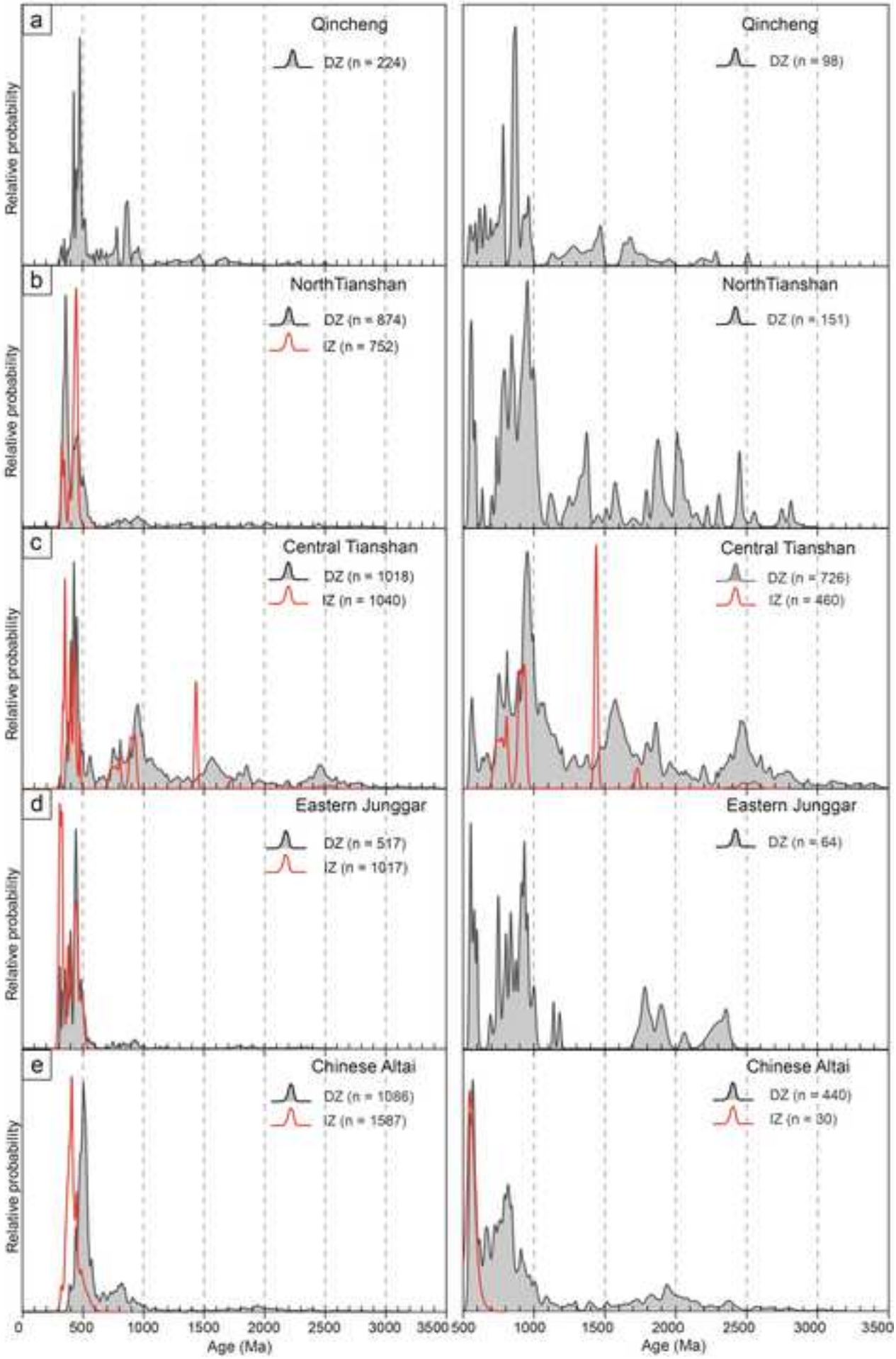

Figure 11

Click here to access/download;Figure;Fig. 11. Tentative cartoon model.jpg

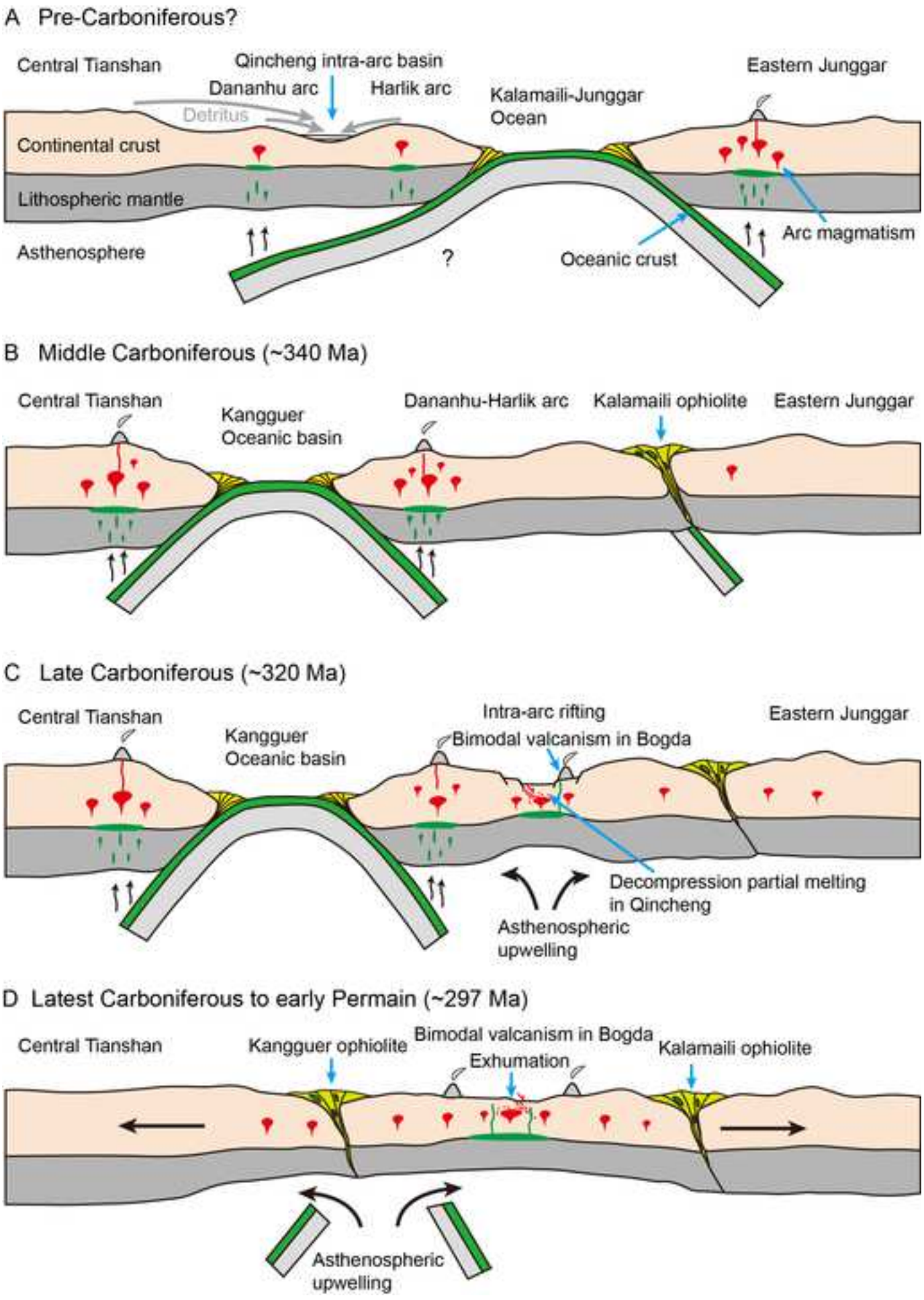

Table 1. Sample description and analytical data summary

Sample No.	Rock type	Petrographic features	Structural features	Age populations
12TS119A	micaschist	Quartz (45-50 vol. %), biotite (20-25 vol. %), plagioclase (10-15 vol. %), muscovite (5-10 vol. %) and a small amount of silimanite	Oriented biotite and muscovite	Similar age spectra, age populations at: 2500-2175, 1800-1600, 1500-1100, 1000-850, 800-500, ~475, ~425, 420-380, ~346, ~322 Ma
12TS119B	mylonitized micaschist	Quartz (30-35 vol. %), biotite (20-25 vol. %), muscovite (30-35 vol. %) and plagioclase (5-10 vol. %)	Preferred orientation of biotite and muscovite flakes and elongated quartz grains	
12TS119E	micaschist	Quartz (30-35 vol. %), chloritized biotite (20-25 vol. %), muscovite (10-15 vol. %), sericite (20-25 vol. %) and sillimanite (<5 vol. %)	Preferred orientation of biotite and elongated quartz grains	
12TS119F	meta-sandstone	Quartz (60-70 vol. %), chloritized mica (10-15 vol. %), plagioclase (15-20 vol. %)	Weakly oriented tabular feldspar and chloritized mica	Age populations at: 1400-1250, 1000-850, ~780, ~580, ~490, ~445, ~425 Ma
12TS119G	migmatitic gneissic-granite	Quartz (40-45 vol. %), K-feldspar (25-30 vol. %), plagioclase (20-25 vol. %) and a small amount of biotite and muscovite	Lattice bending, undulose extinction, deformation bands and subgrains in quartz and feldspar, lobate grain boundaries	Two age peaks at: 322 and 297 Ma
12TS119H	migmatite leucosome	Quartz (40-45 vol. %), K-feldspar (25-30 vol. %), plagioclase (20-25 vol. %) and a small amount of biotite and muscovite	Optically continuous K-feldspar enclosing equant and diamond-shaped quartz, grain boundary migration recrystallization	Two age peaks at: 322 and 297 Ma. Inherited ages of 338-365 Ma

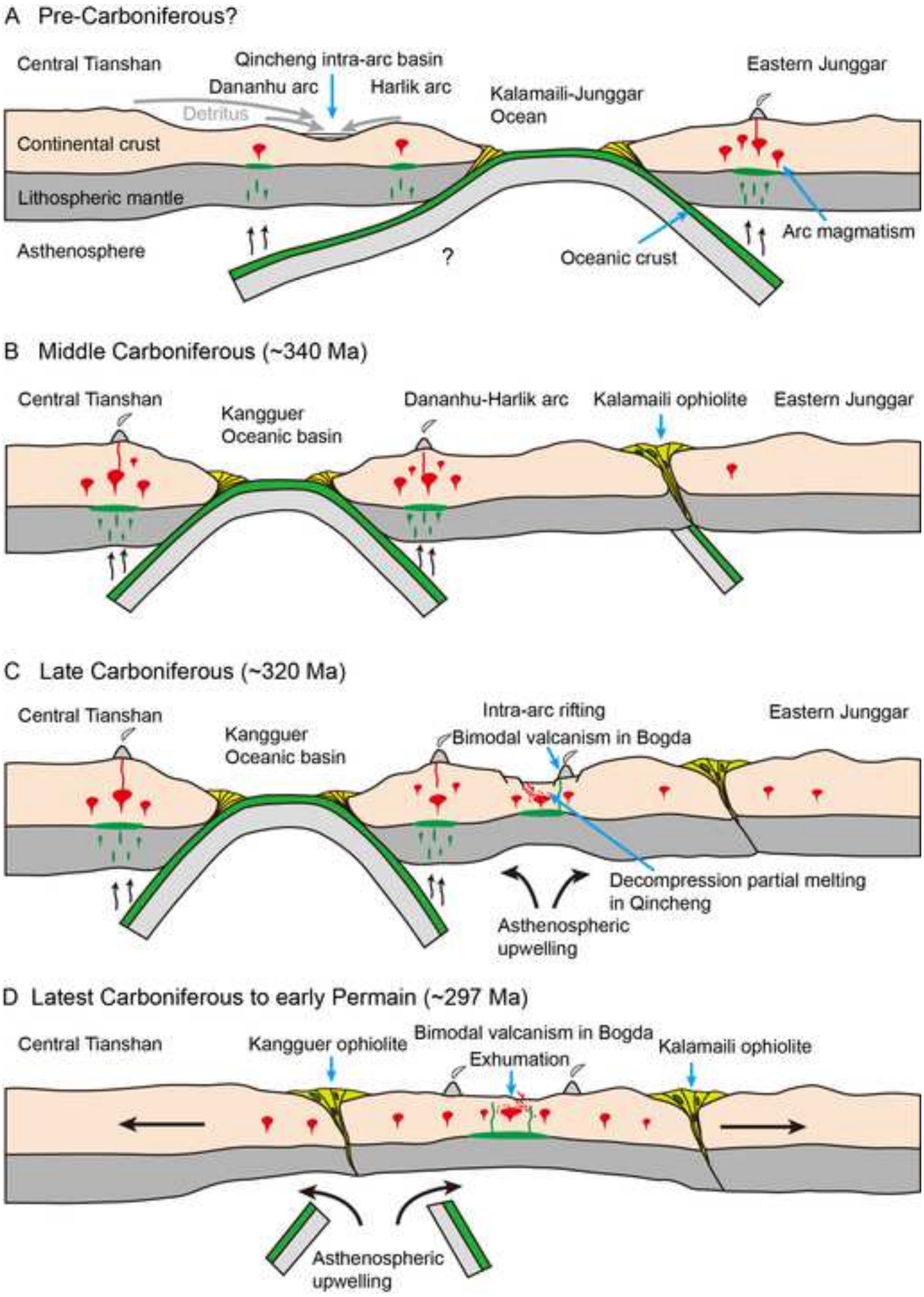

Supplementary Figure S1

Supplementary Figure S2

Click here to access/download

Supplementary Material

Supplementary Table S3.xls

*Declaration of Interest Statement

Declaration of interests

☑ The authors declare that they have no known competing financial interests or personal relationships that could have appeared to influence the work reported in this paper.

☐The authors declare the following financial interests/personal relationships which may be considered as potential competing interests:

Xinghua Ni: Investigation, Conceptualization, Writing-Original Draft, Editing. **Bo Wang:** Supervision, Conceptualization, Funding acquisition, Writing-Reviewing and Editing. **Dominique Cluzel:** Supervision, Investigation, Writing-Reviewing and Editing. **Jiashuo Liu:** Investigation, Writing-Reviewing and Editing. **Zhiyuan He:** Investigation, Writing-Reviewing and Editing.